AN ABSTRACT OF THE THESIS OF

Maynard Carver Falconer for the degree of Doctor of Philosophy in Electrical and Computer Engineering presented on January 23, 1997. Title: Three Dimensional Electromagnetic FDTD Simulation of General Lossy Structures with Nonuniform Grid Spacing.

Abstract approved: Redacted for Privacy

Vijai K. Tripathi

A new second order accurate nonuniform grid spacing technique which does not depend on supraconvergence is developed for Finite Difference Time Domain (FDTD) simulation of general three dimensional structures. The technique is useful for FDTD simulations of systems which require finer details in small regions of the simulation space by providing the ability to utilize nonuniform grid spacing. The stability conditions of the new technique are derived and shown to be consistent with uniform grid formulation and the accuracy of the technique is investigated and shown to be second order. The advantage of the new technique is that it allows for greater simulation detail while reducing the computational and memory requirements compared to the current uniform grid FDTD techniques.

Additionally, the derivation of the expressions associated with the inclusion of material properties in the FDTD simulation with nonuniform grids is presented allowing for the

development of a nonuniform FDTD simulator for general lossy 3D systems associated with on and off chip interconnects, electronic packages and microwave circuits. In order to illustrate the utility of this simulator, time domain electromagnetic simulation of a 3-D lossy interconnect structure associated with a generic surface mount IC package is presented. The time domain currents and fields are computed in the structure to investigate ground bounce, signal degradation, and crosstalk associated with the interconnects and packaging structure. The supply plane conductivities are included in the simulation allowing the observation of the current densities in the power/ground planes as a function of time.

Finally, the FDTD simulation tool is proposed and used as a Virtual TDR (V-TDR) to extract the circuit models associated with complex 3D structures. The time domain response of a multiport structure is used to extract the equivalent circuit parameters to characterize the multiport by using the multiport time domain reflection (TDR) based general deconvolution algorithm. Examples of coupled interconnects and transmission lines are presented to illustrate this technique.

Three Dimensional Electromagnetic FDTD Simulation of General Lossy Structures with Nonuniform Grid Spacing

by

Maynard Carver Falconer

A THESIS

submitted to

Oregon State University

in partial fulfillment of
the requirements for the
degree of

Doctor of Philosophy

Presented January 23, 1997
Commencement June 1997

Doctor of Philosophy thesis of Maynard Carver Falconer presented on January 23, 1997

APPROVED:

Redacted for Privacy

Major Professor, representing Electrical and Computer Engineering

Redacted for Privacy

Head or Chair of Department of Electrical and Computer Engineering

Redacted for Privacy

Dean of Graduate School

I understand that my thesis will become part of the permanent collection of Oregon State University libraries. My signature below authorizes release of my thesis to any reader upon request.

Redacted for Privacy

Maynard Carver Falconer, Author

ACKNOWLEDGMENT

I would like to thank my family for their support and especially my wife Beate who patiently supported me through all the twists and turns that graduate school presents. Prof. Tripathi for always finding me teaching and research assistantships and guiding me through the process. A special thanks to my fellow graduate students, Rick Lutz, Alok Tripathi, Kate Remley, Leonard Hayden, Jhy-Ming Jong, Neven Orhanavic, Dimitry Smolyanski and the many others who contributed by participating the many insightful conversations that helped work out theory, programming bugs, and concepts. Thanks also to Satish Redey of the math department who let me run some of the advanced mathematical concepts by him. Additionally I would like to acknowledge the support of Intel corporation and the National Science Foundation for their financial support in the final stages of this work.

TABLE OF CONTENTS

TABLE OF CONTENTS (Continued)

LIST OF FIGURES

Figure Page

LIST OF FIGURES

LIST OF FIGURES

Figure Page

LIST OF FIGURES

Figure Page

PREFACE

The FDTD technique was first introduced in 1966 and with the recent advances in computational power and the availability of affordable memory the technique has gained widespread popularity. Taflove points out in his recent book on the FDTD method that over 15% of all the papers presented at the 1994 AP-S and URSI conference involved use of the FDTD technique. The FDTD technique has the advantage of allowing electromagnetic simulation of complex structures that were previously intractable by the available methods. Since it is a fullwave technique the simulation gives access to the electrical and magnetic fields throughout the simulation space. This gives the engineer a powerful visualization tool which allows one to observe the behavior of the fields as a function of time and additionally gives great flexibility in the selection of parameters to monitor. However, it is a brute force technique which requires large computational power and large computer memories and is therefore not appropriate for problems which can be solved much more efficiently using other techniques. Overall the FDTD technique is a powerful tool and this thesis presents a nonuniform grid spacing approach for the FDTD technique which further advances the art of electromagnetic simulation.

THREE DIMENSIONAL ELECTROMAGNETIC FDTD SIMULATION OF GENERAL LOSSY STRUCTURES WITH NONUNIFORM GRID SPACING

1. Introduction

1.1. A Brief Evolution of EM simulation

One of the defining points in electomagnetics was Maxwell's unification of electric and magnetic fields into a set of partial differential equations around 1870. Since then electromagnetic source, boundary value, and general mixed problems have been solved using a multitude of approaches. With the advent of computers more computationally intensive techniques have been developed which can solve electromagnetic equations associated with arbitrary useful complex geometries in frequency and time domain or quasi-static fields. These include iterative techniques such as finite difference solution of Laplace's equation, integral equation techniques [1], Moment method in real and spectral domain [2] which uses basis and test functions to approximate the fields in a discretized space, and the finite element method which uses higher order elements of varying size with variational solution approaches. Advances in computational power and memory have lead

to the rise of time domain methods including FDTD and transmission line matrix (TLM) method. The advantage of time stepped approaches is the ability to model highly complex, lossy structures and obtain data over a broadband of frequencies with one simulation. Additionally the time stepped approaches are particularly well suited for massively parallel computers which can currently deliver up to one teraflop of computational power. As further advances in computers arrive, techniques like FDTD can provide many more benefits to EM simulation including completely unstructured grids, frequency dependent materials, nonuniform time stepping, and inclusion of active media such as GaAs and silicon based devices. All of the fore mentioned benefits have already been developed, but await the availability of more computational power for practical implementation of general structures.

1.2. Some Applications of Fullwave EM simulators

Fullwave electromagnetic simulators calculate the electric and magnetic fields throughout the simulations space as a function of time. Since all of the field components are available many different types of metrics can be extracted, including voltage, current, and power. From these S parameters, effective dielectric constant, impedance, inductance, capacitance, radar cross section, and many other parameters can be readily determined for complex structures. This access to all of the field components inside of the simulation space also provides several important additional opportunities to the investigator including;

- Visualization of complex field patterns which can lead to a deeper understanding of the electromagnetic behavior.

- Determination of field patterns such as mapping of antenna lobes, far field strengths and patterns, EMI testing, etc...

- Use as a validation tool to verify the accuracy of CAD-oriented models.

A large body of work using the FDTD method has already been performed by the electromagnetic community for microwave circuits, antennas, radar cross sections, and passive circuit structures. Some specific applications of the FDTD fullwave technique include, but not limited to:

- Extraction of impedance and effective dielectric constant as a function of frequency for microstrips[3].
- Analysis of submicron interconnects[4].
- Analysis of currents in finite conductivity power planes[5].
- Simulation of multi-cavity filters[6].
- Simulation of coupled filters and spiral inductors [7].
- Patch antennas, branch line coupler, microstrip filters [8].
- Open dielectric resonators [9].
- Slotlines and coplanar waveguides [10].
- FDTD coupled with Monte Carlo simulation of optically generated picosecond pulses in a GaAs coplanar waveguide [11].
- Circular waveguides [12].
- PCB vias and performance of vias as shorts [13].
- Modeling of passive and active loads in FDTD simulations [14].
- Modeling of active regions in FDTD [15].

- Radar Cross Section analysis of fighter aircraft [16].

- Hyperthermia treatment of cancer and modeling of human photoreceptors [17].

This wide range of applications of the FDTD technique helps to show the flexibility of the technique and its power as an electromagnetic simulator. As further advances in computer power and memory arise the limitations of the technique, computational time and memory demands, will be diminished to only enhance an already powerful electromagnetic tool.

1.3. Previous Full Wave Methods

Full wave electromagnetic analysis has been dominated over the last decade by the Moment Method (MM) and the Finite Element (FE) methods. Both of these methods were originally frequency domain methods, (although some limited time domain approaches now exist), and required inversion of a matrix to arrive at the solution. The inherent drawback to frequency domain approaches is the necessity to run multiple simulations to extract frequency dependent parameters for wide band characterization. Additionally the matrix inversion requires order of N^3 operations, where N is the number of complex valued field unknowns, (unless the matrix is sparse and conforms to a more efficient matrix inversion technique) [18]. A brief overview of the Moment and Finite Element method is presented to allow a comparison to the FDTD method.

1.3.1. Moment Method

In the moment method the electromagnetic fields are approximated by a linear combination of appropriate basis functions which satisfy the simulation conditions at the grid points (point-matching method) or across the grid cell (Galerkin's method). This requires choosing the appropriate basis functions, then testing it with the same (Galerkin) or another set of testing functions, and finally trying to resolve the error between the two.

However, the complete set of basis functions which approximate the electromagnetic fields in the region and conform to the geometry of the problem are not always easily determined. Additionally a rigorous analysis of the convergence behavior of the solution for the simulation with regard to a set of basis functions is not always easily performed or available. Yamashita points out that the moment method works well for simulation of dielectric waveguides since it requires only a small number of grid locations spanning the cross-section of the waveguide. While the method works well for single and multiple dielectric waveguides it is difficult to apply it to structures with large three dimensional boundary areas, structures with graded dielectric constants, or structures with sharp field concentrations such as occur at corners or edges[19].

The moment method essentially involves setting up and solving a simultaneous set of complex-valued equations (basis functions) by inverting a matrix or by utilizing an iterative technique. Taflove illustrates the computational limitations of the moment method by estimating the requirements of analyzing the radar cross section (RCS) of a military jet fighter at 960 MHz on a Cray Research C-90. He estimated that the simulation would require disk drives to store a 10^{12} word MM matrix, one year and five months of uninterrupted computation time, and assuming that an acceptable error accumulation would result after the 10^{18} floating-point operations on the MM matrix elements having a precision of only 1 part in 10^4 [20]. A problem similar the one presented above, but using FDTD is presented by Taflove demonstrating the ability of the method to handle this previously intractable problem with the additional benefit determining a broad band of frequency data from the single time domain simulation.

1.3.2. Finite Element Method

The finite element method divides the simulation space into 'elements' to which a set of functionals (variational expressions) are set up and solved using a variational method or Galerkin method. Since the elements are not required to be of the same size, the FEM is suitable for application to problems with steep variations in the fields, or with inhomogeneous and anisotropic problems. Some of the difficulties with FEM include the generation of spurious non-physical solutions, dealing with unbounded field problems, and manipulation of ill-conditioned matrices. Additionally, the FEM requires a matrix inversion which is a computationally expensive process. Sometimes the matrix may be sparse which allows use of an iterative technique for matrix manipulation in place of performing an LU decomposition for the inversion thus providing some potential computational savings. However matrix inversion is always computationally expensive and requires that the matrix be well conditioned. One of the major advantages of FEM is the availability of automatic grid generators which conform to the geometry of the problem and significantly reduce the simulation setup time.

Yook et. al., presented a comparison of FDTD and FEM for the solution of several interconnect structures [21]. On an HP 9000/735 workstation the FEM using around 50,000 unknowns took about 30 minutes for each frequency point. The FDTD simulations were performed on a Cray YMP8/864 machine in 2 minutes to 15 minutes and estimated to

require from 3.5 hours to 25 hours on an HP 9000/735 for a time domain result which resulted in a broad range of frequency results after application of a Fourier transform. Additionally he noted that the FEM becomes difficult to apply at low frequencies due to a prohibitive increase in the number of unknowns. For this particular example the frequency resolution desired multiplied by the time for each FEM run may be comparable to the ability of the FDTD to extract a broad band of frequency data from one simulation with out the worry of spurious solutions or ill-conditioned matrices.

1.4. The FDTD method

The finite difference time domain method was first introduced in 1966 by K.S. Yee [22]. It is a full wave simulation technique in the time domain which can perform electromagnetic analysis of highly complex three dimensional structures. The FDTD method is derived by taking the centered differences of Maxwell's curl equations in both space and time. The equations are then solved for the future time field component. The future time field component is a function of only past time field components and, can therefore, be solved for directly and efficiently.

1.4.1. Advantages of the FDTD method

There are several advantages to the FDTD method over MM and FEM techniques. One of the main advantages is the ability to solve directly for the future field components. This results in order T*N operations, where N is the number of complex valued field unknowns and T is the number of time steps, as compared to the order N^2 to N^3 operations for matrix inversion required for MM and FEM. The reduced order of operations is critical for the simulation of a large number of field unknowns. Since the FDTD method does not

require a matrix inversion the difficulty of ill-conditioned matrices and spurious solutions is eliminated. Additionally, since the FDTD is a time domain method, applying a Fourier transform gives results over a broad band of frequencies from one simulation.

The underlying equations in FDTD are easily modified to allow introduction of special cells into the simulation for thin materials, active devices, lumped elements, absorbing boundaries, etc. A further advantage of the FDTD method is that it is extremely well suited for application to massively parallel computer systems when implemented on an orthogonal grid. Access to all of the field components as a function of time allows the investigator to observe the time dependent field patterns possibly leading to better insights and understanding of the structures electromagnetic behavior.

1.4.2. Disadvantages of the FDTD method

One of the largest draw backs to the FDTD method is the need for large computational power and large computer memory. At the current rate of advancement in the computer industry it is anticipated that this draw back will become less and less significant in the near future, especially with the advancements in massively parallel machines. Another limitation to the FDTD method is auto-generation of the grid for general structures. Orthogonal grids require that the structure be approximated by small rectangular cells for which auto-generation software is not widely available. Non-orthogonal unstructured grids can be auto-generated and conform to the structure, but are not easily or efficiently adapted to

massively parallel machines and significantly increase the requirements for computational power and computer memory.

1.4.3. The FDTD grids

The various FDTD implementations can be broken down into two broad categories based on the approach to griding the simulation space. The categories are highly structured orthogonal grids, and unstructured nonorthogonal grids. For the following discussion, only rectangular coordinates will be considered although the discussion can be applied to cylindrical and spherical coordinates as well.

Orthogonal grids are highly structured grids which use rectangular cells to grid up the simulation space. This approach includes Yee's original FDTD implementation. Traditionally the grid is a uniform grid which relies on centered differences to achieve second order accuracy. More recently the concept of supraconvergence was used to allow nonuniform orthogonal griding implementations at the expense of local first order accuracy. Other approaches use special cells which model the behavior of curved surfaces inside of a cell. In this work an alternative technique is presented for implementing nonuniform orthogonal grids without the loss of second order accuracy. Orthogonal grids have the advantage over nonorthogonal grids of being computationally efficient and easily implementable on massively parallel machines. Additionally nonuniform orthogonal grids have most of the location information implied in the indexing that results in a memory

efficient implementation which may out weight the nonorthogonal advantage of using less cells by conforming to the geometry of the problem.

Unstructured nonorthogonal grids divide the simulation space in cells which vary in shape and size conforming to the structure being simulated. By conforming to the geometry of the structure being simulated, unstructured nonorthogonal grids will typically require a smaller number of cells compared to the orthogonal approaches. Additionally the availability of automated grid generators is a major advantage of this approach along with the ability to model complex surfaces with a high degree of accuracy. The disadvantages are the additional mapping information for each cell which must be stored, larger computational burden for calculating each of the field components in an unstructured cell, and the difficulty of efficient implementation on massively parallel machines.

There are also hybrids of the two approaches which use unstructured nonorthogonal subgrids inside of a structured orthogonal grid or structured orthogonal grids inside of an unstructured nonorthogonal gird. Determination of what griding approach is most efficient or appropriate can only be defined for each specific structure to be simulated and not definitively for all generic problems. The use of nonuniform structured orthogonal griding will typically be the most efficient when the simulation structure conforms to rectangular coordinates. Simulation of highly irregular surfaces may require an excessive number of small cells for structured orthogonal approaches resulting in the unstructured nonorthogonal griding approach being more efficient. The focus of this thesis will be on nonuniform orthogonal grids which are second order accurate through out the simulation space since this offers the most computationally and memory efficient implementation of FDTD for the large class of structures which conform to rectangular coordinates.

1.5. Thesis Overview

This thesis presents the derivation of a new FDTD technique for nonuniform orthogonal grids which is computationally efficient, more memory efficient than uniform orthogonal approaches, and retains second order accuracy both globally and locally. Proper handling and calculation of the constitutive material parameters in a nonuniform grid is derived. Accuracy for the nonuniform grid spacing is proven and the stability criteria derived. A comparison is made between the new second order accurate nonuniform approach and the current approach of supraconvergence. The technique is validated by comparing the results obtained with known published results. Simulation of currents in a ground plane in a 3-D structure having finite conductivity, is presented. The FDTD method is also used in a unique novel manner as a virtual TDR (V-TDR) to extract the equivalent SPICE type circuit associated with coupled interconnects in an IC package.

Chapter two covers the basics of FDTD and absorbing boundary conditions. It also presents for the first time the proper derivation and handling of the complete set of constitutive material parameters, (dielectric constant, conductivity, permeability, and equivalent magnetic conductivity), in a nonuniform FDTD grid formulation.

Chapter three covers orthogonal nonuniform space stepping. It presents the current approaches and discusses their limitations. The method of undetermined coefficients is

used to derive the proper finite difference coefficients for a nonuniform grid. A Taylor's series expansion is then used to prove that the new technique is second order accurate. A Fourier analysis is performed to derive the stability criteria for the new technique. Finally it is shown that the new technique does not impose a tighter stability criteria than the current uniform grid spacing FDTD method imposes and therefore does not increase the computational burden by requiring a smaller time step.

Chapter four presents an overview of the FDTD simulator which was written as part of this thesis work and presents the validation of the algorithms developed against published results. A general lossy nonuniform FDTD simulator was developed to simulate complex three dimensional structures and allow the extraction of characteristic electrical parameters of the structures (i.e., impedance, effective dielectric constant, voltage, current, S parameters, resonant frequencies, etc...). The code was written in 'C' and is over six thousand lines long. The validation includes a comparison between the new second order accurate technique and the current supraconvergence approach which allows for local first order accuracy in the FDTD grid. It is seen that the new second order technique is more accurate than the supraconvergence approach.

Chapter five presents results from the FDTD simulator and the application of FDTD as a virtual TDR (V-TDR). A simplified dual inline package (DIP) for an integrated circuit is simulated with finite conductivity ground planes and traces. The ground plane currents and the coupling between the traces are observed as a function of time. Additionally the FDTD method is used as a virtual TDR to extract the equivalent circuit for the DIP.

Chapter six summarizes the original contributions of this work, presents some conclusions and directions for future work. Additionally, applications of the approaches included in this work are presented.

2. FDTD Technique

2.1. Basics of FDTD

The finite-difference time-domain (FDTD) method was first introduced by K.S. Yee[23] to solve electromagnetic scattering problems. The benefits of the FDTD method is that it can be readily implemented and used to solve for the time domain response of three dimensional structures. The main draw backs of the method are the large memory requirements and speed needed for the analysis of complex structures. With modern computers becoming faster and having larger memory capabilities, the above drawbacks are becoming more manageable. The calculation of the electromagnetic fields in FDTD are based on the time and space discretisation of Maxwell's equations[24,25].

$$\nabla \times \vec{E} = -\mu \frac{\partial \vec{H}}{\partial t} \tag{2-1}$$

$$\nabla x \vec{H} = \sigma \vec{E} + \varepsilon \frac{\partial \vec{E}}{\partial t} \tag{2-2}$$

The permeability μ, permittivity ε, and conductivity σ are time-independent for these calculations, but can be altered to be time-dependent. Expanding the curl operation in the previous curl equations and expanding the fields into their x, y, and z components gives:

$$\bar{a}_x\left(\frac{\partial E_z}{\partial y}-\frac{\partial E_y}{\partial z}\right)+\bar{a}_y\left(\frac{\partial E_x}{\partial z}-\frac{\partial E_z}{\partial x}\right)+\bar{a}_z\left(\frac{\partial E_y}{\partial x}-\frac{\partial E_x}{\partial y}\right)= -\mu\frac{\partial}{\partial t}\left(\bar{a}_x H_x+\bar{a}_y H_y+\bar{a}_z H_z\right) \tag{2-3}$$

$$\bar{a}_x\left(\frac{\partial H_z}{\partial y}-\frac{\partial H_y}{\partial z}\right)+\bar{a}_y\left(\frac{\partial H_x}{\partial z}-\frac{\partial H_z}{\partial x}\right)+\bar{a}_z\left(\frac{\partial H_y}{\partial x}-\frac{\partial H_x}{\partial y}\right)= \sigma\left(\bar{a}_x E_x+\bar{a}_y E_y+\bar{a}_z E_z\right)+\varepsilon\frac{\partial}{\partial t}\left(\bar{a}_x E_x+\bar{a}_y E_y+\bar{a}_z E_z\right) \tag{2-4}$$

Taking only the x components of the two equations above gives:

$$\bar{a}_x\left(\frac{\partial E_z}{\partial y}-\frac{\partial E_y}{\partial z}\right)=-\mu\frac{\partial}{\partial t}\left(\bar{a}_x H_x\right) \tag{2-5}$$

$$\bar{a}_x\left(\frac{\partial H_z}{\partial y}-\frac{\partial H_y}{\partial z}\right)=\sigma\left(\bar{a}_x E_x\right)+\varepsilon\frac{\partial}{\partial t}\left(\bar{a}_x E_x\right) \tag{2-6}$$

Taking the centered finite difference of these equations results in:

$$\frac{\left(E_z^n\left(i,j+1,k+0.5\right)-E_z^n\left(i,j,k+0.5\right)\right)}{\Delta y}-\frac{\left(E_y^n\left(i,j+0.5,k+1\right)-E_y^n\left(i,j+0.5,k\right)\right)}{\Delta z}= \frac{-\mu}{\Delta t}\left(H_x^{n+0.5}\left(i,j+0.5,k+0.5\right)-H_x^{n-0.5}\left(i,j+0.5,k+0.5\right)\right) \tag{2-7}$$

and:

$$\frac{\left(H_z^{n+0.5}\left(i+0.5,j+0.5,k\right)-H_z^{n+0.5}\left(i+0.5,j-0.5,k\right)\right)}{\Delta y}$$
$$-\frac{\left(H_y^{n+0.5}\left(i+0.5,j,k+0.5\right)-H_y^{n+0.5}\left(i+0.5,j,k-0.5\right)\right)}{\Delta z}= \tag{2-8}$$
$$\sigma\left(E_x^{n+0.5}\left(i+0.5,j,k\right)\right)+\frac{\varepsilon}{\Delta t}\left(E_x^{n+1}\left(i+0.5,j,k\right)-E_x^{n}\left(i+0.5,j,k\right)\right)$$

Where the superscript is the time step, i is the number of steps in the x direction, j the number of steps i the indices i, j, and k. Solving the previous equations for the new electric and magnetic field components:

$$H_x^{n+0.5}\left(i,j+0.5,k+0.5\right)=H_x^{n-0.5}\left(i,j+0.5,k+0.5\right)-$$
$$\frac{\Delta t}{\mu\cdot\Delta x}\left(E_z^{n}\left(i,j,k+0.5\right)-E_z^{n}\left(i,j,k+0.5\right)+E_y^{n}\left(i,j+0.5,k+1\right)-E_y^{n}\left(i,j+0.5,k\right)\right) \tag{2-9}$$

$$\left(\frac{\Delta t}{\mu\cdot\Delta x}\right)E_x^{n+1}\left(i+0.5,j,k\right)=\left(\frac{2\varepsilon_r\varepsilon_0-\sigma\cdot\Delta t}{2\varepsilon_r\varepsilon_0+\sigma\cdot\Delta t}\right)\left(\frac{\Delta t}{\mu\cdot\Delta x}\right)E_x^{n}\left(i+0.5,j,k\right)+\left(\frac{\left(\frac{c\cdot\Delta t}{\Delta x}\right)^2}{\varepsilon_r+\frac{\sigma\cdot\Delta t}{2\varepsilon_0}}\right) \tag{2-10}$$
$$\left(H_z^{n+0.5}\left(i+0.5,j+0.5,k\right)-H_z^{n+0.5}\left(i+0.5,j-0.5,k\right)+H_y^{n+0.5}\left(i+0.5,j,k-0.5\right)-H_y^{n+0.5}\left(i+0.5,j,k+0.5\right)\right)$$

The other four equations follow the same derivation:

$$H_y^{n+0.5}\left(i,j-0.5,k\right)=H_y^{n-0.5}\left(i,j-0.5,k\right)-$$
$$\frac{\Delta t}{\mu\cdot\Delta x}\left(E_x^{n}\left(i,j-0.5,k+0.5\right)-E_x^{n}\left(i,j-0.5,k-0.5\right)+E_z^{n}\left(i-0.5,j-0.5,k\right)-E_z^{n}\left(i+0.5,j-0.5,k\right)\right) \tag{2-11}$$

$$\left(\frac{\Delta t}{\mu\cdot\Delta x}\right)E_y^{n+1}\left(i+0.5,j,k+0.5\right)=\left(\frac{2\varepsilon_r\varepsilon_0-\sigma\cdot\Delta t}{2\varepsilon_r\varepsilon_0+\sigma\cdot\Delta t}\right)\left(\frac{\Delta t}{\mu\cdot\Delta x}\right)E_y^{n}\left(i+0.5,j,k+0.5\right)+\left(\frac{\left(\frac{c\cdot\Delta t}{\Delta x}\right)^2}{\varepsilon_r+\frac{\sigma\cdot\Delta t}{2\varepsilon_0}}\right) \quad (2\text{-}12)$$

$$\left(H_x^{n+0.5}\left(i+0.5,j,k+1\right)-H_x^{n+0.5}\left(i+0.5,j,k\right)+H_z^{n+0.5}\left(i,j,k+0.5\right)-H_z^{n+0.5}\left(i+1,j,k+0.5\right)\right)$$

$$H_z^{n+0.5}\left(i,j,k+0.5\right)=H_z^{n-0.5}\left(i,j,k+0.5\right)-$$

$$\frac{\Delta t}{\mu\cdot\Delta x}\left(E_x^{n}\left(i,j+0.5,k+0.5\right)-E_x^{n}\left(i,j-0.5,k+0.5\right)+E_y^{n}\left(i-0.5,j,k+0.5\right)-E_y^{n}\left(i+0.5,j,k+0.5\right)\right) \quad (2\text{-}13)$$

$$\left(\frac{\Delta t}{\mu\cdot\Delta x}\right)E_z^{n+1}\left(i+0.5,j-0.5,k\right)=\left(\frac{2\varepsilon_r\varepsilon_0-\sigma\cdot\Delta t}{2\varepsilon_r\varepsilon_0+\sigma\cdot\Delta t}\right)\left(\frac{\Delta t}{\mu\cdot\Delta x}\right)E_z^{n}\left(i+0.5,j-0.5,k\right)+\left(\frac{\left(\frac{c\cdot\Delta t}{\Delta x}\right)^2}{\varepsilon_r+\frac{\sigma\cdot\Delta t}{2\varepsilon_0}}\right) \quad (2\text{-}14)$$

$$\left(H_y^{n+0.5}\left(i+1,j-0.5,k\right)-H_y^{n+0.5}\left(i,j-0.5,k\right)+H_x^{n+0.5}\left(i+0.5,j-1,k\right)-H_x^{n+0.5}\left(i+0.5,j,k\right)\right)$$

As seen in the above equations the new value of a field component is dependent only on the field com since only the field component being solved for is dependent on it's past time information at time n. The other significant observation is that the new field component is solved for directly and independently of the other field components at the same time step. This allows for implementations on massively parallel computers and is why the FDTD does not require a matrix inversion.

Using the discretized Maxwell's equations, boundary conditions, and initial field conditions the electro

The accuracy of the FDTD technique is dependent on the selection of the grid spacing (Δx) and the ti conservative estimates 15*Δx and 20*Δx [28,29]. The stability criteria relating the time and space increments is:

$$\Delta t \leq \frac{\Delta x}{c\sqrt{3}} \tag{2-15}$$

Further modifications can be made to the FDTD equations including irregular grid spacing, incorpora

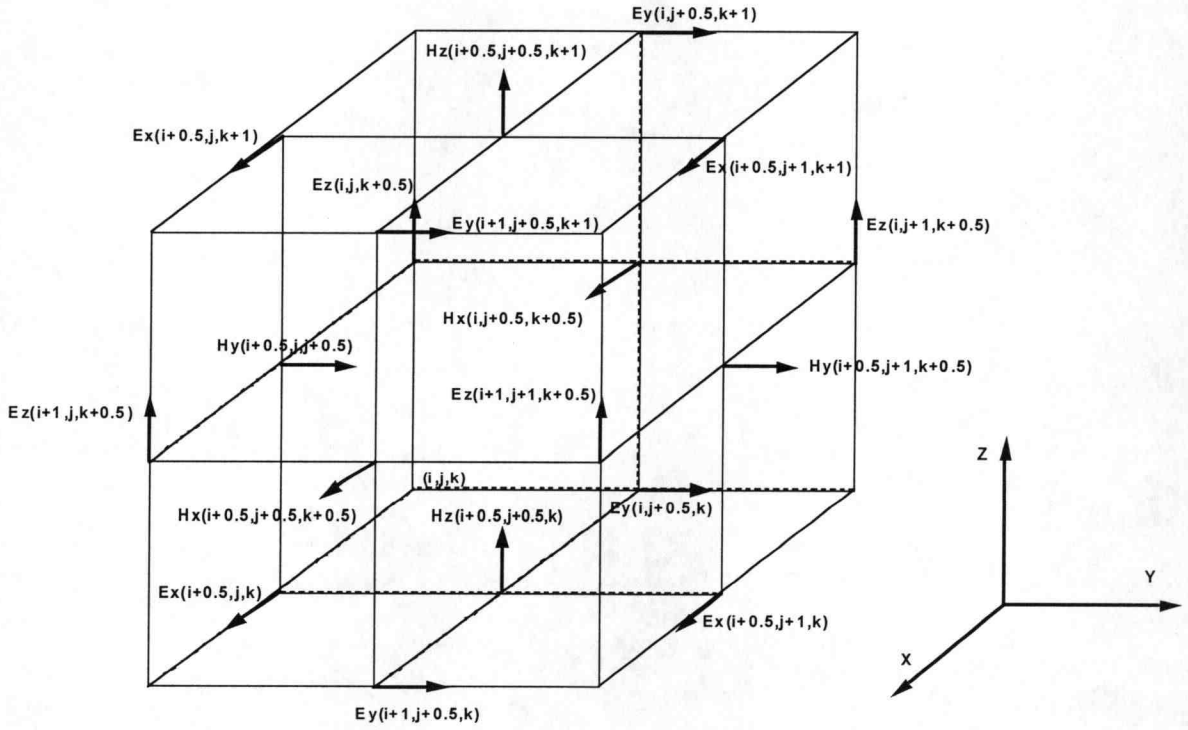

Figure 1 Yee cell or unit cell used in the Finite-Difference Time-Domain technique.

2.1.1. Explicit Exponentially Differenced Time Advancing

Attenuation due to electric or fictitious equivalent magnetic conductivity coupled with a computer's finite number of significant digits may induce instabilities in the standard Yee time stepping method. This problem is particularly significant when implementing highly conductive materials and also of concern when implementing the Perfectly Matched Layer (PML) boundary conditions where both electric and magnetic losses are occurring causing an extremely rapid decay of the outgoing fields[32]. Explicit exponentially differenced time stepping avoids the instabilities in FDTD due to rapid field decay, however it does introduce some further restrictions on the time step size.

Derivation of the exponentially differenced time stepping will be presented in a general format first and then applied to the differential form of Maxwell's Faraday equation.

Assume a general problem of the format:

$$\frac{dy}{dt} + ay = f(t) \tag{2-16}$$

The general solution is:

$$y(\Delta t) = y(0)e^{-at} + \int_0^t e^{-a(t-s)} f(s)ds \tag{2-17}$$

Assuming f(s) is a constant results in:

$$y(\Delta t) = y(0)e^{-at} + (1 - e^{-at})\frac{f}{a} \tag{2-18}$$

Starting with Faraday's law assuming a magnetic loss factor:

$$\nabla xE = -\sigma^* H - \frac{\partial B}{\partial t} \tag{2-19}$$

Rewriting it into the general format results in:

$$\frac{\partial H_x}{\partial t} + \frac{\sigma^*}{\mu_0} H_x = \frac{-1}{\mu_0}\left(\frac{\partial E_z}{\partial y} - \frac{\partial E_y}{\partial z}\right) \tag{2-20}$$

Exponentially differencing in time gives:

$$H_x^{n+1} = e^{-\frac{\sigma^* \Delta t}{\mu_0}} H_x^n + \frac{-1}{\sigma^*}\left(1 - e^{-\frac{\sigma^* \Delta t}{\mu_0}}\right)\left(\frac{\partial E_z}{\partial y} - \frac{\partial E_y}{\partial z}\right) \tag{2-21}$$

The other corresponding five equations follow the same derivation and format. Note that the exponentially differenced equation is only stable if [33]:

$$\frac{\sigma^* \Delta t}{\mu} > 1 \tag{2-22}$$

The FDTD program associated with this body of work was written to automatically determine when to use exponential time stepping and when to use the centered difference time stepping. Recent work has demonstrated that for the PML boundaries the centered time stepping works properly and the exponential time differencing is not required [34]. This is due to the relationship between the electric loss and magnetic loss components required for the implementation of the PML boundaries. The relationship results in a special case in which the centered difference time stepping is stable.

2.1.2. Interface and Material Boundary Conditions

Allowing for the interface between materials with different dielectric constants, conductivities or magnetic properties in the FDTD method requires modification to the basic equations previously presented. However without proper handling of the material interface conditions the FDTD technique typically becomes unstable. First an illustrative derivation for a discontinuity involving an interface between a dielectric and a conductor is presented followed by the more general results for arbitrary electric and magnetic material properties.

Suppose Ex is tangential on the interface between two different materials, media 1 and media 2. The interface plane of the two materials is in the X-Z plane. The relevant equations in the two materials are:

$$\varepsilon_1\left(\frac{\partial E_1 x}{\partial t}\right)+\sigma_1 E_1 x=\frac{\partial H_1 z}{\partial y}-\frac{\partial H_1 y}{\partial z} \tag{2-23}$$

$$\varepsilon_2\left(\frac{\partial E_2 x}{\partial t}\right)+\sigma_2 E_2 x=\frac{\partial H_1 z}{\partial y}-\frac{\partial H_1 y}{\partial z} \tag{2-24}$$

Where the superscript 1 and 2 signify the field components in their respective media. The tangential electric fields across a boundary are continuous:

$$E_1 x = E_2 x \tag{2-25}$$

Adding the previous equations and utilizing (2-25) yields:

$$\left(\frac{\varepsilon_1+\varepsilon_2}{2}\right)\frac{\partial Ex}{\partial t}+\left(\frac{\sigma_1+\sigma_2}{2}\right)Ex=\frac{\partial Hz}{\partial y}-\frac{\partial Hy}{\partial z} \tag{2-26}$$

Discretisation of equation (2-26) leads to a modified version of the original FDTD equation as given by:

$$\left(\frac{\Delta t}{\mu\cdot\Delta x}\right)E_x^{n+1}(i+0.5,j,k)=\frac{\left(\varepsilon_{r1}+\varepsilon_{r2}\right)\varepsilon_0-\left(\frac{\sigma_1+\sigma_2}{2}\right)\Delta t}{\left(\varepsilon_{r1}+\varepsilon_{r2}\right)\varepsilon_0+\left(\frac{\sigma_1+\sigma_2}{2}\right)\Delta t}\left(\frac{\Delta t}{\mu\cdot\Delta x}\right)E_x^{n}(i+0.5,j,k)+$$
$$\left(\frac{\left(\frac{c\cdot\Delta t}{\Delta x}\right)^2}{\frac{\left(\varepsilon_{r1}+\varepsilon_{r2}\right)}{2}+\frac{\sigma\cdot\Delta t}{2\varepsilon_0}}\right)\left[H_z^{n+0.5}(i+0.5,j+0.5,k)-H_z^{n+0.5}(i+0.5,j-0.5,k)+\right. \tag{2-27}$$
$$\left.H_y^{n+0.5}(i+0.5,j,k-0.5)-H_y^{n+0.5}(i+0.5,j,k+0.5)\right]$$

The example above shows the modified electric field equation for a specific material interface case. The more general approach calculates an effective material coefficient dependent on the material properties in the neighboring cells and the cell itself. These effective material coefficients are calculated once, before the simulation time stepping begins, and stored for use throughout the simulation period. The simulator is designed to utilize materials which have non-isotropic dielectrics, electric conductivities, magnetic permeabilities, and fictitious magnetic conductivities. Additionally the simulator does not assume uniform space stepping in calculating the effective material constants.

Calculating the X component of the dielectric constant and the conductivity is based on the weighted mean of the material properties in the cells tangential to the electric field

component. Figure 2 shows the material properties in relation to the vertical Ex component, represented by the black dot.

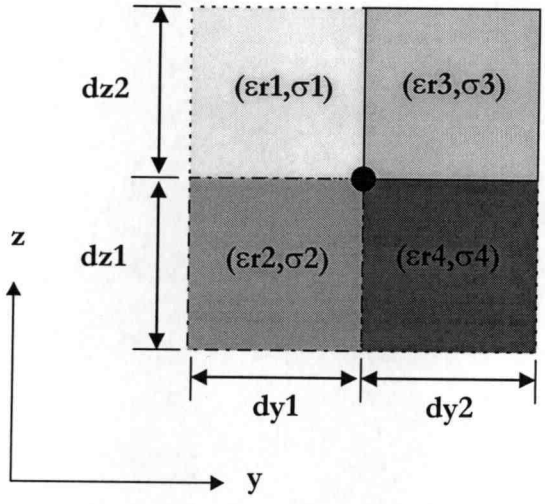

Figure 2 Calculation of Effective Electric Constants

The effective dielectric and conductivity constants are calculated as follows with the variables defined in Figure 2:

$$\varepsilon r_{eff} = \frac{\varepsilon r1 dy1 dz2 + \varepsilon r2 dy1 dz2 + \varepsilon r3 dy2 dz2 + \varepsilon r4 dy2 dz1}{(dy1 + dy2)\cdot(dz1 + dz2)} \tag{2-28}$$

$$\sigma_{eff} = \frac{\sigma 1 dy1 dz2 + \sigma 2 dy1 dz1 + \sigma 3 dy2 dz2 + \sigma 4 dy2 dz1}{(dy1 + dy2)\cdot(dz1 + dz2)} \tag{2-29}$$

The effective magnetic constants are computed as a weighted harmonic mean of the cell properties normal to the magnetic field component. Figure 3 shows the material properties in relation to the Hx component for the calculation of the effective material constants.

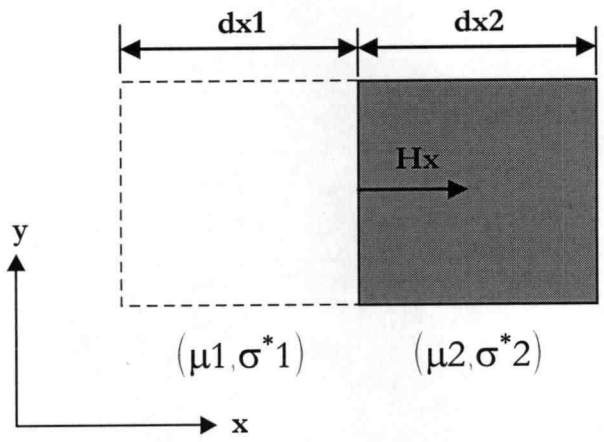

Figure 3 Calculation of Effective Magnetic Constants

The effective permeability[35] and magnetic conductivity constants are calculated as follows with the variables defined in Figure 3:

$$\mu r_{eff} = \frac{\mu 1 \mu 2(dx1 + dx2)}{\mu 1 dx2 + \mu 2 dx1} \tag{2-30}$$

$$\sigma^* r_{eff} = \frac{\sigma^* 1 \sigma^* 2(dx1 + dx2)}{\sigma^* 1 dx2 + \sigma^* 2 dx1} \tag{2-31}$$

These derivations of the electric and magnetic material properties are necessary for the development of a general lossy FDTD simulator with a nonuniform grid and are implemented in the simulator developed for this work. To reduce the computational and memory demands the material properties are calculated as a preprocessing step and redundant values are eliminated. Only the index, size of an integer, of the material properties needs to be stored in the large three dimensional array.

2.2. Absorbing Boundary Conditions

There are several absorbing boundary conditions (ABCs) to handle truncation of the simulation space. While none of the ABCs are perfect, recent advances have produced new techniques that can result in less then -60[dB] of reflection over the frequency band of interest[36]. A brief overview of absorbing boundary conditions will be presented in this chapter followed by a more in depth explanation of the perfectly matched layer (PML) technique which was implemented for this work.

2.2.1. Overview of Absorbing Boundary Conditions

The first simulation space truncation technique comprised of implementing Dirchlet and Neumann boundary conditions which resulted in total reflection of the incident wave from the edge of the simulation space. The Dirchlet and Neumann boundaries were implemented by setting the appropriate tangential fields to zero at the edges of the simulation space. The first absorbing boundary condition (ABC) is often referred to as the Mur ABC[37]. The Mur ABC assumes that the outgoing fields are approximated by a plane wave and then uses the following relationship between position and time to solve for the electric field values at the simulation edges.

$$\left(\frac{\partial}{\partial x}+\frac{\partial}{V_i \partial t}\right)=0 \tag{2-32}$$

Where V_i is the velocity of light in the media. This approximation would then be expanded typically using a Taylor series, but other expansions have been used such as Pade, Chebyshev, Newman, and other expansions[38]. The first order expansion leads to a stable ABC that has a significant reflection coefficient for most applications. The second order approximation leads to an ABC which is unstable over long periods of time[39] and the absorption of the outgoing wave is dependent on the angle of incident and sensitive to the value of v_i. Additionally the Mur ABC has difficulty with evanescent wave absorption.

Another limitation of Mur's ABC is that it does not handle dispersive systems. A modification referred to as the dispersive boundary condition[40] (DBC) was proposed based on the following relationship.

$$\left(\frac{\partial}{\partial x}+\frac{\partial}{V_i \partial t}\right)\left(\frac{\partial}{\partial x}+\frac{\partial}{V_k \partial t}\right)=0 \tag{2-33}$$

Where v_i and v_k are different velocities of electromagnetic waves in the simulation space. Proper selection of the velocities allows for absorption of dispersive outgoing waves in structures like microstrips, however this procedure still suffers from the stability, angle of incidence, and evanescent wave absorption problems of the original Mur ABC.

To solve the evanescent wave absorption problem the following modification to Mur's ABC was introduced[41].

$$\left(\frac{\partial}{\partial x}+\frac{\partial}{V_i \partial t}+\alpha\right)=0 \tag{2-34}$$

To solve the angle of incidence problem the ABC was modified as follows[42].

$$\prod_{i=1}^{N}\left(\frac{\partial}{\partial x}+\frac{\cos(\theta i)\partial}{V_i \partial t}\right)=0 \tag{2-35}$$

Where θi is the angle of incidence. In general the above techniques can be combined to form a more robust ABC in the following manner[43].

$$\prod_{i=1}^{N}\left(\frac{\partial}{\partial x}+\frac{\partial}{V_i \partial t}+\alpha_i\right)=0 \tag{2-36}$$

The main drawback the above approach occurs in determining the values for v_i and α_i. Typically an educated guess needs to be made for the constants and then they are iteratively refined until the desired result is obtained. This can be extremely time consuming for large simulations that take several hours for each iteration.

An additional technique called super absorption[44] can be applied to the Mur ABC to improve the accuracy. Super absorption is not an ABC, but rather a technique which can be applied to some ABCs, such as Mur's ABC, to improve their accuracy. In many ABCs, only the tangential electric field needs to be determined at the edge of the simulation space. The idea behind super absorption is to solve additionally for the magnetic field component which is half a space step away from the boundary. By mixing these two results the reflection can be reduced by partial cancellation of the absorbing boundary condition errors.

2.2.2. Berengers Perfectly Matched Layers ABC

Berengers perfectly matched layers[45] (PML) absorbing boundary condition provides orders of magnitude improvement in performance over all previous ABCs for the FDTD method[46]. The PML relies on introducing a fictitious magnetic loss and on decomposing Maxwell's equations into twelve equations instead of the typical six equations for three dimensional problems. This increases the complexity and requires additional memory usage around the edges of the simulation space. However the PML does not make a plane wave assumption and can therefore be placed closer to the simulation structure resulting in significantly less memory demand in many cases.

The fictitious magnetic loss, denoted as σ^*, provides two functions; impedance matching between cells and additional attenuation of outgoing waves. The equivalent magnetic conductivity is introduced into Maxwell's equations as follows.

$$\nabla \times \vec{E} = -\sigma^* \vec{H} - \mu \frac{\partial \vec{H}}{\partial t} \tag{2-37}$$

$$\nabla x \vec{H} = \sigma \vec{E} + \varepsilon \frac{\partial \vec{E}}{\partial t} \tag{2-38}$$

Letting ψ be any component of a wave in the PML region interfacing with a vacuum region, Berenger has shown that[47]:

$$\psi = \psi_o e^{j\omega\left(t-\frac{x\cdot\cos\phi+y\cdot\sin\phi}{c\cdot G}\right)} e^{-\frac{\sigma_x\cdot\cos\phi}{\varepsilon_o\cdot c\cdot G}x} e^{-\frac{\sigma_y\cdot\sin\phi}{\varepsilon_o\cdot c\cdot G}y} \tag{2-39}$$

$$Z = \frac{\sqrt{\frac{\mu_o}{\varepsilon_o}}}{G} \tag{2-40}$$

where Z is the wave impedance, c is the speed of light, ϕ is the angle between the wave field vector and the y axis, and

$$G = \sqrt{\omega_x \cos^2\phi + \omega_y \sin^2\phi} \tag{2-41}$$

$$\omega_x = \frac{1-\frac{j\sigma_x}{\omega\varepsilon_o}}{1-\frac{j\sigma_x^*}{\omega\mu_o}} \quad , \omega_y = \frac{1-\frac{j\sigma_y}{\omega\varepsilon_o}}{1-\frac{j\sigma_y^*}{\omega\mu_o}} \tag{2-42}$$

Choosing the electric and magnetic losses so they satisfy:

$$\frac{\sigma}{\varepsilon_o} = \frac{\sigma^*}{\mu_o} \tag{2-43}$$

results in ω_x, ω_y, and G equal to one at all frequencies. This results in the wave components and the wave impedance becoming:

$$\psi = \psi_o e^{j\omega\left(t-\frac{x\cdot\cos\phi+y\cdot\sin\phi}{c}\right)} e^{-\frac{\sigma_x\cdot\cos\phi}{\varepsilon_o\cdot c}x} e^{-\frac{\sigma_y\cdot\sin\phi}{\varepsilon_o\cdot c}y} \tag{2-44}$$

$$Z = \sqrt{\frac{\mu_o}{\varepsilon_o}} \tag{2-45}$$

This shows that in the PML media the wave propagates at the speed of light, is attenuated exponentially along x and y axes, and that the wave impedance matches the impedance of the vacuum independent of frequency and angle of incidence. Ideally the attenuation could be extremely high, by choosing large σ and σ^*, thus requiring a PML layer only one cell thick. However the large attenuation causes large numerical dispersion in the FDTD technique resulting in a reflection. To compensate for the reflections due to numerical dispersion Berenger proposed that the loss should increase gradually with depth through several layers of PML media as follows:

$$\sigma(\rho) = \sigma_{max}\left(\frac{\rho}{\delta}\right)^n \tag{2-46}$$

where ρ is the depth into the PML, δ is the total PML thickness, and n is the growth factor. Deriving a theoretical reflection coefficient, R_{th}, for waves normally incident on the PML boundary the value of σ_{max} can be defined as:

$$\sigma_{max} = -\frac{(n+1)\varepsilon_o c}{2\delta}\ln(R_{th}) \tag{2-47}$$

This results in three user defined parameters for the implementation of PML boundary conditions: 1) the number of PML layers, 2) n, the growth factor, 3) Rt_h, the theoretical reflection coefficient. Numerical studies have been performed to determine optimum selections of the user defined parameters[48].

Splitting Maxwell's equations into twelve equations allows the attenuation to be provided on only the outgoing component of the wave, leaving the tangential components of the wave unaffected. The loss components are defined in the twelve equations as follows:

$$\mu_o \frac{\partial H_{xy}}{\partial t} + \sigma_y^* H_{xy} = -\frac{\partial\left(E_{zx} + E_{zy}\right)}{\partial y} \tag{2-48}$$

$$\mu_o \frac{\partial H_{xz}}{\partial t} + \sigma_z^* H_{xz} = \frac{\partial\left(E_{yx} + E_{yz}\right)}{\partial z} \tag{2-49}$$

$$\mu_o \frac{\partial H_{yz}}{\partial t} + \sigma_z^* H_{yz} = -\frac{\partial\left(E_{xy} + E_{xz}\right)}{\partial z} \tag{2-50}$$

$$\mu_o \frac{\partial H_{yx}}{\partial t} + \sigma_x^* H_{yx} = \frac{\partial\left(E_{zx} + E_{zy}\right)}{\partial x} \tag{2-51}$$

$$\mu_o \frac{\partial H_{zx}}{\partial t} + \sigma_x^* H_{zx} = -\frac{\partial\left(E_{yx} + E_{yz}\right)}{\partial x} \tag{2-52}$$

$$\mu_o \frac{\partial H_{zy}}{\partial t} + \sigma_y^* H_{zy} = \frac{\partial\left(E_{xy} + E_{xz}\right)}{\partial y} \tag{2-53}$$

$$\varepsilon_o \frac{\partial E_{xy}}{\partial t} + \sigma_y E_{xy} = \frac{\partial\left(H_{zx} + H_{zy}\right)}{\partial y} \tag{2-54}$$

$$\varepsilon_o \frac{\partial E_{xz}}{\partial t} + \sigma_z E_{xz} = -\frac{\partial\left(H_{yx} + H_{yz}\right)}{\partial z} \tag{2-55}$$

$$\varepsilon_o \frac{\partial E_{yz}}{\partial t} + \sigma_z E_{yz} = \frac{\partial\left(H_{xy} + H_{xz}\right)}{\partial z} \tag{2-56}$$

$$\varepsilon_o \frac{\partial E_{yx}}{\partial t} + \sigma_x E_{yx} = -\frac{\partial\left(H_{zx} + H_{zy}\right)}{\partial x} \tag{2-57}$$

$$\varepsilon_o \frac{\partial E_{zx}}{\partial t} + \sigma_x E_{zx} = \frac{\partial\left(H_{yx} + H_{yz}\right)}{\partial x} \tag{2-58}$$

$$\varepsilon_o \frac{\partial E_{zy}}{\partial t} + \sigma_y E_{zy} = -\frac{\partial\left(H_{xy} + H_{xz}\right)}{\partial y} \tag{2-59}$$

There are currently several papers on implementing the PML using approaches that differ from the twelve component equations, however the implementation here uses the original twelve equation approach proposed by Berenger.

3. Orthogonal Nonuniform Space Stepping

Orthogonal nonuniform space stepping allows finer details of the simulation structure to be accurately represented without using special cells while saving memory and computing time by using larger space steps where the simulation step size is not restricted by fine details in the structure. The present use of nonuniform space steps has been restricted to special cases or the acceptance of first order accuracy at the junction of the nonuniformity. This section will present the theory behind nonuniform stepping, the current state of the art, and a new approach which will allow general nonuniform space stepping while retaining the local second order accuracy of the FDTD technique.

3.1. Current Techniques For Orthogonal Nonuniform Space Stepping

There are two current approaches for nonuniform space stepping in the FDTD method. The first is a second order accurate method presented by Sheen which utilizes a special case of space stepping[49]. If the grid space is changed by a factor of three, or a third, a second order centered difference approach can be performed at the interface by keeping the

magnetic fields centered between the electric field components and placing the electric field at the interface as shown in Figure 4. The electric field at the interface is now centered between two of the magnetic field components resulting in a second order accurate approach.

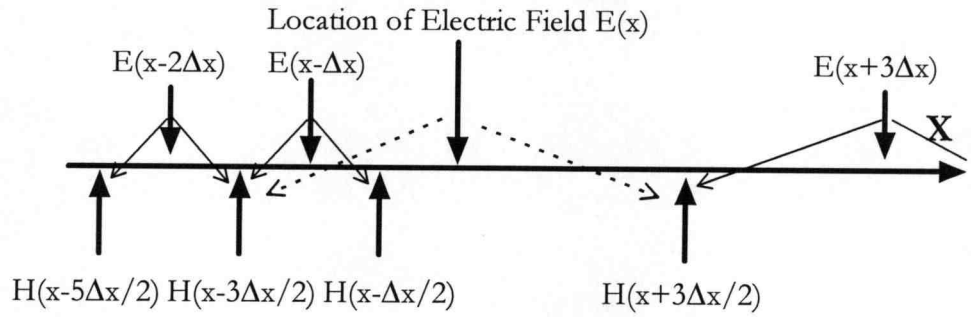

Figure 4 Factor of Three Nonuniform Grid Stepping

The second approach to nonuniform stepping relies on the concept of supraconvergence[50,51]. A supraconvergent system is one which may have local first order errors, but behaves as a second order accurate system globally. The typical FDTD implementation using supraconvergence is implemented by keeping the magnetic fields centered, thus second order accurate, and relying on first order accuracy for the noncentered electric fields. The first order accurate coefficients for differencing are generated by essentially averaging the space step magnitudes to both sides of the field and then proceeding as if the field was centered, but using the averaged step size[52].

There are several problems with using supraconvergence including difficulty in defining when a system is or isn't supraconvergent, measurements which are sensitive to local errors present in a supraconvergent system, and what is the meaning of convergence in the FDTD method. The difficulty with defining when a system is or isn't supraconvergent has been observed by Navarro[53]. Navarro observed that the accuracy of the boundary conditions strongly influences whether the system exhibits the global second order supraconvergent behavior or global first order accuracy. He observed that a waveguide simulation exhibited supraconvergence when perfect electric, perfect magnetic, or the highly accurate PML boundaries were used, Figure 6. However, the same waveguide simulation did not exhibit supraconvergence when the imperfect first order dispersive boundary conditions (DBC) were used, Figure 5. First order absorbing boundary conditions are widely used in the FDTD community due to the their ease of implementation and therefore currently pose a significant limitation to the use of supraconvergence.

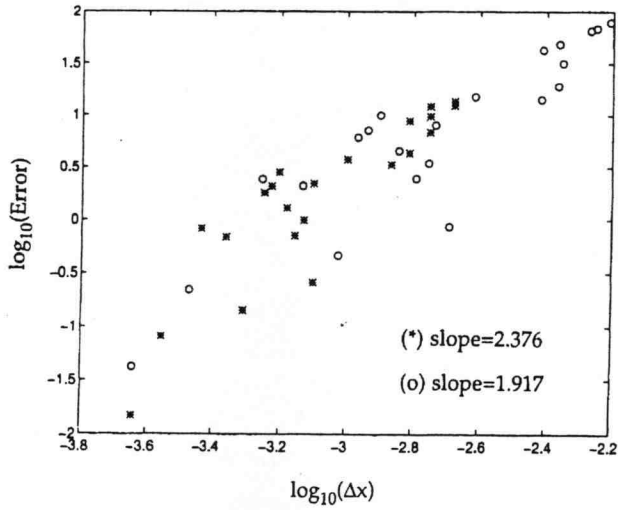

Numerical error in calculating TM_{11} mode using a gradual nonuniform mesh. Inset: slope for a least square adjust. (o) Error = maximum Error, $\Delta x = \Delta x_{\text{maximum}}$. (*) Error = average Error, $\Delta x = \Delta x_{average}$.

Figure 5 Supraconvergence Results from Navarro for First Order ABCs

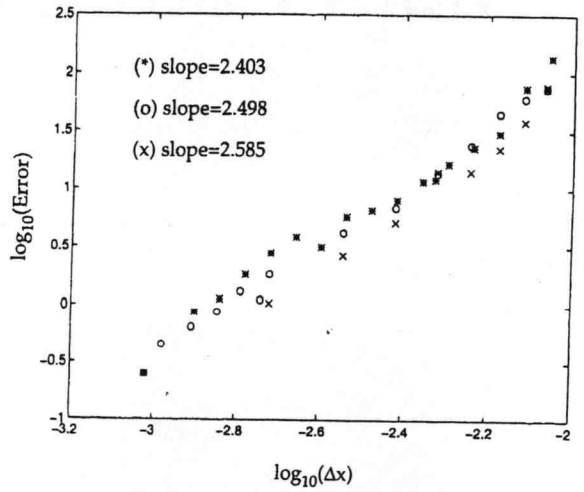

Maximum error versus maximum cell size using the perfect dispersive boundary condition: (×) Uniform mesh. (o) Nonuniform with abrupt change. (*) Gradual nonuniform.

Figure 6 Supraconvergence Results from Navarro for Near Perfect ABCs

Local errors which are present in a supraconvergent system occur because of the first order accurate differencing performed on the nonuniformly spaced electric field components. These errors manifest themselves as small reflections at the nonuniform interfaces and can potentially distort parameters extracted from the simulation. Additionally, these local errors are shown, later in the validation section, to be frequency dependent thereby making them more difficult to compensate or mitigate.

The concept of convergence is typically used to describe the behavior of an iterative numerical technique, such as a finite-difference Laplace solver which uses successive over relaxation (SOR). Convergence refers to whether a technique 'converges' or goes towards the correct answer in the limit as the number of iterations goes to infinity. The rate at which the SOR technique converges is determined by the accuracy of the numerical method employed. For a SOR technique the convergence and accuracy are interrelated. However, these SOR techniques solve for a steady state solution. In FDTD convergence only makes sense if the simulation is allowed to run for a very long period of time, tending to infinity, in which case the simulation space would contain only the steady state solution at the end of the simulation. Since the FDTD method is often employed to investigate transitory events, or events which occur over a small period of time, the concept of convergence is not as significant as the accuracy, since the investigators are not looking for steady state solutions. This ties back into the previous concern about local errors, which are essentially ignored when analyzing a system for convergence.

When analyzing a system's convergence behavior, or how a system converges, the behavior of the local errors may be observed. Navarro showed several plots of the log of the step size verses the log of the error, as shown in Figure 6. For the uniform mesh, the

plots were a straight line with a slope which corresponded to a second order accurate system. A straight line was seen for none of his nonuniform grid plots due to the effects of the local errors in the simulation results. Additionally, all of Navarro's results were for a single frequency and thus did not include any frequency dependent effects.

The two current techniques of one third stepping and supraconvergence are useful, but impose limitations on the flexibility of the FDTD technique. The next section will derive a technique for nonuniform space stepping which is less limiting than the two current approaches.

3.2. Determination of Finite Difference Coefficients

The derivative at a point in space can be approximated by a linear combination of the neighboring field values assuming that the derivative exists everywhere between the fields to be utilized. By using the method of undetermined coefficients one can derive a proper function to approximate the derivative. The following will illustrate how the method can be used to derive the standard centered difference scheme, then derive a nonuniform difference scheme, and then present an algorithm for the determination of coefficients for second order nonuniform differencing.

The method of undetermined coefficients approximates the derivative as a linear combination of neighboring field values by noting that any function which is continuous on an interval can be approximated to any desired accuracy by a polynomial of sufficiently high degree. An example of how the method of undetermined coefficients can be used to derive the standard centered difference formula is illustrated below;

First, approximate the derivative as a linear combination of the neighboring field values:

$$f'(x) \cong C_0 f(x-h) + C_1 f(x) + C_2 f(x+h) \tag{3-1}$$

Then, assume that the fields take the values of x^2, x, and 1. This results in the following three equations:

$$0 = C_0(-h)^2 + C_1(0)^2 + C_2(h)^2 \qquad \text{assuming } f(x)=x^2 \tag{3-2}$$

$$1 = C_0(-h) + C_1(0) + C_2(h) \qquad \text{assuming } f(x)=x \tag{3-3}$$

$$0 = C_0(1) + C_1(1) + C_2(1) \qquad \text{assuming } f(x)=1 \tag{3-4}$$

Converting the above equations to matrix form:

$$\begin{bmatrix} 0 \\ 1 \\ 0 \end{bmatrix} = \begin{bmatrix} h^2 & 0 & h^2 \\ -h & 0 & h \\ 1 & 1 & 1 \end{bmatrix} \cdot \begin{bmatrix} C_0 \\ C_1 \\ C_2 \end{bmatrix} \tag{3-5}$$

and solving for the constants yields:

$$C_0 = \frac{-1}{2h} \qquad C_1 = 0 \qquad C_2 = \frac{1}{2h} \tag{3-6}$$

Substituting back into the original formula gives:

$$f'(x) \cong \frac{f(x+h) - f(x-h)}{2h} \tag{3-7}$$

which is the standard centered difference formula. To show that the centered difference formula is second order accurate, a Taylor's series expansion is applied to each of the terms.

$$f(x-h) = f(x) - hf'(x) + \frac{h^2 f''(x)}{2} - \frac{h^3 f'''(\xi)}{6} \tag{3-8}$$

$$f(x+h) = f(x) + hf'(x) + \frac{h^2 f''(x)}{2} + \frac{h^3 f'''(\xi)}{6} \tag{3-9}$$

Taking the difference between the two expansions:

$$f(x+h) - f(x-h) = 2hf'(x) + \frac{h^3 f'''(\xi)}{3} \tag{3-10}$$

Solving for f'(x) results in:

$$f'(x) = \frac{f(x+h) - f(x-h)}{2h} + \frac{h^2 f'''(\xi)}{6} \qquad \text{for } x-h < \xi < x+h \tag{3-11}$$

$$f'(x) = \frac{f(x+h) - f(x-h)}{2h} + O(h^2) \tag{3-12}$$

Which confirms that the centered difference is 2nd order accurate, as it is known to be. The same procedure will be repeated for a piecewise uniform grid which is uniformly spaced then abruptly changes to a uniform grid of a different spacing as shown in Figure 7.

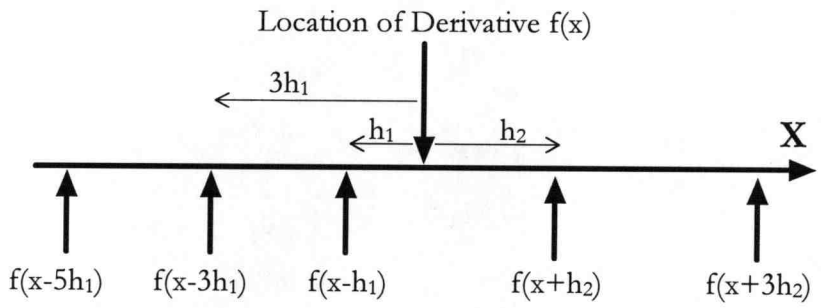

Figure 7 Location of Fields for Abrupt Space Step Example

First, approximate the derivative as a linear combination of the neighboring field values:

$$f'(x) \cong C_1 f(x-3h_1) + C_2 f(x-h_1) + C_3 f(x+h_2) \tag{3-13}$$

Assuming that the fields take the values of x^2, x, and 1.

$$0 = C_1(-3h_1)^2 + C_2(-h_1)^2 + C_3(h_2)^2 \quad \text{assuming } f(x)=x^2 \tag{3-14}$$

$$1 = C_1(-3h_1) + C_2(-h_1) + C_3(h_2) \quad \text{assuming } f(x)=x \tag{3-15}$$

$$0 = C_1(1) + C_2(1) + C_3(1) \quad \text{assuming } f(x)=1 \tag{3-16}$$

Converting to matrix form:

$$\begin{bmatrix} 0 \\ 1 \\ 0 \end{bmatrix} = \begin{bmatrix} 9h_1^2 & h_1^2 & h_2^2 \\ -3h_1 & -h_1 & h_2 \\ 1 & 1 & 1 \end{bmatrix} \cdot \begin{bmatrix} C_1 \\ C_2 \\ C_3 \end{bmatrix} \tag{3-17}$$

Solving for the constants results in:

$$C_1 = \frac{h_1^2 - h_2^2}{2h_1(3h_1 + h_2)(h_1 + h_2)} \tag{3-18}$$

$$C_2 = \frac{-9h_1^2 + h_2^2}{2h_1(3h_1 + h_2)(h_1 + h_2)} \tag{3-19}$$

$$C_3 = \frac{8h_1^2}{2h_1(3h_1 + h_2)(h_1 + h_2)} \tag{3-20}$$

To show that the formula is second order accurate a Taylor's series expansion is applied to each of the terms.

$$f(x - 3h_1) = f(x) - 3h_1 f'(x) + \frac{9h_1^2 f''(x)}{2} - \frac{27h_1^3 f'''(\xi_1)}{6} \quad \text{for } x - 3h_1 < \xi_1 < x \tag{3-21}$$

$$f(x - h_1) = f(x) - h_1 f'(x) + \frac{h_1^2 f''(x)}{2} - \frac{h_1^3 f'''(\xi_2)}{6} \quad \text{for } x - h_1 < \xi_2 < x \tag{3-22}$$

$$f(x + h_2) = f(x) + h_2 f'(x) + \frac{h_2^2 f''(x)}{2} + \frac{h_2^3 f'''(\xi_3)}{6} \quad \text{for } x < \xi_3 < x + h_2 \tag{3-23}$$

Where the three errors are not required to be identical. Substituting the expansions and coefficients into the original equation and solving for $f'(x)$ results in:

$$\left(C_1 f(x-3h_1)+C_2 f(x-h_1)+C_3 f(x+h_2)\right)=\left(C_1+C_2+C_3\right)f(x)+$$
$$\left(-3h_1C_1-h_1C_2+h_2C_3\right)f'(x)+\left(9h_1^2C_1+h_1^2C_2+h_2^2C_3\right)f''(x)+ \quad (3\text{-}24)$$
$$\frac{\left(-3h_1\right)^3C_1}{6}f'''(\xi_1)+\frac{\left(-h_1\right)^3C_2}{6}f'''(\xi_2)+\frac{\left(h_2\right)^3C_3}{6}f'''(\xi_3)$$

where:

$$\left(C_1+C_2+C_3\right)=0 \quad (3\text{-}25)$$

$$\left(-3h_1C_1-h_1C_2+h_2C_3\right)=1 \quad (3\text{-}26)$$

$$\left(9h_1^2C_1+h_1^2C_2+h_2^2C_3\right)=0 \quad (3\text{-}27)$$

Solving for f'(x) results in:

$$f'(x)=\left(C_1 f(x-3h_1)+C_2 f(x-h_1)+C_3 f(x+h_2)\right)-$$
$$\frac{\left(-3h_1\right)^3C_1}{6}f'''(\xi_1)-\frac{\left(-h_1\right)^3C_2}{6}f'''(\xi_2)-\frac{\left(h_2\right)^3C_3}{6}f'''(\xi_3) \quad (3\text{-}28)$$

As the limit of h goes to zero the three errors approach the same value resulting in:

$$f'(x)=\left(C_1 f(x-3h_1)+C_2 f(x-h_1)+C_3 f(x+h_2)\right)-$$
$$\left(\left(-3h_1\right)^3C_1+\left(-h_1\right)^3C_2+\left(h_2\right)^3C_3\right)\frac{f'''(\xi)}{6} \quad (3\text{-}29)$$

After substituting the values for C_1, C_2, and C_3 into the error term it is seen that the error is 2nd order.

$$f'(x) = \left(C_1 f(x - 3h_1) + C_2 f(x - h_1) + C_3 f(x + h_2)\right) + O(h^2) \tag{3-30}$$

Finally, the procedure will be repeated for a grid which is nonuniformly spaced as shown in Figure 8. The three closest fields are chosen for the derivative. If the grid is uniformly spaced, the results presented here will automatically reduce to the centered difference equations presented previously.

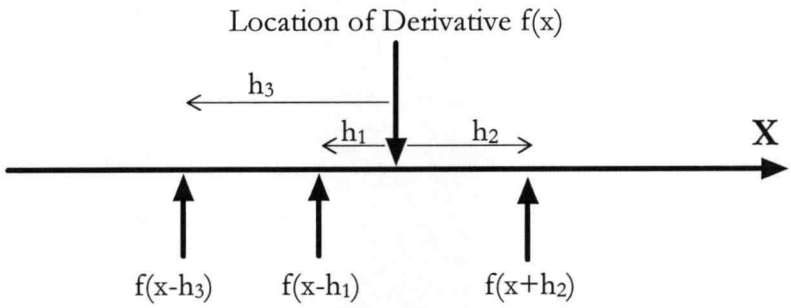

Figure 8 Location of Fields for Nonuniform
Space Step Example

First, approximate the derivative as a linear combination of the neighboring field values:

$$f'(x) \cong C_1 f(x - h_3) + C_2 f(x - h_1) + C_3 f(x + h_2) \tag{3-31}$$

Assuming that the fields take the values of x^2, x, and 1.

$$0 = C_1(-h_3)^2 + C_2(-h_1)^2 + C_3(h_2)^2 \qquad \text{assuming } f(x)=x^2 \tag{3-32}$$

$$1 = C_1(h_1) + C_2(-h_1) + C_3(h_2) \qquad \text{assuming } f(x)=x \tag{3-33}$$

$$0 = C_1(1) + C_2(1) + C_3(1) \qquad \text{assuming } f(x)=1 \tag{3-34}$$

Rewriting the above equation in a matrix form:

$$\begin{bmatrix} 0 \\ 1 \\ 0 \end{bmatrix} = \begin{bmatrix} h_3^2 & h_1^2 & h_2^2 \\ -h_3 & -h_1 & h_2 \\ 1 & 1 & 1 \end{bmatrix} \cdot \begin{bmatrix} C_1 \\ C_2 \\ C_3 \end{bmatrix} \tag{3-35}$$

and solving for the constants results in:

$$C_1 = \frac{h_1^2 - h_2^2}{(h_3 - h_1)(h_2 + h_1)(h_3 + h_2)} \tag{3-36}$$

$$C_2 = \frac{h_2^2 - h_3^2}{(h_3 - h_1)(h_2 + h_1)(h_3 + h_2)} \tag{3-37}$$

$$C_3 = \frac{h_3^2 - h_1^2}{(h_3 - h_1)(h_2 + h_1)(h_3 + h_2)} \tag{3-38}$$

To show that the solution is second order accurate, a Taylor's series expansion is applied to each of the terms.

$$f(x-h_3)=f(x)-h_3f'(x)+\frac{h_3^2f''(x)}{2}-\frac{h_3^3f'''(\xi_1)}{6} \quad \text{for } x-h_3<\xi_1<x \tag{3-39}$$

$$f(x-h_1)=f(x)-h_1f'(x)+\frac{h_1^2f''(x)}{2}-\frac{h_1^3f'''(\xi_2)}{6} \quad \text{for } x-h_1<\xi_2<x \tag{3-40}$$

$$f(x+h_2)=f(x)+h_2f'(x)+\frac{h_2^2f''(x)}{2}+\frac{h_2^3f'''(\xi_3)}{6} \quad \text{for } x<\xi_3<x+h_2 \tag{3-41}$$

Where the three errors are not required to be identical. Substituting the expansions and coefficients into the original equation and solving for f'(x) gives:

$$\begin{aligned}&\left(C_1f(x-h_3)+C_2f(x-h_1)+C_3f(x+h_2)\right)=\left(C_1+C_2+C_3\right)f(x)+\\&\left(-h_3C_1-h_1C_2+h_2C_3\right)f'(x)+\left(h_3^2C_1+h_1^2C_2+h_2^2C_3\right)f''(x)+\\&\frac{\left(-h_3\right)^3C_1}{6}f'''(\xi_1)+\frac{\left(-h_1\right)^3C_2}{6}f'''(\xi_2)+\frac{\left(h_2\right)^3C_3}{6}f'''(\xi_3)\end{aligned} \tag{3-42}$$

where:

$$\left(C_1+C_2+C_3\right)=0 \tag{3-43}$$

$$\left(-h_3C_1-h_1C_2+h_2C_3\right)=1 \tag{3-44}$$

$$\left(h_3^2C_1+h_1^2C_2+h_2^2C_3\right)=0 \tag{3-45}$$

Solving for f'(x) results in:

$$f'(x) = \left(C_1 f(x-h_3) + C_2 f(x-h_1) + C_3 f(x+h_2)\right) - \frac{(-h_3)^3 C_1}{6} f'''(\xi_1) - \frac{(-h_1)^3 C_2}{6} f'''(\xi_2) - \frac{(h_2)^3 C_3}{6} f'''(\xi_3) \tag{3-46}$$

As the limit of h goes to zero, the three errors approach the same value resulting in:

$$f'(x) = \left(C_1 f(x-h_3) + C_2 f(x-h_1) + C_3 f(x+h_2)\right) - \left((-h_3)^3 C_1 + (-h_1)^3 C_2 + (h_2)^3 C_3\right)\frac{f'''(\xi)}{6} \tag{3-47}$$

After substituting the values for C_1, C_2, and C_3 into the error term it is seen that the error is 2nd order.

$$f'(x) = \left(C_1 f(x-h_3) + C_2 f(x-h_1) + C_3 f(x+h_2)\right) + O(h^2) \tag{3-48}$$

The method of undetermined coefficients was used to derive a second order accurate finite difference formulation for nonuniform grid spacing. The formulation uses the closest three fields to determine the derivative at the desired location. If the grid is uniform, the formulation will automatically reduce to the centered difference formulation. A more general formulation could be created using four field components, two to the left and two to the right, this would automatically select the three closest components and reduce to the formulation presented above. However, in the case of a uniform grid the four component approach would automatically reduce to a fourth order accurate centered differencing formulation with much tighter restrictions on stability.

3.3. Implementation in FDTD Code of Arbitrarily Spaced Grids

In the preceding section a derivation for a 2^{nd} order accurate finite difference equation was presented for the general case of an arbitrarily spaced grid and shown to be 2^{nd} order. A recursive algorithm for the generation of finite difference coefficients has been developed by Bengt Fornberg[54] and has been implemented in the FDTD code of this work for the coefficient generation. The algorithm is general in that it allows for arbitrarily spaced grids, any specified derivative (including the 0^{th} derivative), to any specified accuracy. It is implemented in the FDTD code to provide second order accurate results for any arbitrarily specified grid spacing and can be modified to provide higher order accuracy results. The implementation of higher than the second order accurate finite difference formulation is not typically necessary and requires a different stability criteria for the selection of the time step in FDTD routines.

The following is the pseudo code version of the algorithm for the generation of finite difference formulas on arbitrarily spaced grids taken directly from Fornberg's paper:

$\text{EnterM, N, } x_o, \alpha_0, \alpha_1, \alpha_2, \ldots, \alpha_N$

$\delta^0_{0,0} := 1$

$c1 := 1$

$\text{for. n} := 1. \text{ to. N. do}$

$\ldots c2 := 1$

$\ldots \text{for. } \upsilon := 0. \text{ to. n} - 1. \text{ do}$

$\ldots\ldots c3 := \alpha_n - \alpha_\upsilon$

$\ldots\ldots c2 := c2 \cdot c3$

$\ldots\ldots \text{if. n} \le \text{M. then. } \delta^n_{n-1,\upsilon} := 0$

$\ldots\ldots \text{for. m} := 0. \text{ to. min(n, M). do}$

$\ldots\ldots\ldots \delta^m_{n,\upsilon} := \left(\left(\alpha_n - x_o\right)\delta^m_{n-1,\upsilon} - m\delta^{m-1}_{n-1,n-1}\right) / c3$

$\ldots\ldots \text{next. m}$

$\ldots \text{next. } \upsilon$

$\ldots \text{for. m} := 0. \text{ to. min(n, M). do}$

$\ldots\ldots \delta^m_{n,n} := \frac{c1}{c2}\left(m\delta^{m-1}_{n-1,n-1} - \left(\alpha_{n-1} - x_o\right)\delta^m_{n-1,n-1}\right)$

$\ldots \text{next. m}$

$\ldots c1 = c2$

next. n

Where M is the highest order derivative desired, N+1 is the number of grid points, alpha contains the location of the grid points, and x_o is the location where the derivative is desired. If the grid is uniformly spaced, the algorithm above will return the standard 2nd order centered difference solution for the first derivative.

The implementation of the FDTD code incorporating arbitrarily spaced grids selects the location of the magnetic fields to always be centered between the electric fields. This allows the centered difference formulation to be valid for the calculation of the magnetic field components even when the grid is arbitrarily spaced. However, the electric field

components require that the coefficients for the finite differencing be generated as described above when the grid in not uniformly spaced.

The following table shows some first order coefficients for Δz=1e-5 as calculated by Fornberg's algorithm. These results are identical to the first order coefficients generated using the technique presented by Navarro[55].

Step Change Δz=1e-5	**C2**	**C1**
1.1Δz	9.5238e4	-9.5238e4
1.5Δz	8.0000e4	-8.0000e4
2.0Δz	6.66667e4	-6.66667e4
3.0Δz	5.0000e4	-5.0000e4
4.0Δz	4.0000e4	-4.0000e4

Some second order results are presented in the following table and show complete agreement between Fornberg's algorithm and the values calculated using the method of undetermined coefficients presented earlier.

Step Change Δz=1e-5	**C3**	**C2**	**C1**
1.1Δz	9.2915e4	-9.0476e4	-2.439e3
1.5Δz	7.1111e4	-6.00e4	-1.1111e4
2.0Δz	5.3333e4	-3.3333e4	2.0e4
3.0Δz	3.3333e4	0.0	-3.3333e4
4.0Δz	2.2857e4	2.0000e4	-4.2857e4

3.4. Stability of Nonuniform FDTD

The Courant stability criteria limits the size of the time step to a function of the space step. If the time step is allowed to be larger than the limit specified by the stability criteria, the high frequency components will increase with time leading to false results. Typically this increase is dramatic and quite noticeable. If the time step is chosen to be significantly smaller than the upper limit of the stability criteria, then increased numerical dispersion will occur and must be considered if the simulation results are sensitive to phase errors. It is also important that the initial assumption of FDTD is not forgotten, simulation wavelengths are long compared to the grid spacing, or instabilities will occur even if the Courant stability criteria is met. To investigate the stability of the nonuniform FDTD technique the stability for one and three dimensional uniform FDTD will be derived first followed by the stability of nonuniform FDTD technique.

To derive the stability of a numerical method a Fourier analysis is typically performed. The Fourier analysis allows the method to be put into a matrix form as follows:

$$\hat{u}^{n+1} = G\hat{u}^{n} \tag{3-49}$$

The stability criteria is then found by setting the determinant of the matrix to zero and solving for the time increment. The Fourier analysis consists of a direct substitution of the

Fourier modes into the initial set of equations. The generic form of the Fourier modes is expressed as follows:

$$\hat{u}_j^n = \hat{u}e^{i(\omega n\Delta t - kj\Delta x)} \tag{3-50}$$

The analysis of the of the one dimensional uniform FDTD technique starts with the original equations:

$$E_j^{n+1/2} = E_j^{n-1/2} - \frac{\Delta t}{\varepsilon \Delta x}\left(H_{j+1/2}^n - H_{j-1/2}^n\right) \tag{3-51}$$

$$H_{j+1/2}^n = H_{j+1/2}^{n-1} - \frac{\Delta t}{\mu \Delta x}\left(E_{j+1}^{n-1/2} - E_j^{n-1/2}\right) \tag{3-52}$$

The Fourier modes for each of the components are:

$$E_j^{n+1/2} = Ee^{i(\omega(n+1/2)\Delta t - kj\Delta x)} \qquad E_j^{n-1/2} = Ee^{i(\omega(n-1/2)\Delta t - kj\Delta x)} \tag{3-53}$$

$$E_{j+1}^{n-1/2} = Ee^{i(\omega(n-1/2)\Delta t - k(j+1)\Delta x)} \tag{3-54}$$

$$H_{j+1/2}^n = He^{i(\omega n\Delta t - k(j+1/2)\Delta x)} \tag{3-55}$$

$$H_{j+1/2}^{n-1} = He^{i(\omega(n-1)\Delta t - k(j+1/2)\Delta x)} \tag{3-56}$$

$$H_{j-1/2}^{n-1} = He^{i(\omega(n-1)\Delta t - k(j-1/2)\Delta x)} \tag{3-57}$$

Substituting in the Fourier modes:

$$Ee^{i(\omega(n+1/2)\Delta t-kj\Delta x)} = Ee^{i(\omega(n-1/2)\Delta t-kj\Delta x)} - \frac{\Delta t}{\varepsilon\Delta x}\left(He^{i(\omega n\Delta t-k(j+1/2)\Delta x)} - He^{i(\omega n\Delta t-k(j-1/2)\Delta x)}\right) \tag{3-58}$$

$$He^{i(\omega n\Delta t-k(j+1/2)\Delta x)} = He^{i(\omega(n-1)\Delta t-k(j+1/2)\Delta x)} - \frac{\Delta t}{\mu\Delta x}\left(Ee^{i(\omega(n-1/2)\Delta t-k(j+1)\Delta x)} - Ee^{i(\omega(n-1/2)\Delta t-kj\Delta x)}\right) \tag{3-59}$$

Eliminating common factors results in:

$$Ee^{i(1/2\omega\Delta t)} = Ee^{i(-1/2\omega\Delta t)} - \frac{\Delta t}{\varepsilon\Delta x}\left(He^{i(1/2k\Delta x)} - He^{i(-1/2k\Delta x)}\right) \tag{3-60}$$

$$He^{i(1/2\omega\Delta t)} = He^{i(-1/2\omega\Delta t)} - \frac{\Delta t}{\mu\Delta x}\left(Ee^{i(1/2k\Delta x)} - Ee^{i(-1/2k\Delta x)}\right) \tag{3-61}$$

Applying Euler's equations and setting equal to zero:

$$0 = -E\sin(1/2\omega\Delta t) - \frac{\Delta t}{\varepsilon\Delta x}H(\sin(1/2k\Delta x)) \tag{3-62}$$

$$0 = -H\sin(1/2\omega\Delta t) - \frac{\Delta t}{\mu\Delta x}E(\sin(1/2k\Delta x)) \tag{3-63}$$

Putting into matrix form results in:

$$0 = \begin{bmatrix} \sin(1/2\omega\Delta t) & \frac{\Delta t}{\varepsilon\Delta x}(\sin(1/2k\Delta x)) \\ \frac{\Delta t}{\mu\Delta x}(\sin(1/2k\Delta x)) & \sin(1/2\omega\Delta t) \end{bmatrix}\begin{bmatrix} E \\ H \end{bmatrix} \tag{3-64}$$

The determinate of the matrix is:

$$\det(M) = \sin^2(1/2\omega\Delta t) - \left(\frac{c\Delta t}{\Delta x}\right)^2 \sin^2(1/2k\Delta x) \tag{3-65}$$

Setting to zero and solving for the time increment:

$$\Delta t \le \frac{\left|\sin(1/2\omega\Delta t)\right|}{\left|\sin(1/2k\Delta x)\right|}\left(\frac{\Delta x}{c}\right) \tag{3-66}$$

The sine terms can vary between zero and one due to the absolute value requirements. The most restrictive condition will occur when the spacial sine function is at the value of one. However this leaves the temperal sine function. Assuming:

$$\Delta t = A\left(\frac{\Delta x}{c}\right) \tag{3-67}$$

and knowing:

$$\omega^2 - k^2c^2 = 0 \tag{3-68}$$

the constant A can be solved for.

$$A = \frac{\left|\sin(1/2\omega\Delta t)\right|}{\left|\sin(1/2k\Delta x)\right|} = \frac{\left|\sin(1/2kcA\Delta x/c)\right|}{\left|\sin(1/2k\Delta x)\right|} = \frac{\left|\sin(1/2kA\Delta x)\right|}{\left|\sin(1/2k\Delta x)\right|} \tag{3-69}$$

This is only valid if A equals one or zero. Zero is a trivial case and one results in the Courant stability condition of:

$$\Delta t \leq \frac{\Delta x}{c} \tag{3-70}$$

For the three dimensional uniform FDTD the same technique is summarized below.

The Fourier modes are:

$$E_x^{n+1/2}(I, J, K) = E_x e^{i\left(\omega\left(n+1/2\right)\Delta t - \left(a\left(I+1/2\right)\Delta x + bJ\Delta y + cK\Delta z\right)\right)} \tag{3-71}$$

$$E_y^{n+1/2}(I, J, K) = Eye^{i\left(\omega\left(n+1/2\right)\Delta t - \left(aI\Delta x + b\left(J+1/2\right)\Delta y + cK\Delta z\right)\right)} \tag{3-72}$$

$$E_z^{n+1/2}(I, J, K) = E_z e^{i\left(\omega\left(n+1/2\right)\Delta t - \left(aI\Delta x + bJ\Delta y + c\left(K+1/2\right)\Delta z\right)\right)} \tag{3-73}$$

$$H_x^{n}(I, J, K) = H_x e^{i\left(\omega n\Delta t - \left(aI\Delta x + b\left(J+1/2\right)\Delta y + c\left(K+1/2\right)\Delta z\right)\right)} \tag{3-74}$$

$$H_y^{n}(I, J, K) = H_y e^{i\left(\omega n\Delta t - \left(a\left(I+1/2\right)\Delta x + bJ\Delta y + c\left(K+1/2\right)\Delta z\right)\right)} \tag{3-75}$$

$$H_z^{n}(I, J, K) = H_z e^{i\left(\omega n\Delta t - \left(a\left(I+1/2\right)\Delta x + b\left(J+1/2\right)\Delta y + cK\Delta z\right)\right)} \tag{3-76}$$

Substituting the Fourier modes into the FDTD equations, applying Euler's equation and putting into matrix form results in:

$$\begin{bmatrix} W & 0 & 0 & 0 & -\frac{C}{\varepsilon} & \frac{B}{\varepsilon} \\ 0 & W & 0 & \frac{C}{\varepsilon} & 0 & -\frac{A}{\varepsilon} \\ 0 & 0 & W & -\frac{B}{\varepsilon} & \frac{A}{\varepsilon} & 0 \\ 0 & \frac{C}{\mu} & -\frac{B}{\mu} & W & 0 & 0 \\ -\frac{C}{\mu} & 0 & \frac{A}{\mu} & 0 & W & 0 \\ \frac{B}{\mu} & -\frac{A}{\mu} & 0 & 0 & 0 & W \end{bmatrix} \begin{bmatrix} E_x \\ E_y \\ E_z \\ H_x \\ H_y \\ H_z \end{bmatrix} = 0 \tag{3-77}$$

where:

$$W = \frac{2\sin(\omega\Delta t/2)}{\Delta t} \tag{3-78}$$

$$A = \frac{2\sin(a\Delta x/2)}{\Delta x} \tag{3-79}$$

$$B = \frac{2\sin(b\Delta y/2)}{\Delta y} \tag{3-80}$$

$$C = \frac{2\sin(c\Delta z/2)}{\Delta z} \tag{3-81}$$

Setting the determinate to zero gives:

$$W^2 - \frac{\left(A^2 + B^2 + C^2\right)}{\varepsilon\mu} = 0 \tag{3-82}$$

or

$$0 = \frac{1}{\varepsilon\mu}\left(\left(\frac{\sin(1/2a\Delta x)}{\Delta x}\right)^2 + \left(\frac{\sin(1/2b\Delta y)}{\Delta y}\right)^2 + \left(\frac{\sin(1/2c\Delta z)}{\Delta z}\right)^2\right) - \left(\frac{\sin(1/2\omega\Delta t)}{\Delta t}\right)^2 \tag{3-83}$$

Solving for the time step:

$$\Delta t = \frac{\left|\sin(1/2\omega\Delta t)\right|}{c\sqrt{\left(\frac{\sin(1/2a\Delta x)}{\Delta x}\right)^2 + \left(\frac{\sin(1/2b\Delta y)}{\Delta y}\right)^2 + \left(\frac{\sin(1/2c\Delta z)}{\Delta z}\right)^2}} \tag{3-84}$$

Selecting:

$$a = \frac{\pi}{\Delta x} \quad b = \frac{\pi}{\Delta y} \quad c = \frac{\pi}{\Delta z} \tag{3-85}$$

This results in the three dimensional stability condition of:

$$\Delta t = \frac{1}{c\sqrt{\left(\frac{1}{\Delta x}\right)^2 + \left(\frac{1}{\Delta y}\right)^2 + \left(\frac{1}{\Delta z}\right)^2}} \tag{3-86}$$

The analysis of the one dimensional nonuniform FDTD technique starts with the original equations based on the field locations shown in Figure 9:

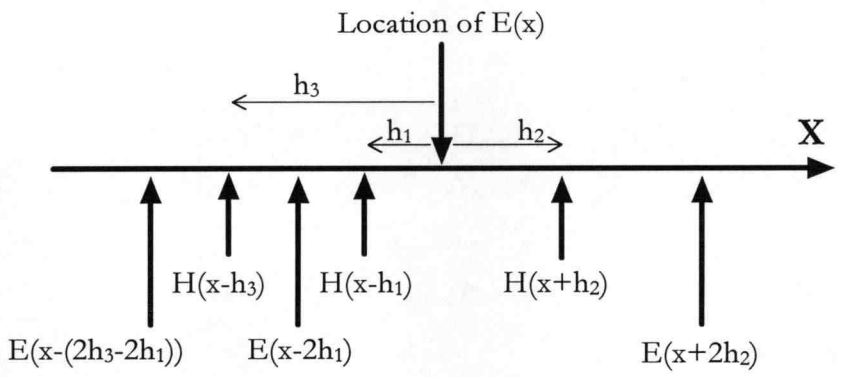

Figure 9 Field Locations for Nonuniform case

$$E_x^{n+1/2} = E_x^{n-1/2} - \frac{\Delta t}{\varepsilon}\left(C_1 H_{x-h3}^n + C_2 H_{x-h1}^n + C_3 H_{x+h2}^n\right) \tag{3-87}$$

$$H_{x+h2}^n = H_{x+h2}^{n-1} - \frac{\Delta t}{\mu 2h2}\left(E_{x+h2}^{n-1/2} - E_x^{n-1/2}\right) \tag{3-88}$$

The Fourier modes for each of the components are:

$$E_x^{n+1/2} = Ee^{i(\omega(n+1/2)\Delta t - kx)} \tag{3-89}$$

$$E_x^{n-1/2} = Ee^{i(\omega(n-1/2)\Delta t - kx)} \tag{3-90}$$

$$E_{x+2h2}^{n-1/2} = Ee^{i(\omega(n-1/2)\Delta t - k(x+2h2))} \tag{3-91}$$

$$H_{x+h2}^n = He^{i(\omega n\Delta t - k(x+h2))} \tag{3-92}$$

$$H_{x-h1}^{n} = He^{i(\omega n\Delta t - k(x-h1))} \tag{3-93}$$

$$H_{x-h3}^{n} = He^{i(\omega n\Delta t - k(x-h3))} \tag{3-94}$$

$$H_{x-h1}^{n-1} = He^{i(\omega (n-1)\Delta t - k(x-h1))} \tag{3-95}$$

Substituting in the Fourier modes:

$$Ee^{i(\omega(n+1/2)\Delta t - kx)} = Ee^{i(\omega(n-1/2)\Delta t - kx)} - \frac{\Delta t}{\varepsilon}\begin{pmatrix} C_1 He^{i(\omega n\Delta t - k(x-h3))} \\ + C_2 He^{i(\omega n\Delta t - k(x-h1))} \\ + C_3 He^{i(\omega n\Delta t - k(x+h2))} \end{pmatrix} \tag{3-96}$$

$$He^{i(\omega n\Delta t - k(x+h2))} = He^{i(\omega(n-1)\Delta t - k(x+h2))} - \frac{\Delta t}{\mu 2h2}\begin{pmatrix} Ee^{i(\omega(n-1/2)\Delta t - k(x+2h2))} \\ - Ee^{i(\omega(n-1/2)\Delta t - k(x))} \end{pmatrix} \tag{3-97}$$

Eliminating common factors results in:

$$Ee^{i(1/2\omega\Delta t)} = Ee^{i(-1/2\omega\Delta t)} - \frac{\Delta t}{\varepsilon}\begin{pmatrix} C_1 He^{i(kh3)} + C_2 He^{i(kh1)} \\ + C_3 He^{i(-kh2)} \end{pmatrix} \tag{3-98}$$

$$He^{i(1/2\omega\Delta t)} = He^{i(-1/2\omega\Delta t)} - \frac{\Delta t}{\mu 2h2}\left(Ee^{i(kh2)} - Ee^{i(-kh2)}\right) \tag{3-99}$$

Applying Euler's equations and setting equal to zero:

$$0 = -2Ei\sin(1/2\omega\Delta t) + \frac{\Delta t}{\varepsilon} H\left(C_1 e^{ikh3} + C_2 e^{ikh1} + C_1 e^{-ikh2}\right) \tag{3-100}$$

$$0 = -H\sin(1/2\omega\Delta t) - \frac{\Delta t}{\mu 2h2} E(\sin(kh2)) \tag{3-101}$$

Putting into matrix form results in:

$$0 = \begin{bmatrix} 2i\sin(1/2\omega\Delta t) & -\frac{\Delta t}{\varepsilon}\left(C_1 e^{ikh3} + C_2 e^{ikh1} + C_3 e^{-ikh2}\right) \\ \frac{\Delta t}{\mu 2h2}(\sin(kh2)) & \sin(1/2\omega\Delta t) \end{bmatrix} \begin{bmatrix} E \\ H \end{bmatrix} \tag{3-102}$$

The determinant of the matrix is:

$$\det(M) = 2i\sin^2(1/2\omega\Delta t) + \frac{\Delta t^2}{\mu\varepsilon 2h2}(\sin(kh2))\left(C_1 e^{ikh3} + C_2 e^{ikh1} + C_3 e^{-ikh2}\right) \tag{3-103}$$

Setting to zero and solving for the time increment:

$$\Delta t^2 = \frac{-4i\mu\varepsilon h2\sin^2(1/2\omega\Delta t)}{(\sin(kh2))\left(C_1 e^{ikh3} + C_2 e^{ikh1} + C_3 e^{-ikh2}\right)} \tag{3-104}$$

or,

$$\Delta t = \frac{|\sin(1/2\omega\Delta t)|}{c} \sqrt{\frac{-4ih2}{(\sin(kh2))\left(C_1 e^{ikh3} + C_2 e^{ikh1} + C_3 e^{-ikh2}\right)}} \tag{3-105}$$

Selecting:

$$k = \frac{\pi}{2h} \qquad \omega = \frac{\pi}{\Delta t} \quad , \tag{3-106}$$

results in the in the sine terms going to one and the exponential terms go to the following:

$$e^{ikh} = \cos(kh) + i\sin(kh) = \cos\left(\frac{\pi}{2}\right) + i\sin\left(\frac{\pi}{2}\right) = i \tag{3-107}$$

This reduces the stability criteria to:

$$\Delta t \le \frac{1}{c}\sqrt{\frac{4h_2}{\left(C_3 - C_2 - C_1\right)}} \tag{3-108}$$

Substituting the values of constants as determined previously using the method of undetermined coefficients gives:

$$\Delta t \le \frac{1}{c\sqrt{\dfrac{h_3 + h_1}{2h_2\left(h_2 + h_1\right)\left(h_3 + h_2\right)}}} \tag{3-109}$$

Converting this the space step sizes of the grid in the X dimension as defined in Figure 10 gives:

$$\Delta t \le \frac{1}{c\sqrt{\dfrac{2\Delta x_3 + 6\Delta x_1}{\Delta x_2\left(\Delta x_1 + \Delta x_2\right)\left(\Delta x_3 + 2\Delta x_1 + \Delta x_2\right)}}} \tag{3-110}$$

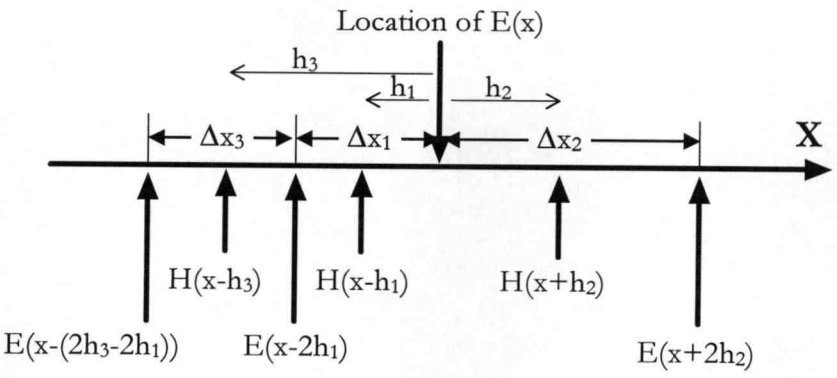

Figure 10 Relationship Between h and Δx

To check the result one can assume a uniform grid where $\Delta x_1 = \Delta x_2 = \Delta x_3 = \Delta x$:

$$\Delta t \le \frac{1}{c\sqrt{\frac{8\Delta x}{\Delta x(2\Delta x)(4\Delta x)}}} = \frac{1}{c\sqrt{\frac{1}{\Delta x^2}}} = \frac{\Delta x}{c} \tag{3-111}$$

Which is the one dimensional Courant stability criteria as expected. Often simulations will consist of a region of small, uniformly spaced griding which will limit the simulation time step to the Courant stability condition for that region. Therefore it would be convenient to know the relationship between the nonuniform stability criteria and the courant stability criteria for the smallest space step, Δx_s. Δt_s will be defined as the time step required by the Courant stability condition based on the smallest space step in the simulation:

$$\Delta t_s = \frac{1}{c\sqrt{\frac{1}{\Delta x_s^2}}} \tag{3-112}$$

Since the three closest fields are chosen for the nonuniform diffencing, either Δx_1 or Δx_3 will be the smallest space step, Δx_s. Therefore the analysis will be performed investigating the relationship between the nonuniform and Courant stability conditions for the cases of $\Delta x_1=\Delta x_s$ and $\Delta x_3=\Delta x_s$.

Δt_1 will be defined as the time step required by the nonuniform stability assuming that $\Delta x_1=\Delta x_s$.

$$\Delta t_1 = \frac{1}{c\sqrt{\frac{2\Delta x_3 + 6\Delta x_s}{2\Delta x_2\left(\Delta x_s + \Delta x_2\right)\left(\frac{\Delta x_3}{2} + \Delta x_s + \frac{\Delta x_2}{2}\right)}}} \tag{3-113}$$

The region of interest is defined by:

$$\Delta t_s \le \Delta t_1 \quad \text{or} \quad \frac{\Delta t_s}{\Delta t_1} \le 1 \tag{3-114}$$

$$1 \ge \frac{\Delta t_s}{\Delta t_1} = \frac{\sqrt{\frac{2\Delta x_3 + 6\Delta x_s}{2\Delta x_2\left(\Delta x_s + \Delta x_2\right)\left(\frac{\Delta x_3}{2} + \Delta x_s + \frac{\Delta x_2}{2}\right)}}}{\sqrt{\frac{1}{\Delta x_s^2}}} \tag{3-115}$$

$$1 \ge \frac{\Delta x_s^2\left(2\Delta x_3 + 6\Delta x_s\right)}{2\Delta x_2\left(\Delta x_s + \Delta x_2\right)\left(\frac{\Delta x_3}{2} + \Delta x_s + \frac{\Delta x_2}{2}\right)} \tag{3-116}$$

$$\left(2\Delta x_2\Delta x_s + 2\Delta x_2^2\right)\left(\frac{\Delta x_3}{2} + \Delta x_s + \frac{\Delta x_2}{2}\right) \ge \Delta x_s^2\left(\Delta x_3 + 3\Delta x_s\right) + \Delta x_s^2\left(\Delta x_3 + 3\Delta x_s\right) \tag{3-117}$$

$$\Delta x_2^2\left(\Delta x_3 + 3\Delta x_s\right) + \Delta x_2 \Delta x_s \Delta x_3 + \Delta x_2\left(2\Delta x_s^2 + \Delta x_2^2\right) \geq \Delta x_s^2\left(\Delta x_3 + 3\Delta x_s\right) + \Delta x_s \Delta x_s \Delta x_3 + 3\Delta x_s^3 \tag{3-118}$$

Breaking into three pieces results in:

$$\Delta x_2^2\left(\Delta x_3 + 3\Delta x_s\right) \geq \Delta x_s^2\left(\Delta x_3 + 3\Delta x_s\right) \quad \text{Always true} \tag{3-119}$$

$$\Delta x_2 \Delta x_s \Delta x_3 \geq \Delta x_s \Delta x_s \Delta x_3 \qquad \text{Always true} \tag{3-120}$$

$$\Delta x_2\left(2\Delta x_s^2 + \Delta x_2^2\right) \geq 3\Delta x_s^3 \qquad \text{Always true} \tag{3-121}$$

This shows that the Courant stability criteria based on the smallest space step is more stringent than the nonuniform stability criteria when $\Delta x_1 = \Delta x_s$. It is also possible that $\Delta x_3 = \Delta x_s$ and therefore this stability criteria relationship needs to be investigated. Δt_3 will be defined as the time step required by the nonuniform stability criteria assuming that $\Delta x_3 = \Delta x_s$.

$$\Delta t_3 = \frac{1}{c\sqrt{\dfrac{2\Delta x_s + 6\Delta x_1}{2\Delta x_2\left(\Delta x_1 + \Delta x_2\right)\left(\dfrac{\Delta x_s}{2} + \Delta x_1 + \dfrac{\Delta x_2}{2}\right)}}} \tag{3-122}$$

The region of interest is defined by:

$$\Delta t_s \leq \Delta t_3 \quad \text{or} \quad \frac{\Delta t_s}{\Delta t_3} \leq 1 \tag{3-123}$$

$$1 \geq \frac{\Delta t_s}{\Delta t_2} = \frac{\sqrt{\dfrac{2\Delta x_s + 6\Delta x_1}{2\Delta x_2(\Delta x_1 + \Delta x_2)\left(\dfrac{\Delta x_s}{2} + \Delta x_1 + \dfrac{\Delta x_2}{2}\right)}}}{\sqrt{\dfrac{1}{\Delta x_s^2}}} \tag{3-124}$$

$$1 \geq \frac{\Delta x_s^2(2\Delta x_s + 6\Delta x_1)}{2\Delta x_2(\Delta x_1 + \Delta x_2)\left(\dfrac{\Delta x_s}{2} + \Delta x_1 + \dfrac{\Delta x_2}{2}\right)} \tag{3-125}$$

$$\Delta x_2(\Delta x_1 + \Delta x_2)(\Delta x_s + 2\Delta x_1 + \Delta x_2) \geq \Delta x_s^2(2\Delta x_s + 6\Delta x_1) \tag{3-126}$$

$$\Delta x_2\left(\Delta x_1 \Delta x_s + 2\Delta x_1^2 + \Delta x_2 \Delta x_s + 3\Delta x_1 \Delta x_2 + \Delta x_2^2\right) \geq \Delta x_s\left(2\Delta x_s^2 + 6\Delta x_1 \Delta x_s\right) \tag{3-127}$$

$$\begin{aligned} &\Delta x_2(\Delta x_1 \Delta x_s + \Delta x_2 \Delta x_2) + \Delta x_2(2\Delta x_1 \Delta x_1 + \Delta x_2 \Delta x_s + 3\Delta x_1 \Delta x_2) \\ &\geq \Delta x_s(\Delta x_s \Delta x_s + \Delta x_s \Delta x_s) + \Delta x_s(2\Delta x_1 \Delta x_s + \Delta x_1 \Delta x_s + 3\Delta x_1 \Delta x_s) \end{aligned} \tag{3-128}$$

Comparing term by term it can be seen that the right hand side is always less than the left hand side when Δx_s is the smallest grid spacing as defined previously.

Therefore, the stability analysis above shows that the nonuniform stability criteria will always be less stringent than the Courant stability condition based on the smallest grid spacing in the simulation. Consequently, the nonuniform griding will not require smaller time stepping than either the standard uniform technique or the supraconvergent first order nonuniform technique.

The three dimensional nonuniform stability criteria follows the same procedure as the derivation for the uniform three dimensional stability criteria. The nonuniform stability matrix becomes:

$$\begin{bmatrix} W & 0 & 0 & 0 & -\frac{C}{\varepsilon} & \frac{B}{\varepsilon} \\ 0 & W & 0 & \frac{C}{\varepsilon} & 0 & -\frac{A}{\varepsilon} \\ 0 & 0 & W & -\frac{B}{\varepsilon} & \frac{A}{\varepsilon} & 0 \\ 0 & \frac{C}{\mu} & -\frac{B}{\mu} & W & 0 & 0 \\ -\frac{C}{\mu} & 0 & \frac{A}{\mu} & 0 & W & 0 \\ \frac{B}{\mu} & -\frac{A}{\mu} & 0 & 0 & 0 & W \end{bmatrix} \begin{bmatrix} E_x \\ E_y \\ E_z \\ H_x \\ H_y \\ H_z \end{bmatrix} = 0 \tag{3-129}$$

where:

$$W = \frac{i2\sin(\omega\Delta t/2)}{\Delta t} \tag{3-130}$$

$$A = C_{x1}e^{ik_{x3}h_{x3}} + C_{x2}e^{ik_{x1}h_{x1}} + C_{x3}e^{-ik_{x2}h_{x2}} \tag{3-131}$$

$$B = C_{y1}e^{ik_{y3}h_{y3}} + C_{y2}e^{ik_{y1}h_{y1}} + C_{y3}e^{-ik_{y2}h_{y2}} \tag{3-132}$$

$$C = C_{z1}e^{ik_{z3}h_{z3}} + C_{z2}e^{ik_{z1}h_{z1}} + C_{z3}e^{-ik_{z2}h_{z2}} \tag{3-133}$$

After manipulating the determinate in the same manner as for the one dimensional case the three dimensional stability criteria is found to be:

$$\Delta t \le \frac{1}{c\sqrt{\left(\frac{2\Delta x_3 + 6\Delta x_1}{\Delta x_2(\Delta x_1 + \Delta x_2)(\Delta x_3 + 2\Delta x_1 + \Delta x_2)}\right) + \left(\frac{2\Delta y_3 + 6\Delta y_1}{\Delta y_2(\Delta y_1 + \Delta y_2)(\Delta y_3 + 2\Delta y_1 + \Delta y_2)}\right) + \left(\frac{2\Delta z_3 + 6\Delta z_1}{\Delta z_2(\Delta z_1 + \Delta z_2)(\Delta z_3 + 2\Delta z_1 + \Delta z_2)}\right)}} \tag{3-134}$$

In this section the stability criteria for the nonuniform griding was derived for the three dimensional case and it is shown that this criteria is less stringent than the Courant stability criteria based on the smallest grid spacing in each dimension of the simulation. This is significant in that it shows that the time step limit for a nonuniformly girded simulation will be the same as the time step limit for a uniformly gridded simulation. Therefore the nonuniform grid spacing technique will not require more time iterations than the current nonuniform techniques or the standard FDTD uniform grid spacing approach.

4. Validation

4.1. Implementation of FDTD Method

The nonuniform lossy orthogonal FDTD simulator written as part of this body of work was designed to be general and adaptable to the whole class of structures which conform to rectangular grid spacing. Special attention was given to minimizing the computer memory requirements and to minimizing the computational burden. All the work was performed on an HP715 work station which had 300 [MB] of available RAM. The following sections will describe some of the preprocessing steps and conventions used to achieve computational and memory efficiency in the FDTD simulator.

4.1.1. Simulator Organization

The simulator is divided into two separate pieces of code, one which contains all of the specific simulation structure information (setup code) and the second which contains the FDTD engine (engine code) that performs the actual electromagnetic simulation. The

concept is to only modify the setup code and design the engine code to be capable of handling any simulation space regardless of the specific simulation structure information.

In the setup code the space stepping, materials, boundary conditions, input cells, reporting, and time stepping information is set and written to a data file. The engine code reads in the data file and performs the electromagnetic simulation while reporting the requested information, see Figure 11.

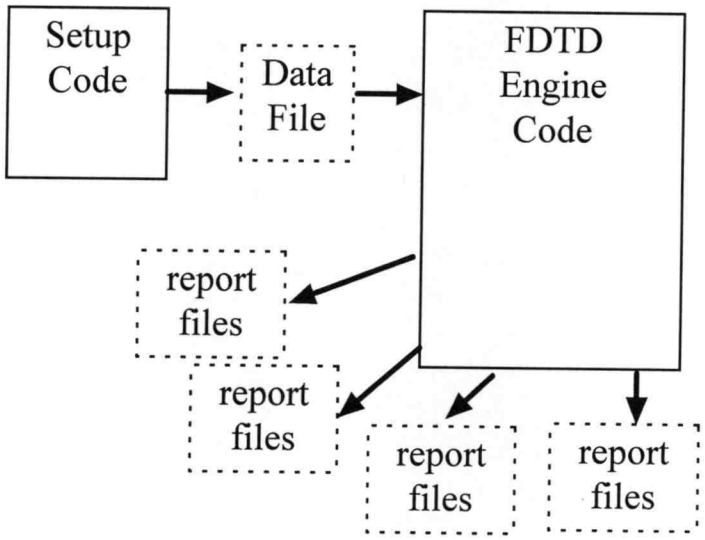

Figure 11 Organization of FDTD simulator

4.1.2. Preprocessing

To minimize the memory and computational burdens, a preprocessing step is performed before the FDTD simulation begins. The standard FDTD equation can be rewritten from its standard form:

$$\left(\frac{\Delta t}{\mu}\right)E_z^{n+1}\left(i+0.5,j-0.5,k\right)=\left(\frac{2\varepsilon_r\varepsilon_0-\sigma\cdot\Delta t}{2\varepsilon_r\varepsilon_0+\sigma\cdot\Delta t}\right)\left(\frac{\Delta t}{\mu}\right)E_z^{n}\left(i+0.5,j-0.5,k\right)+\left(\frac{(c\cdot\Delta t)^2}{\varepsilon_r+\frac{\sigma\cdot\Delta t}{2\varepsilon_0}}\right) \tag{4-1}$$
$$\left(\frac{H_y^{n+0.5}\left(i+1,j-0.5,k\right)-H_y^{n+0.5}\left(i,j-0.5,k\right)}{\Delta x}+\frac{H_x^{n+0.5}\left(i+0.5,j-1,k\right)-H_x^{n+0.5}\left(i+0.5,j,k\right)}{\Delta y}\right)$$

into a less computationally intensive form of:

$$E_z^{n+1}\left(i+0.5,j-0.5,k\right)=C_A E_z^{n}\left(i+0.5,j-0.5,k\right)+C_B\left(\begin{array}{l}C_1H_y^{n+0.5}\left(i+1,j-0.5,k\right)+C_2H_y^{n+0.5}\left(i,j-0.5,k\right)\\+C_3H_x^{n+0.5}\left(i+0.5,j-1,k\right)+C_4H_x^{n+0.5}\left(i+0.5,j,k\right)\end{array}\right) \tag{4-2}$$

Where C_A, C_B, C_1, C_2, C_3, and C_4 are all constants which do not vary in value during the simulation. The actual values of the constants are not stored in each cell with the field information, but a short integer which is used as an index to locate the proper constant value is stored in each cell. The results in a large computer memory savings by storing only a type short integer in each cell instead of two type doubles (C_A and C_B). Additionally many of the cells will have the same C_A and C_B pair, so the redundant information is eliminated and only the unique constant pairs are stored as double precision numbers.

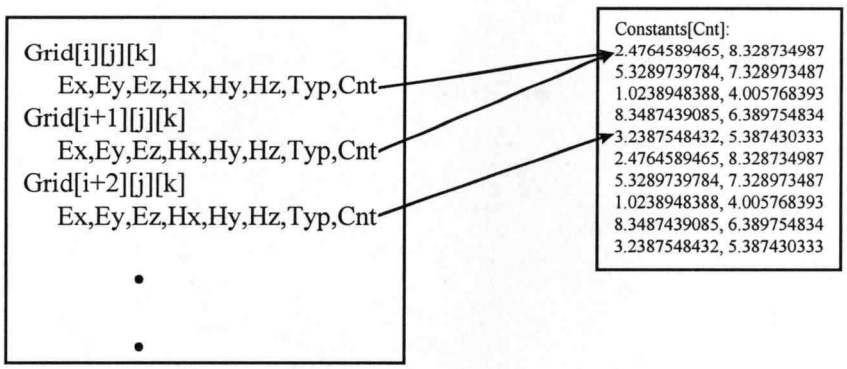

Figure 12 FDTD Handling of Material Constants

The spacial constants, (C_1, C_2, C_3, and C_4) are looked up by using the grid indexes (i, j, k) and since the grid is orthogonal the information is stored in three one dimensional arrays representing each the X, Y, and Z axes. The spacial constants are preprocessed to determine the value of each constant and which neighboring cells will need to be accessed for the calculation of the spacial derivatives, see Figure 13. This results in both a memory savings and a reduction in computational burden.

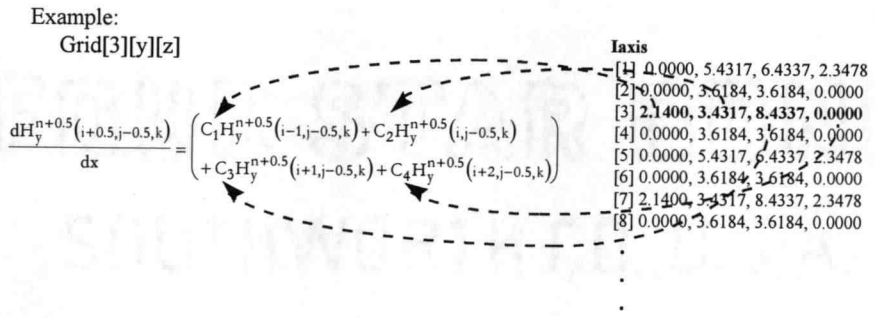

Figure 13 Storage of Spacial Constant Information

After both the material constants and spacial constants have been calculated, there are no divisions performed inside of the main FDTD loops for typical cells. Some special case cells may perform divisions, but these are few in number compared to the overall number of cells.

4.2. Microstrip Validation Examples

4.2.1. FDTD Extraction of Effective Dielectric Constant

To validate the simulator a microstrip structure is simulated and a comparison of the FDTD results is made with the results obtained by Kirsching and Jansen [56]. Kirsching and Jansen's results are recognized as the most reliable empirical expressions for simple and coupled microstrips. A typical microstrip structure is shown in Figure 14.

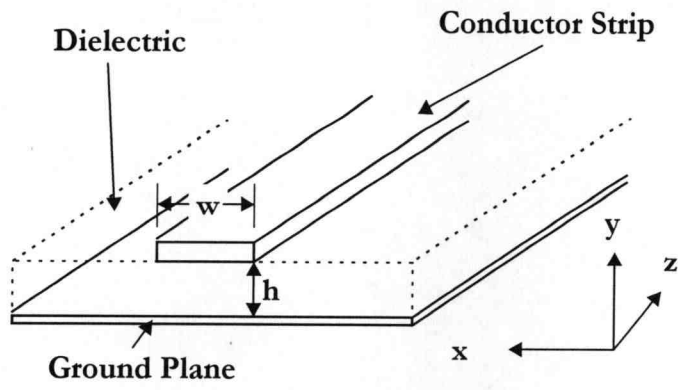

Figure 14 Microstrip Structure

The simulated microstrip used PML boundaries and a dielectric constant of 4. The strip was 1 [mm] wide, 0.5 [mm] thick, and had a W/H ratio of 2. The effective dielectric constant was determined by monitoring the vertical electric field component directly under the metal conductor at two points separated by a known distance. The transfer function between the two observation points is given by:

$$e^{-\gamma(\omega)L} = \frac{E(\omega, z = L)}{E(\omega, z = 0)} \tag{4-3}$$

where:

$$\gamma(\omega) = \alpha(\omega) + j\beta(\omega) \tag{4-4}$$

The effective dielectric constant is then determined by:

$$\varepsilon_{eff}(\omega) = \frac{\beta^2(\omega)}{\omega^2 \varepsilon_0 \mu_0} \tag{4-5}$$

The results in Figure 15 show good agreement with Kirsching and Jansen's results. In previous work by Zhang, Figure 16, it has been shown that effective dielectric constant determined by various formulas tend to form a band of agreement rather than an exact agreement[57]. These particular results match quite well considering the typical disagreement between the various formulations for microstrips.

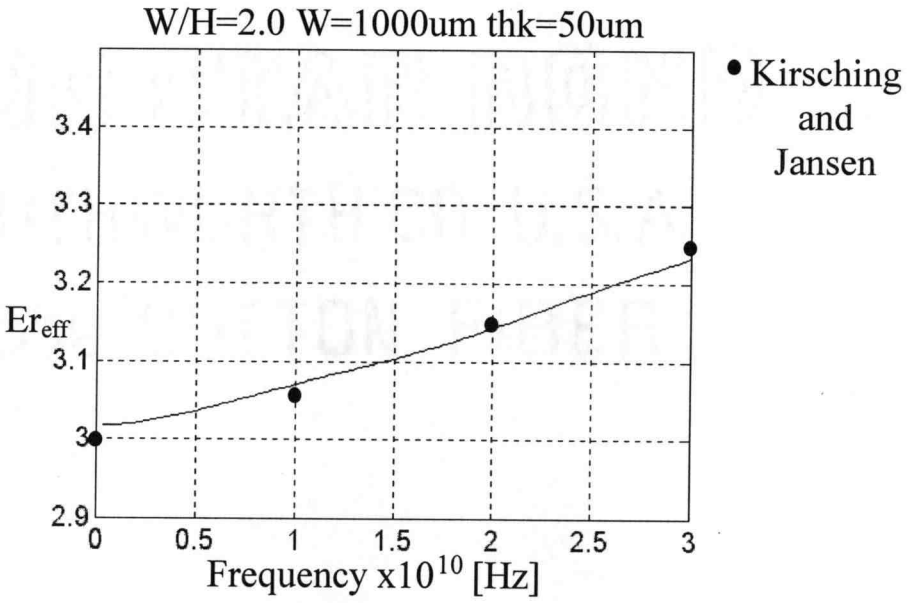

Figure 15 Microstrip Results of Effective Dielectric Constant

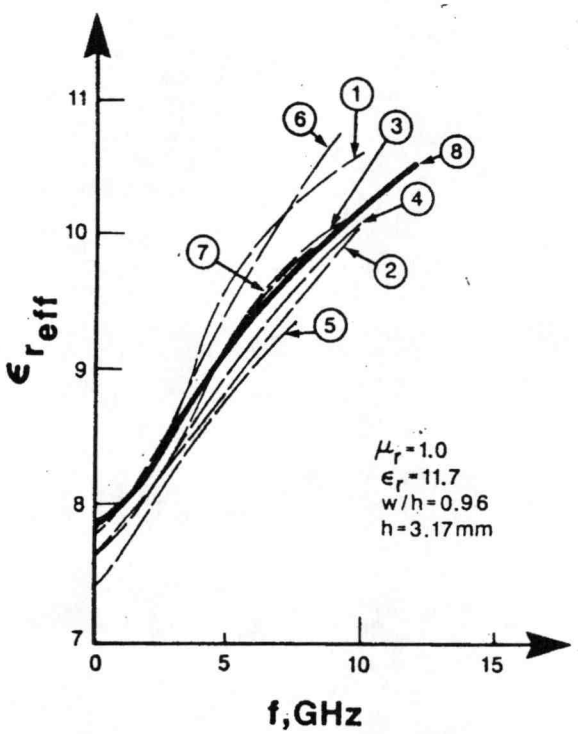

Comparison of effective dielectric constant ϵ_{reff} as computed by different authors [1) Farrar and Adam, 2) Itoh and Mittra, 3) Van de Capelle and Luypaert, 4) Denlinger, 5) Schmitt and Sarges (ϵ_r = 11.2), 6) Chang and Kuester, 7) Pregla and Kowalaki, 8) time-domain result in this paper]. All of the results except the last one are from Kuester and Chang's paper [1].

Figure 16 Effective Dielectric Constant Results
as Predicted by Various Formulas

4.2.2. Previous FDTD Results for Effective Dielectric Constant

Zhang presented results for an infinitely thin microstrip with a W/H ratio of 0.75 and er=13.0, Figure 17. This simulation was repeated using the FDTD code written for this

thesis and showed good agreement with Zhang's effective dielectric constant results, Figure 18.

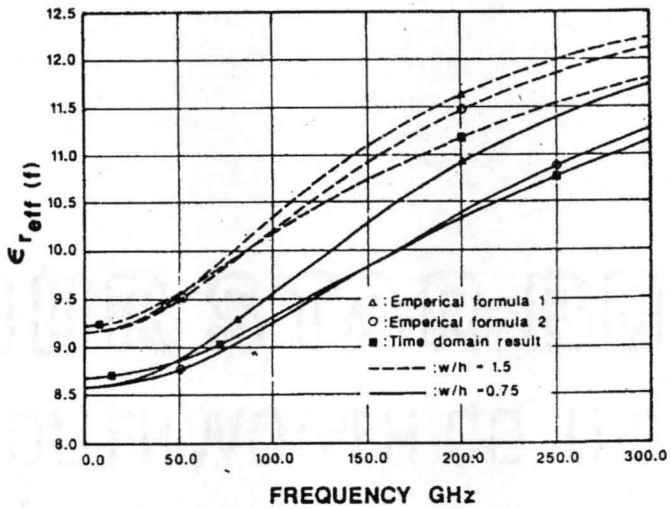

Effective dielectric constant ($\epsilon_r = 13.0$). Comparison of the results from time-domain method with two empirical formulas: 1) Edward and Owen [5], 2) Pramanick and Bhartia [6], [4].

Figure 17 Zhangs FDTD Results for a Microstrip with W/H=0.75

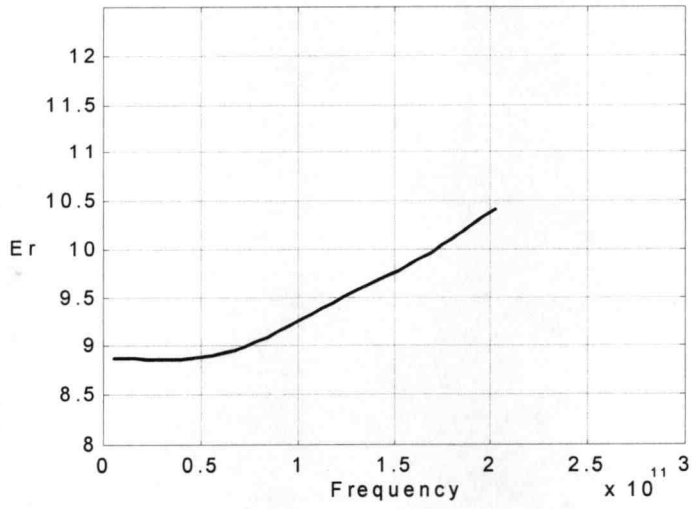

Figure 18 Effective Dielectric Constant from FDTD simulation for W/H=0.75

4.2.3. Previous FDTD Results for Microstrip Impedance

For the same structure described above Zhang extracted the impedance as a function of frequency, Figure 19. Again the FDTD results compare favorably with Zhangs FDTD results, Figure 20.

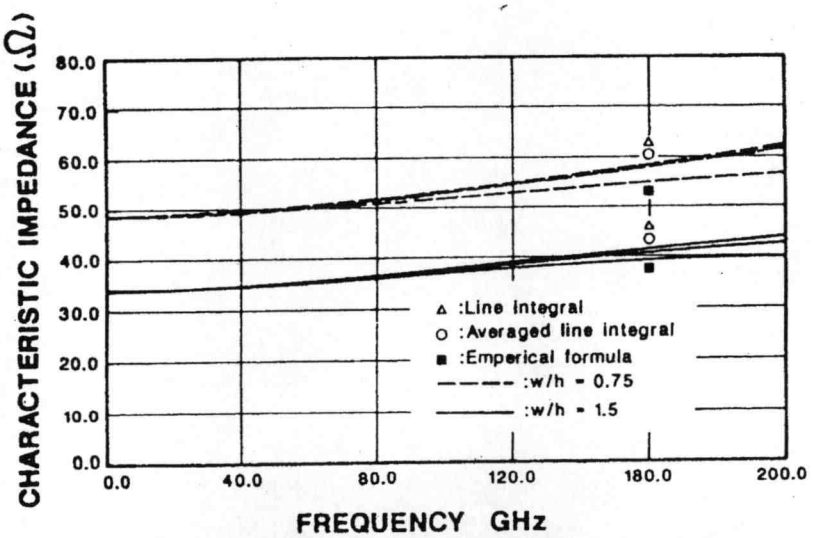

Characteristic impedance ($\varepsilon_r = 13.0$). Comparison of the results from time-domain method with empirical formula (Bianco *et al.* [5]).

Figure 19 Zhangs FDTD Impedance Results for a Microstrip with W/H=0.75

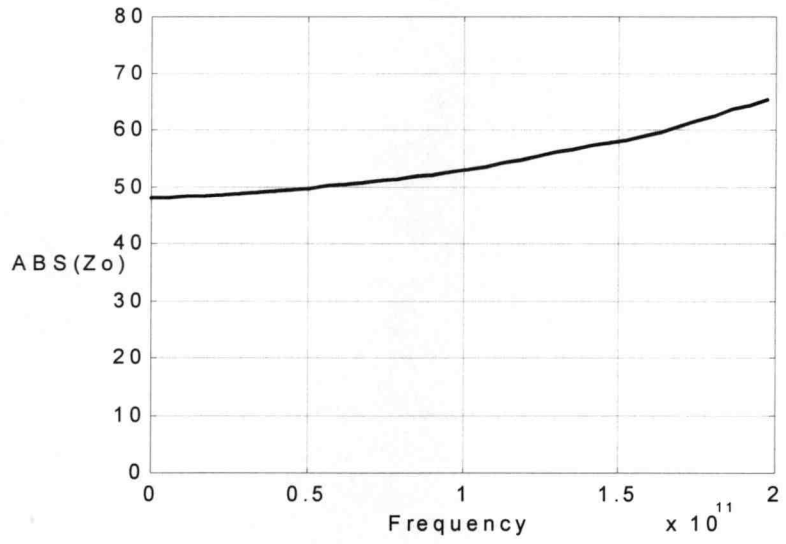

Figure 20 Microstrip Impedance from FDTD simulation for W/H=0.75

4.3. Characteristic Impedance of a Stripline

To further validate the algorithms a stripline structure was simulated and the impedance of the line was extracted as a function of frequency. The strip was 90 μm wide, 100 μm from the ground planes and was infinitely thin. The FDTD simulator produced an impedance of 102.5[Ohms] which was flat with frequency. The details of this simulation are presented in the validation section for the nonuniform grid spacing. This result compares to an impedance of 107[Ohms] predicted by Collins based on conformal mapping[58]. It was expected that the two impedances would match closer than they did, however, Collins made some approximations that may contribute to the small discrepancy. Additionally the FDTD simulations used perfectly conducting walls to enclose the stripline,

but experiments which moved these walls further from the strip did not vary the impedance enough to account for the small discrepancy.

Both of the above experiments show that the general lossy FDTD simulator written as part of this body of work produces results which agree reasonably with other techniques. The effective dielectric constant for a microstrip was compared to the results from a commercial software package and the characteristic impedance of a stripline was extracted and compared to the results predicted by conformal mapping.

4.4. Nonuniform space stepping

An enclosed stripline, Figure 21, is used to test the second order technique compared to the first order technique. The comparison is of the FDTD measured impedance of the transmission line as a function of frequency for various grid discontinuities. The impedance of the enclosed stripline is calculated one cell away from the discontinuity in the grid spacing using the procedure described by Taflove[59].

The structure is excited by a Gaussian pulse in a cross sectional plane perpendicular to the direction of propagation. The field pattern of the input plane is determined by a 2-D Laplace solver which insures that the fields in the enclosed stripline are essentially TEM. The input plane was located near the center of the enclosed stripline structure and the simulation was terminated before reflections from the end of the stripline could interact with the measurements.

For all of the experiments described here, $\Delta x=\Delta y=\Delta z=10[\mu m]$ and the time step was set to 0.45 of the time step determined by the standard FDTD stability criteria. All metal structures were modeled as ideal conductors and were infinitely thin.

Figure 22 shows the results of the stripline impedance measurement using uniform grid spacing. Note that the frequency axis is stopped at 3[THz] which corresponds to a wavelength that is ten grid spaces in length[60,61]. Wavelengths smaller than ten grid spacings violate the assumption that wavelength is large compared to grid spacing and

significant numerical distortion occurs to these frequency components. Some authors suggest that wavelengths smaller than 15 or 20 grid spaces should be disregarded, but for illustrative purposes the most liberal interpretation of 10 grid spaces will be used in the following discussion. In the nonuniform plots, the vertical line corresponds to the frequency at which the largest grid spacing is equal to a tenth of a wavelength.

Figure 23 and Figure 24 compare the results for an abrupt change in the grid spacing from Δz to $2*\Delta z$. The performance of the second order nonuniform differencing is much better than the first order results in the region where wavelength is greater than ten grid spacings. Figure 25 and Figure 26 show the results for a decreasing grid size of Δz to $1/2*\Delta z$. Again as expected the second order nonuniform technique performs better than the first order technique.

Figure 27 shows a composite of first and second order results for $1.5*\Delta z$, $2.0*\Delta z$, and $3.0*\Delta z$. The frequencies for a tenth of a wavelength are 2[THz], 1.5[THz], and 1[THz] respectively.

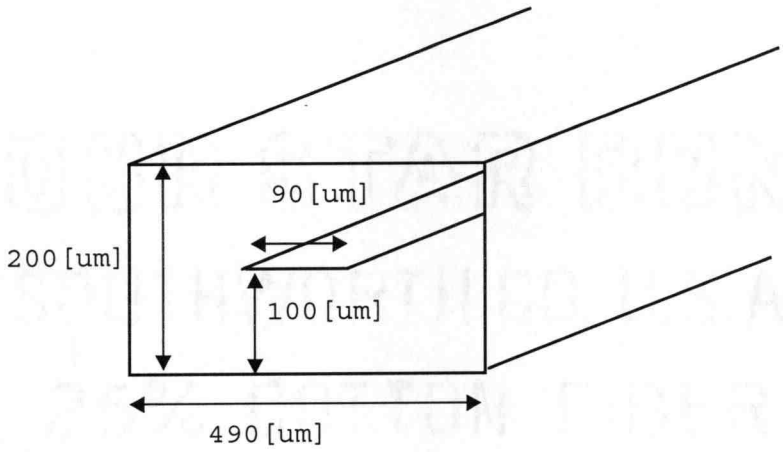

Figure 21 Enclosed Stripline Structure

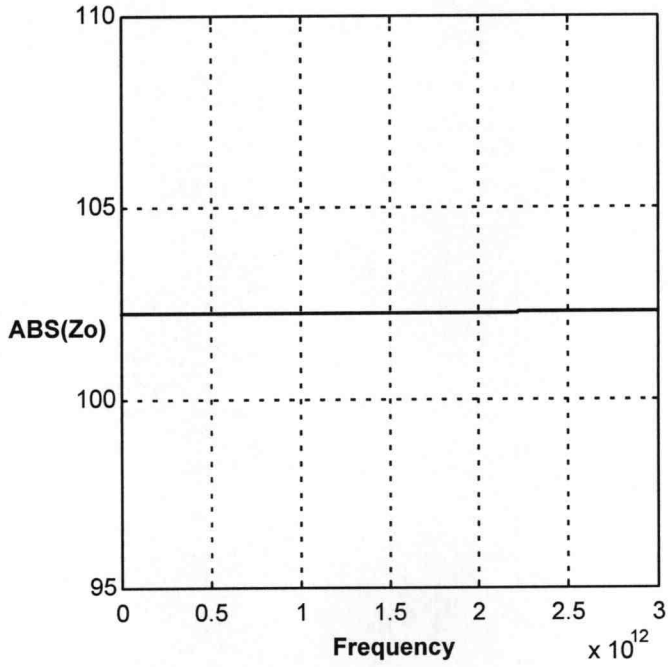

Figure 22 Uniform Grid Results

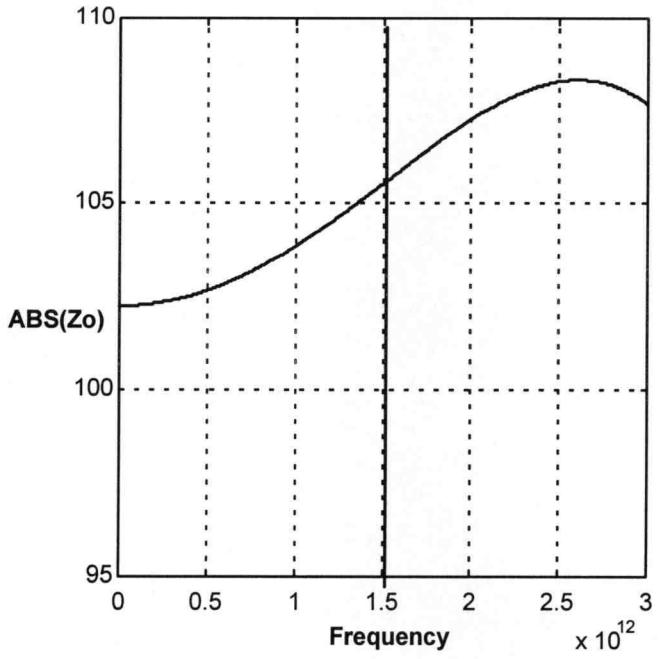

Figure 23 First Order dz=>2.0 dz

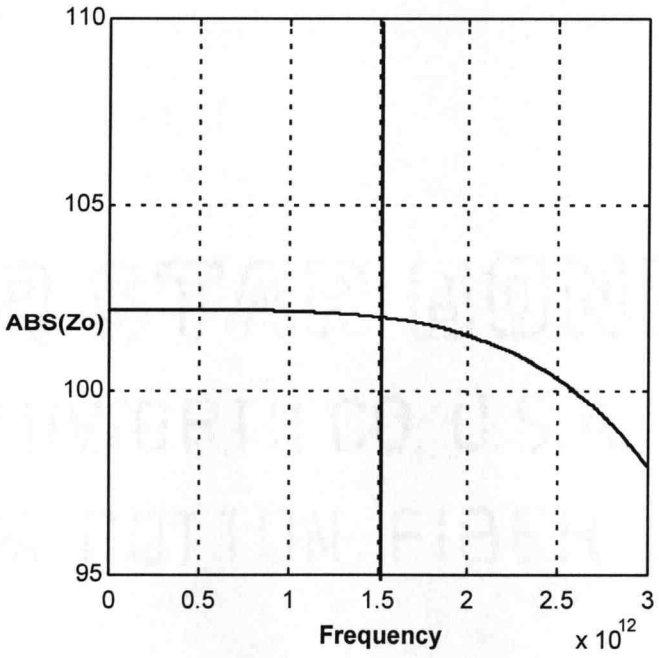

Figure 24 Second Order dz=>2.0dz

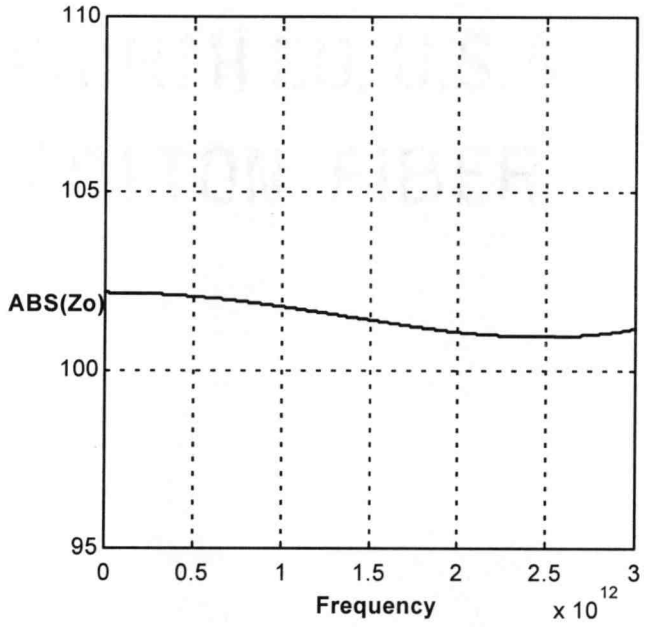

Figure 25 First Order dz=>0.5dz

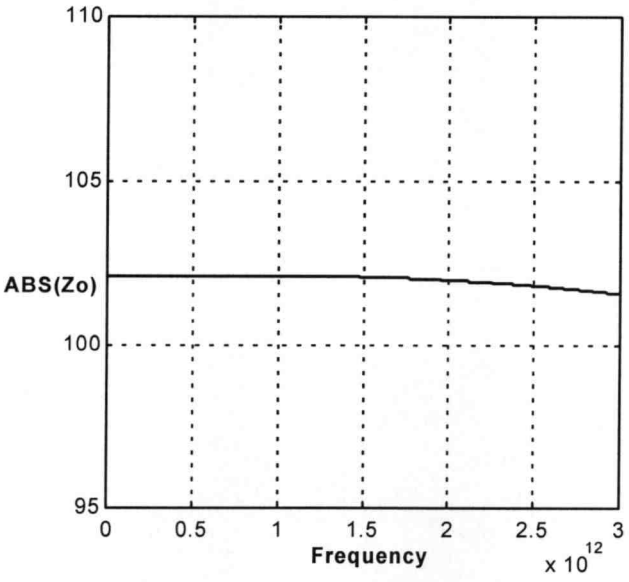

Figure 26 Second Order dz=>0.5dz

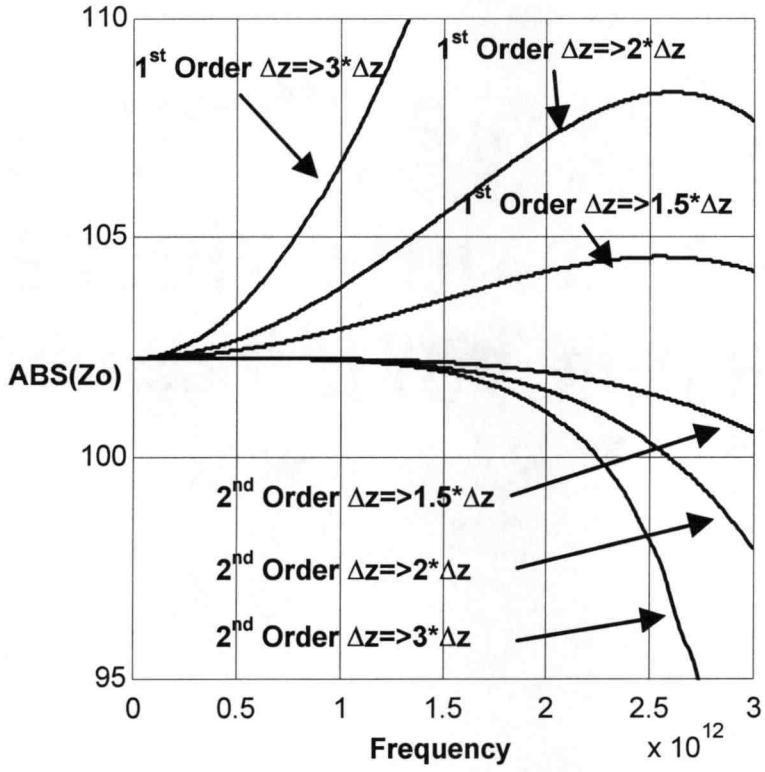

Figure 27 Composite of First and Second Order Results

Often the accuracy of a technique is shown by plotting the maximum error versus the maximum step size in the simulation grid[62]. This is a valid approach when looking at a single frequency component. More generally one is concerned with the full time domain response. The problem with applying this approach to a full time domain response is that the error is strongly frequency dependent as is shown in the previous impedance plots. The max error versus max step plots do not show this frequency dependence and the results are strongly colored by the frequency content of the input pulse. However they are present

here for consistency and they illustrate the variation of error between the first order and second order nonuniform griding approaches (see Figure 28 thru Figure 30).

The simulation to produce the max error versus max step plots was an enclosed stripline similar, but smaller, to Figure 21. The cross sectional fields, Ex, Ey, and Ez, were stored every tenth time step and compared to the uniform grid spacing results. The maximum absolute error over the cross section and over time was determined and plotted for each of the field components.

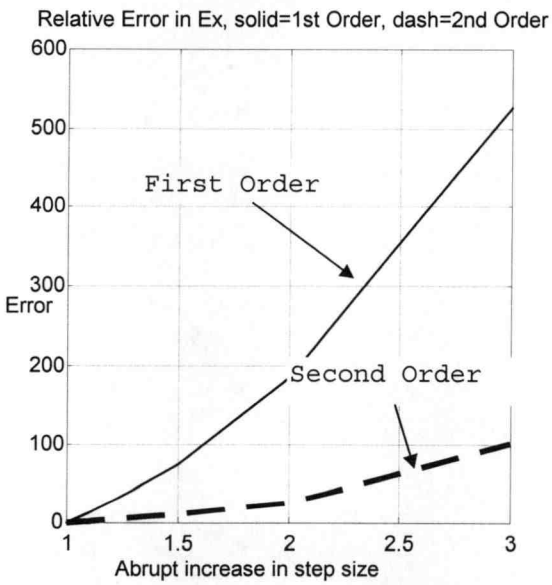

Figure 28 Error in Ex of First versus Second Order Techniques

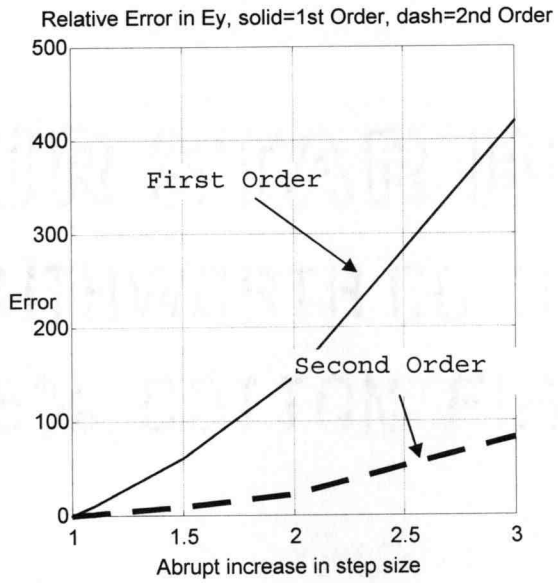

Figure 29 Error in Ey of First versus Second Order Techniques

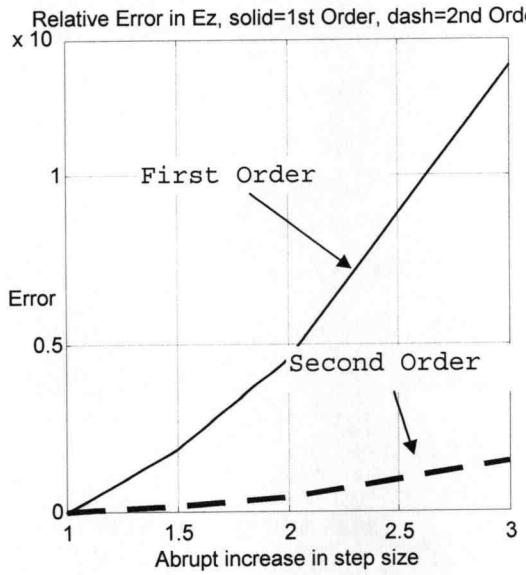

Figure 30 Error in Ez of First versus Second Order Techniques

A second order accurate technique for nonuniform FDTD has been implemented and compared to the current first order techniques. It is seen on nonuniform grids that the new second order technique produces better results for a broader frequency range than the first order techniques.

Since the grid is orthogonal, the nonuniform second order technique requires virtually no additional memory and requires up to six additional multiplications and additions per nonuniform cell. The standard lossy FDTD can be implemented using 36 multiplies and 24 additions per uniform cell. There was no noticeable speed difference between the first and second order nonuniform techniques during the simulations presented in this thesis. The same algorithm for generating the nonuniform space stepping can also be applied to the time stepping. Although nonuniform time stepping would increase the memory requirements, more past time information needs to be stored, it would allow for the FDTD method to be coupled with nonlinear simulators which rely on variable time stepping. The nonuniform second order technique also works within nonuniform PML boundaries and may lead to more efficient implementations.

5. Results

5.1. Simulation of DIP Package

A simplified Dual Inline Pins (DIP) package as shown in Figure 31 has been simulated with lossy conductivities to investigate ground bounce and current flow in an Integrated Circuit (IC) ground plane. Pins 1 and 4 are connecting the IC ground plane to the Printed Circuit Board (PCB) ground plane. A Gaussian pulse is induced on pin 2 by exciting the vertical electric field components between the trace and the IC ground plane. Pin 3 is a passive trace and has no excitation.

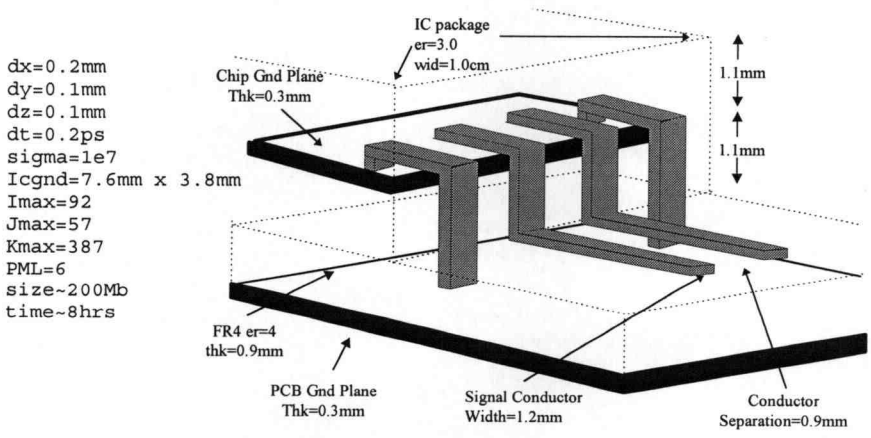

Figure 31 Simplified DIP package with finite conductivities

5.1.1. Ground Plane Currents

The conductors and ground planes have a nominal finite conductivity of 1e7 which allows the currents in the metallic regions to be determined by multiplying the electric fields by the conductivity of the region. This allows observation of the currents as a function of time. The following figures show the current density on the top surface of the IC ground plane at various time steps. The figures show the current flowing away from the excitation point, a negative voltage Gaussian pulse, and as the time continues the location of the ground connections can clearly be seen. In the figures showing Jx the current density along the leading is large relative to the other current densities due to the edge effects and is therefore not shown in the following figures to more easily observe the current densities on the top surface of the IC ground plane. This edge effect can be seen along the trailing rim of the IC ground plane in the later time steps.

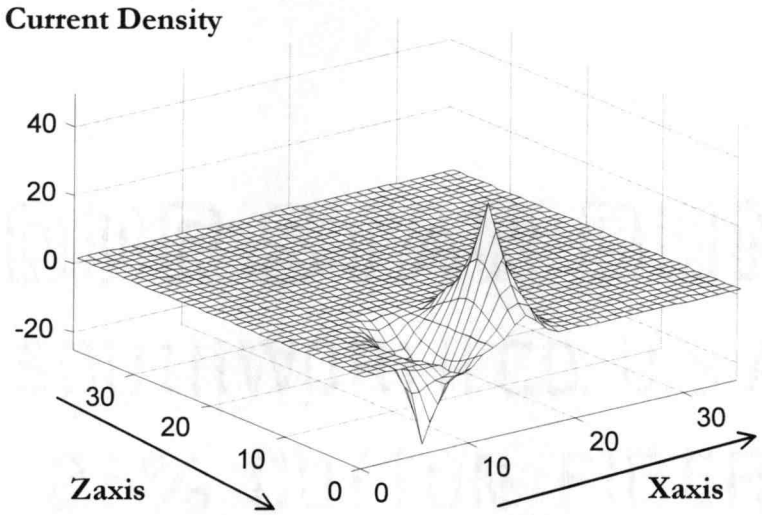

Figure 32 Jx on top surface of IC ground plane
at Time 25*0.2[psec]

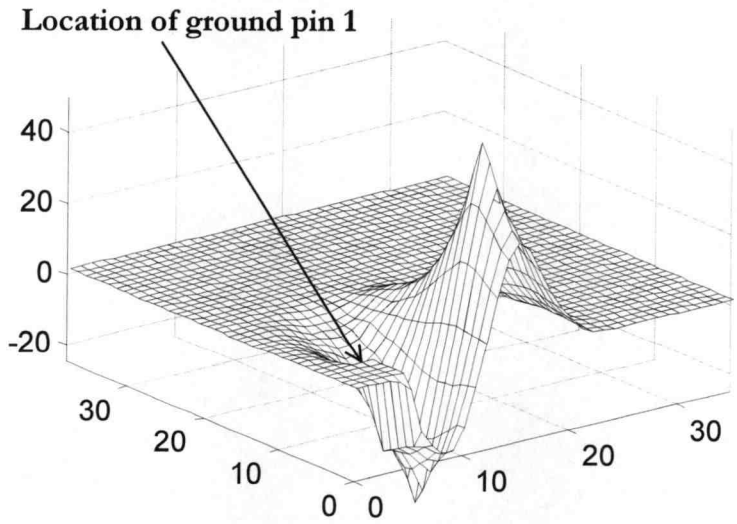

Figure 33 Jx on top surface of IC ground plane
at Time 50*0.2[psec]

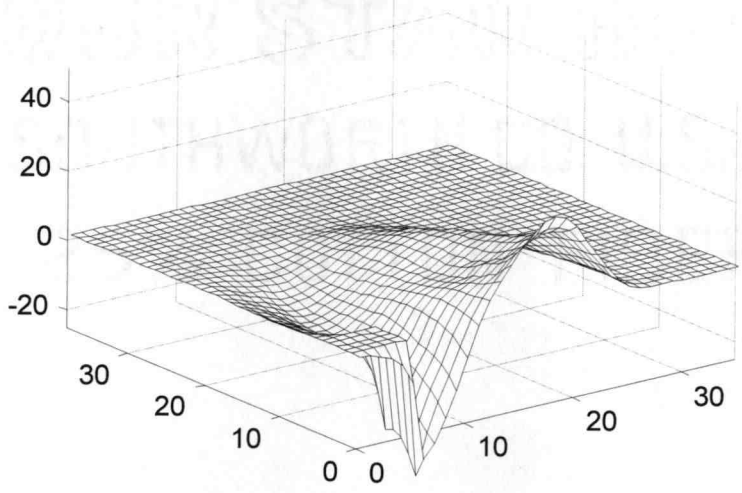

Figure 34 Jx on top surface of IC ground plane
at Time 75*0.2[psec]

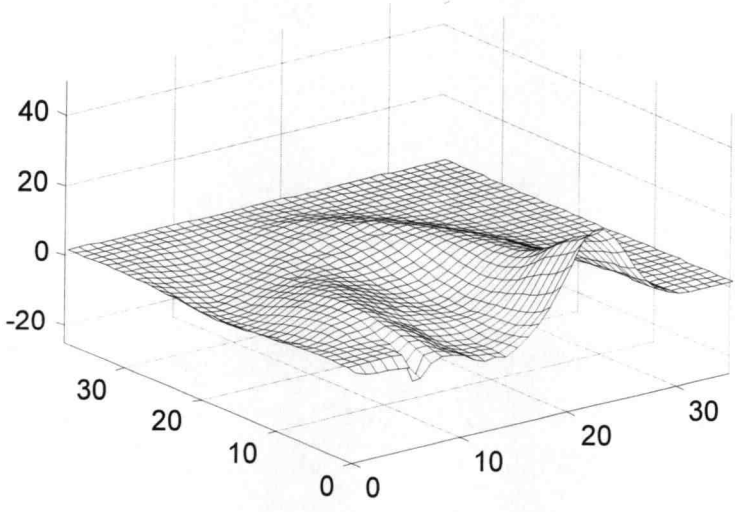

Figure 35 Jx on top surface of IC ground plane
at Time 100*0.2[psec]

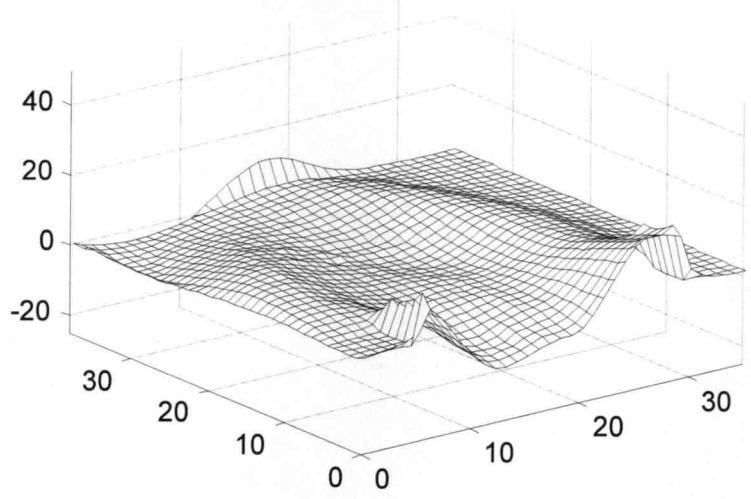

Figure 36 Jx on top surface of IC ground plane
at Time 125*0.2[psec]

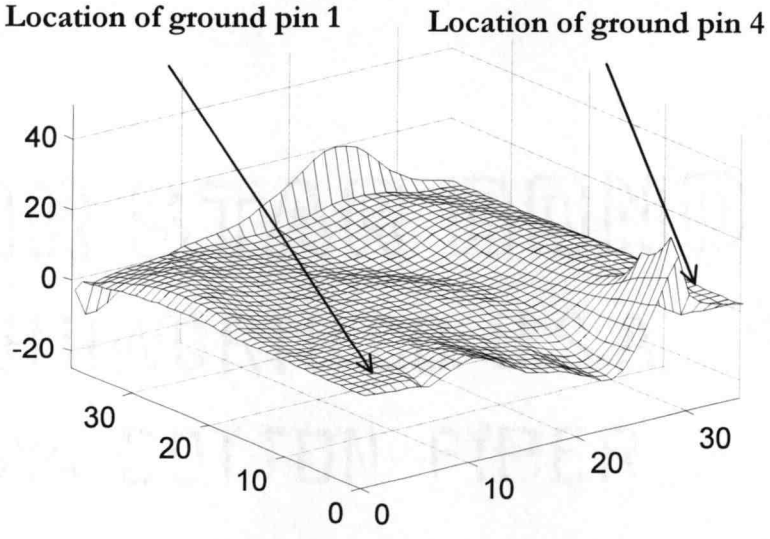

Figure 37 Jx on top surface of IC ground plane
at Time 150*0.2[psec]

The following set of figures shows the Jz component of the current densities corresponding to the above figures. In these figures both the left and right edges were cropped due to the dominating edge effects explained previously. The Jz current should go to zero at the leading edge of the ground plane unlike seen in the appropriate figures. The non-zero value is because the location of the Ez field component used to determine the current densities is located half a cell width from the edge of the metal IC ground plane, not at the edge. As can be seen the Jz current density is beginning to head towards zero along the leading edge.

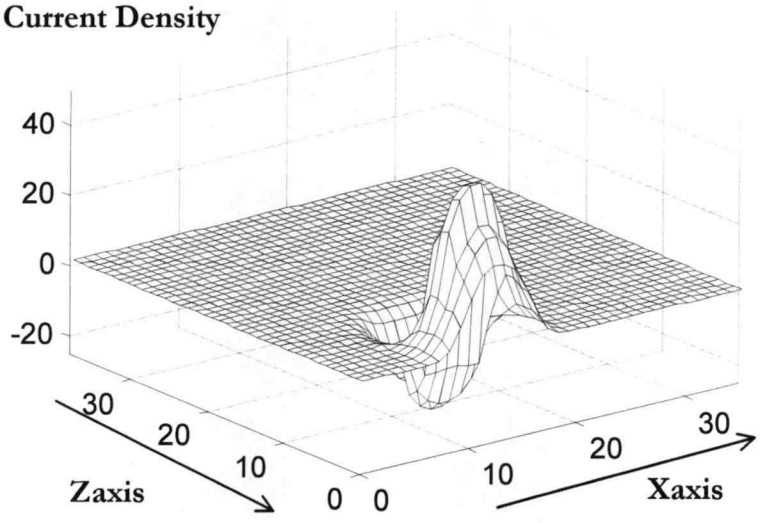

Figure 38 Jz on top surface of IC ground plane
at Time 25*0.2[psec]

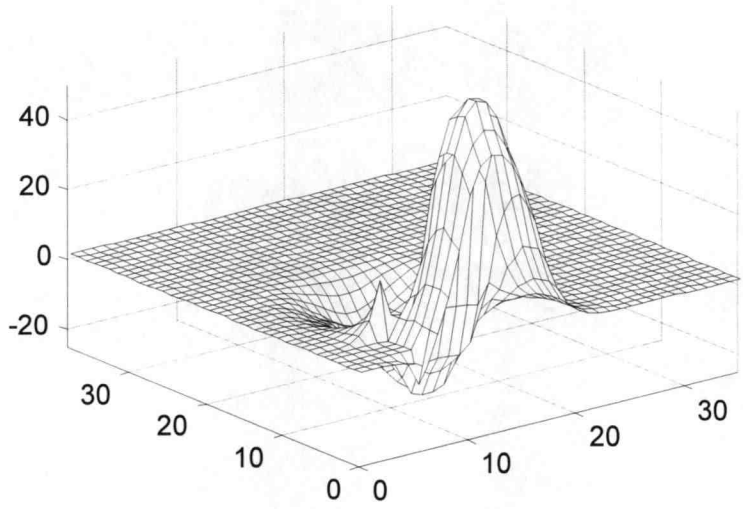

Figure 39 Jz on top surface of IC ground plane
at Time 50*0.2[psec]

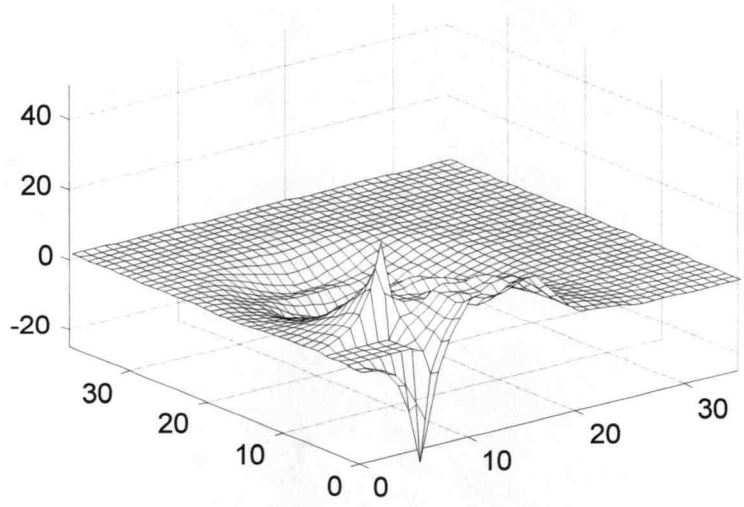

Figure 40 Jz on top surface of IC ground plane
at Time 75*0.2[psec]

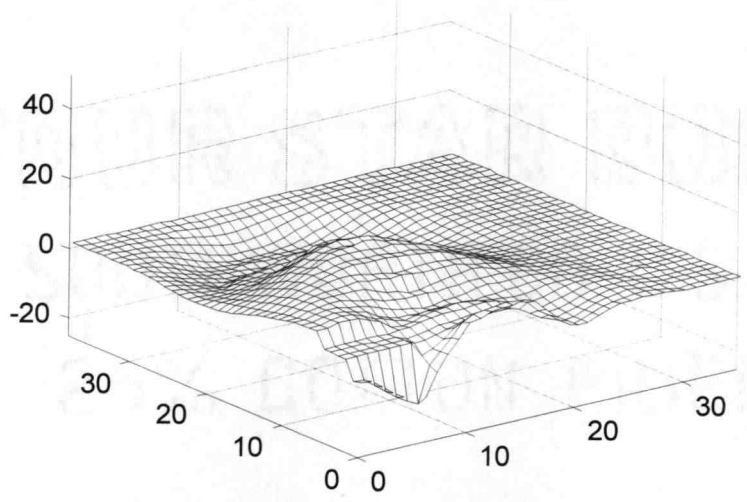

Figure 41 Jz on top surface of IC ground plane
at Time 100*0.2[psec]

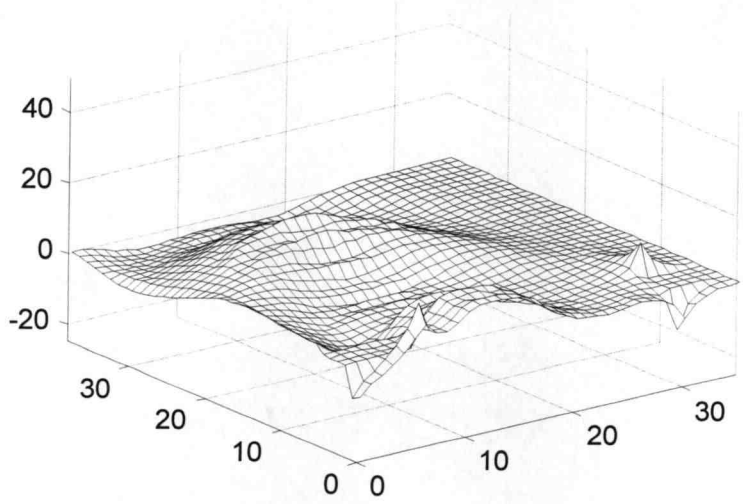

Figure 42 Jz on top surface of IC ground plane
at Time 125*0.2[psec]

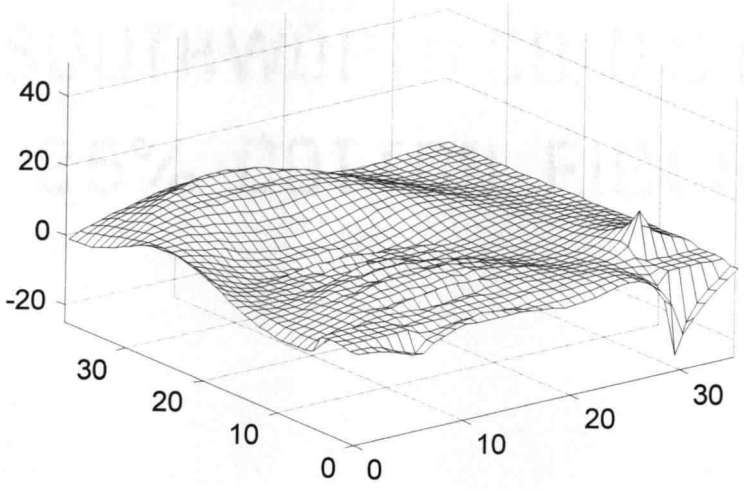

Figure 43 Jz on top surface of IC ground plane
at Time 150*0.2[psec]

Additional insights into the effects of the ground bounce can found by integrating the electric fields between the two ground planes to obtain the induced voltage and a function of time and as a function of frequency by using an FFT.

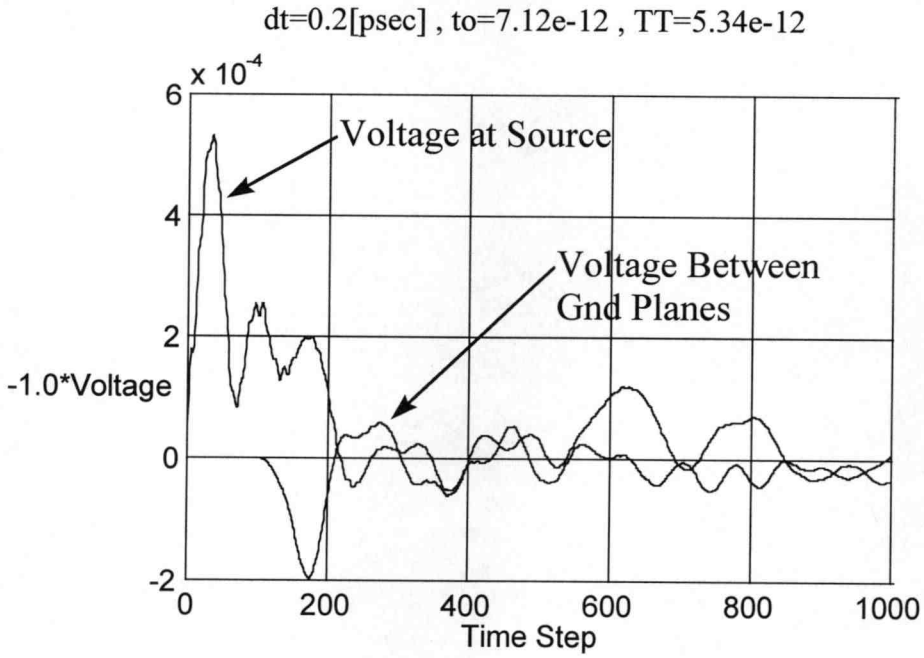

Figure 44 Voltage versus time between IC ground and PCB ground

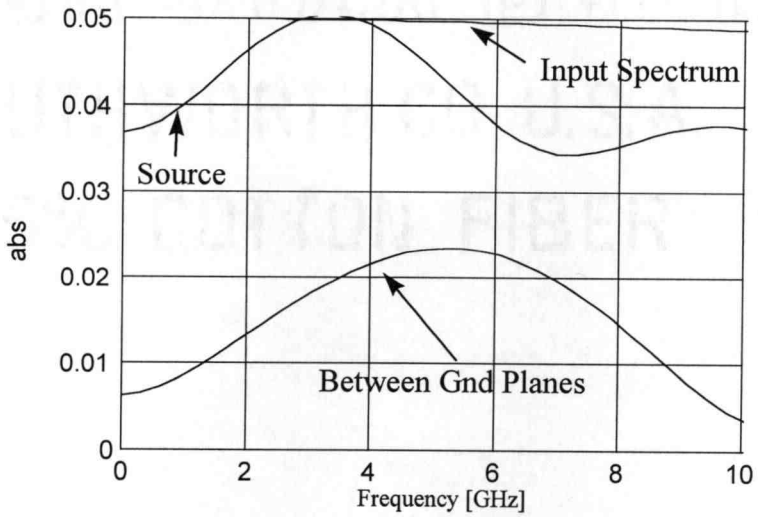

Figure 45 Voltage versus frequency between IC ground and PCB ground

Placement of the ground pins is often of concern for ground/power bounce and crosstalk. To demonstrate the utility of the FDTD the previous DIP simulation is repeated, but with the third and fourth pins swapped as shown in Figure 46. The following mesh plots illustrate the effect of the alternative grounding scheme on the ground currents.

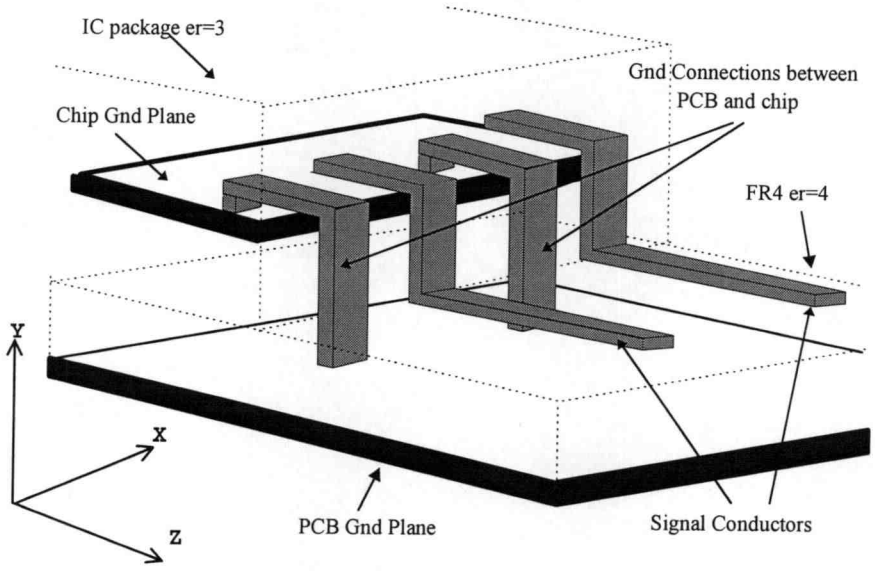

Figure 46 Alternative grounding scheme for DIP package

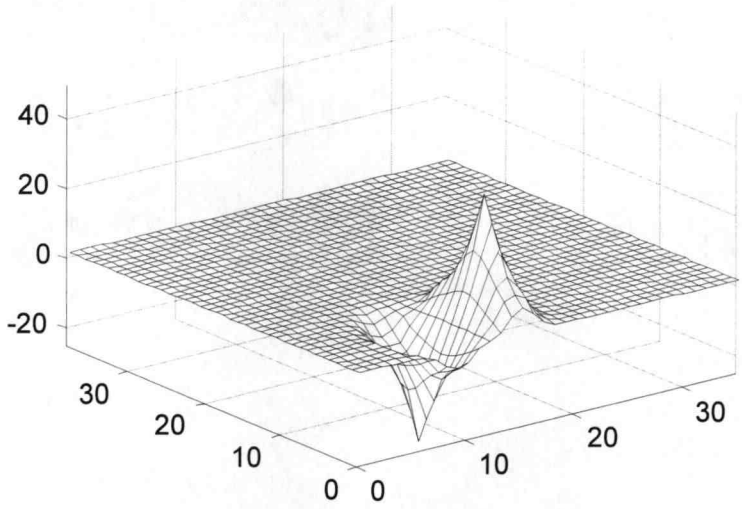

Figure 47 Jx on top surface of alternative IC ground plane at Time 25*0.2[psec]

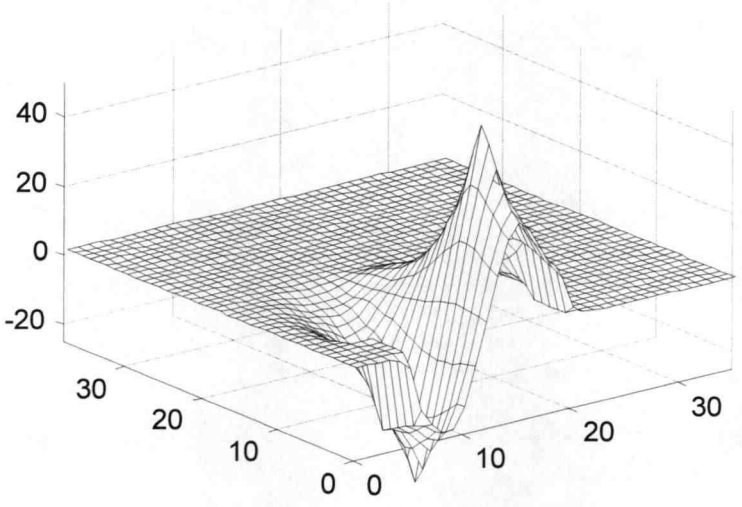

Figure 48 Jx on top surface of alternative IC ground plane at Time 50*0.2[psec]

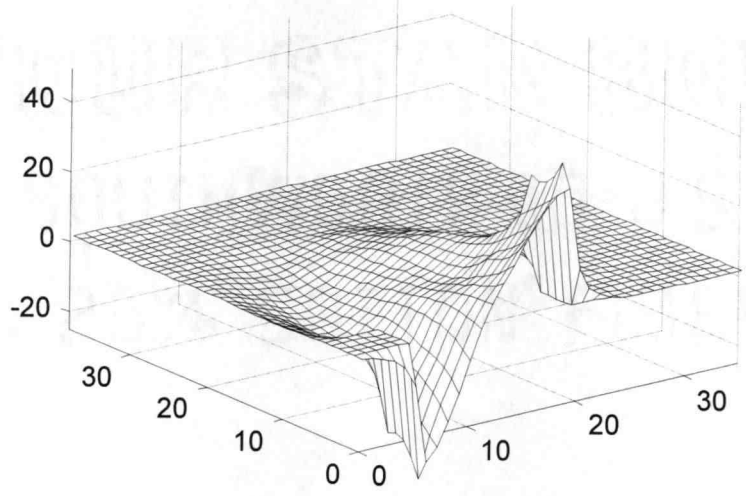

Figure 49 Jx on top surface of alternative IC ground plane at Time 75*0.2[psec]

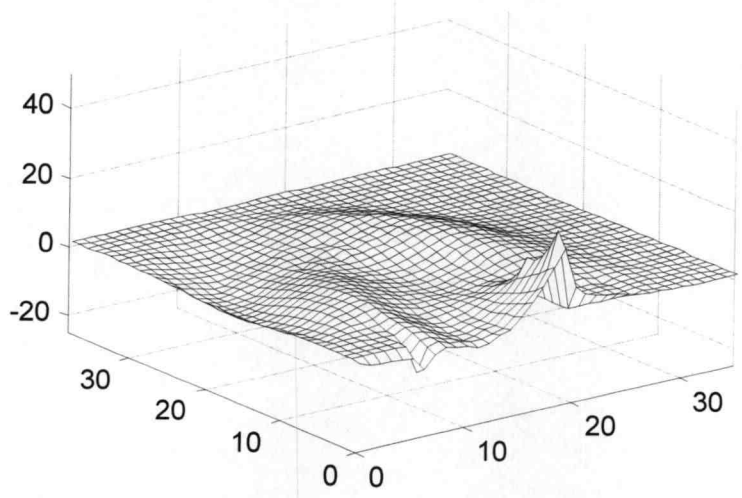

Figure 50 Jx on top surface of alternative IC ground plane at Time 100*0.2[psec]

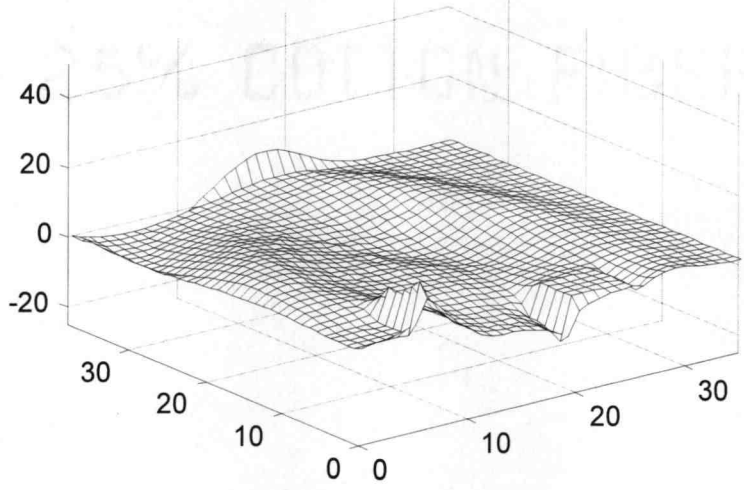

Figure 51 Jx on top surface of alternative IC ground plane at Time 125*0.2[psec]

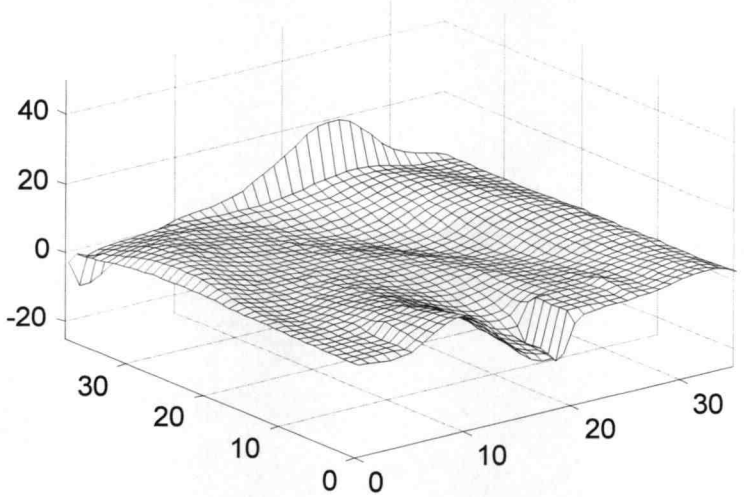

Figure 52 Jx on top surface of alternative IC ground plane at Time 150*0.2[psec]

5.1.2. Coupling and Crosstalk in the DIP

The coupling effects in the interconnect structure is apparent when observing the vertical electric field components (Ey) directly under the PCB traces as shown in Figure 53.

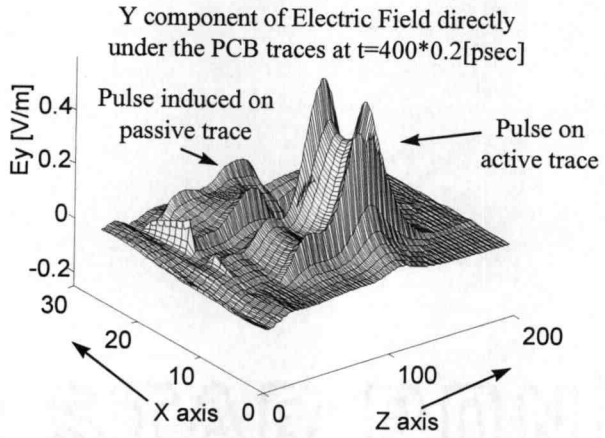

Figure 53 Electric Fields showing Crosstalk Effect

The voltage on both traces can be obtained by integrating the electric fields between the PCB ground plane and the center of the conductor as shown in Figure 54. Additional insight can be gained from the Fourier transform of the voltages as shown in Figure 55.

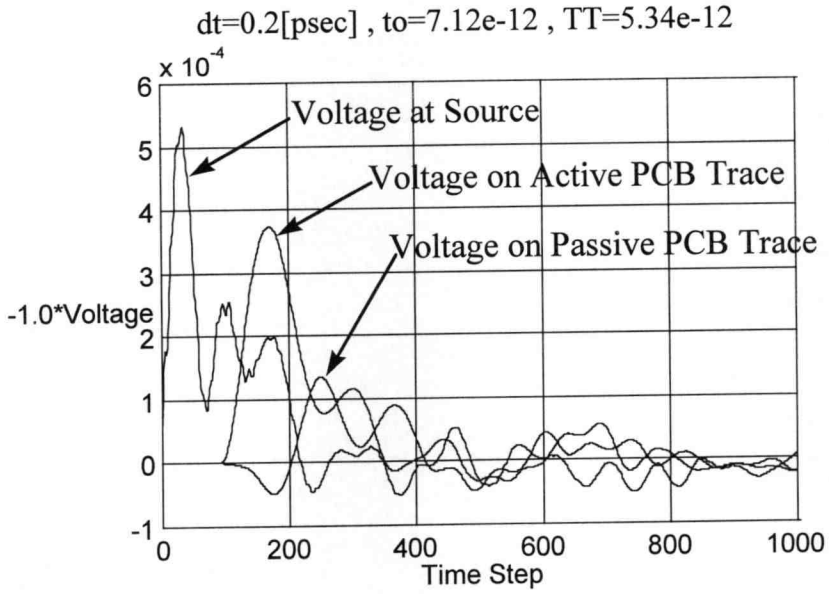

Figure 54 Voltage versus time for active and passive traces

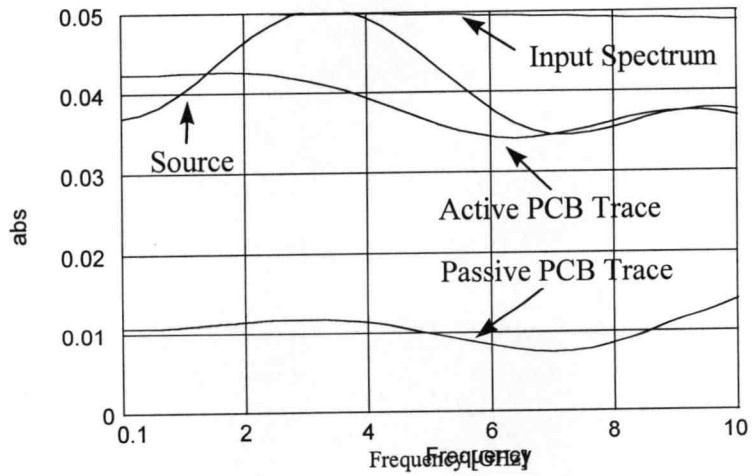

Figure 55 Voltage versus frequency for active and passive traces

5.2. FDTD as a V-TDR

The FDTD simulation tool is proposed and used as a Virtual TDR (V-TDR) to extract the equivalent SPICE type coupled circuit models associated with complex 3D structures. The extracted circuit models can be used in accurate, reliable board level simulations of high speed digital and RF/microwave systems incorporating interconnects, vias, and complex coupling between structures such as these in IC packages. The technique is exemplified by the characterization and SPICE modeling of coupled package pins and vias. The concept can be used to evaluate design options before prototyping, thus saving time and resources by eliminating electrically poor options. In this section it is shown that the simulation can be used as a virtual time domain reflection/transmission system to characterize complex coupled interconnect structures[63].

Coupling effects are becoming increasingly critical as digital integrated circuits continue to use smaller rail to rail voltage swings with faster risetimes. These same trends taken in conjunction with higher packing density of electronic package pins potentially leads to the problem of signal degradation and crosstalk in RF, mixed signal, and digital IC's. It is becoming increasingly important to select proper configurations for the conductors in IC packages in order to minimize the crosstalk and signal degrading effects.

Additionally, it is important to have accurate circuit models when performing integrated circuit board level analysis and design. As the packing density rises, the line lengths do not

correspondingly decrease which can create difficulty in simulation due to the differences in scale between the smallest features and the largest features of the circuit which require modeling. SPICE type simulators can efficiently model long symmetrically coupled transmission lines and lumped elements for a board level analysis, but are not capable of simulating three dimensional highly complex structures such as coupled vias or IC packages. The FDTD method is an excellent tool for simulating highly complex three dimensional structures, but maybe inefficient at simulating board level circuits. The V-TDR concept uses the ability of the FDTD technique to model highly complex three dimensional structures and extracts equivalent coupled circuits which can be efficiently used in SPICE type simulators for system level simulations.

For the V-TDR a 50[Ω] source with a Gaussian step function was used to excite the PCB traces. Voltages are obtained by integrating the electric field, and current densities in the conducting planes are obtained by multiplying the electric field components by the corresponding conductivities.

Figure 56 shows one of the structures investigated to exemplify the lossy FDTD technique to simulate power/ground bounce and crosstalk. Here, pins 1 and 4 are connected to the IC ground and the PCB ground planes. Pin 3 represents a passive interconnect and Pin 2 is excited by a 50[Ω] source between the PCB trace and the PCB ground plane. The IC package is assumed to be 1cm by 0.5cm with a ground plane which is 7.6mm by 3.8mm. The IC pins are 1mm wide, 0.3mm thick, and are separated by 1.2mm. The IC package is assumed to have a relative dielectric constant of 3 and the printed circuit

board substrate is assumed to have a relative dielectric constant of 4. The conductivity of all metals is assumed to be nominally 1e7(S/m).

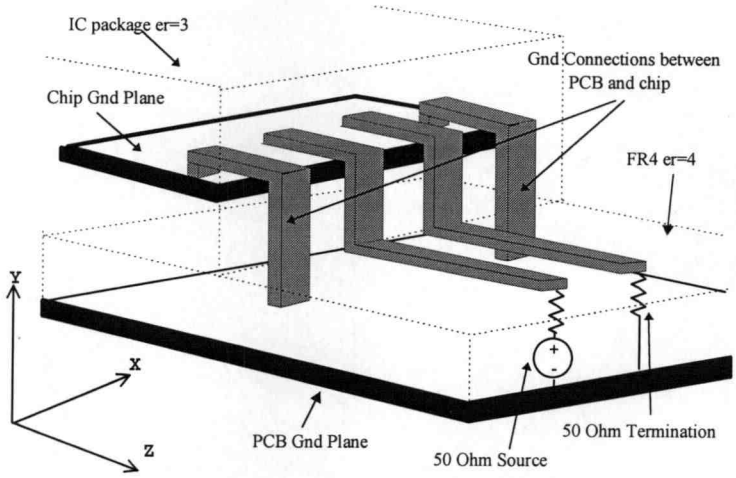

Figure 56 IC Package Test Structure

Figure 57 is the voltage between the PCB interconnect and the PCB ground plane as a function of time as excited by the V-TDR. The impedance mismatch along the interconnect and at the input end lead to reflections in the waveforms shown in Figure 57.

Figure 58 shows the self and mutual admittance and impedance profiles associated with the characteristic admittance and impedance matrices of the nonuniform coupled interconnects. The profiles were obtained by applying a two dimensional peeling algorithm to the V-TDR results in Figure 57. Each time step of the admittance profile can be turned into a SPICE type circuit, see Figure 59, consisting of three transmission line sections. This results in a SPICE type equivalent circuit derived from the FDTD results. The characteristic admittance of each line is determined as follows:

$$Y_A = Y_{11} + Y_{12} \tag{5-1}$$

$$Y_{AB} = -Y_{12} \tag{5-2}$$

$$Y_B = Y_{22} + Y_{21} \tag{5-3}$$

where Y_{11}, Y_{12}, and Y_{22} correspond to the self and mutual characteristic admittance of the transmission lines in the configuration oriented model of coupled interconnect structures.

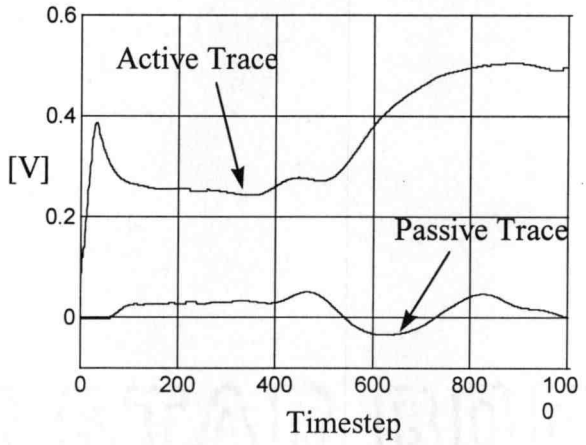

Figure 57 Virtual TDR Voltages of IC package

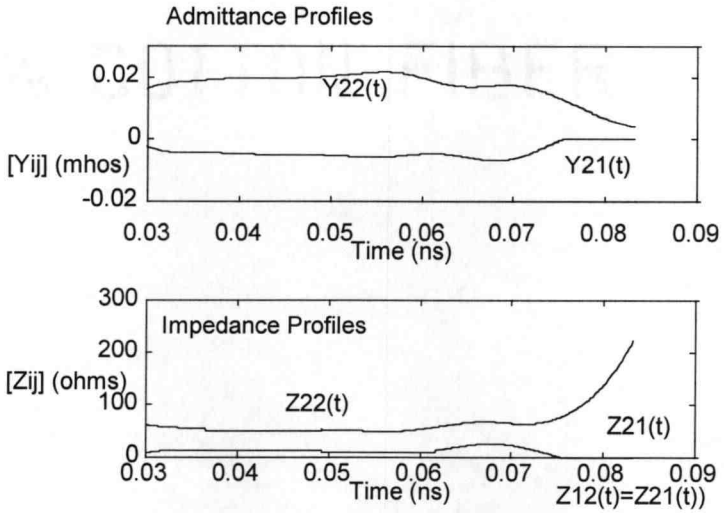

Figure 58 Admittance/Impedance Profiles of IC Package

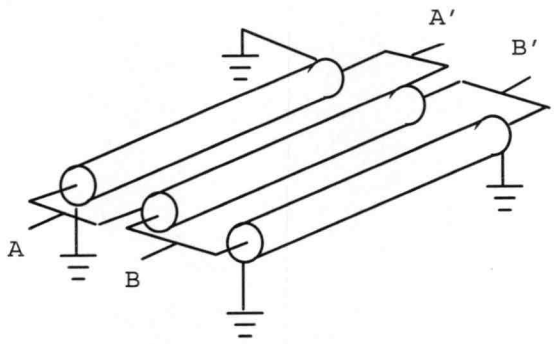

Figure 59 Transmission Line Model for each
SPICE like Simulation Section

The SPICE type transmission line model shown in Figure 59 was used with the admittance profile in Figure 58 to produce an equivalent circuit. The equivalent circuit was simulated using HSPICE and the resulting waveforms are shown in Figure 60 and Figure 61.

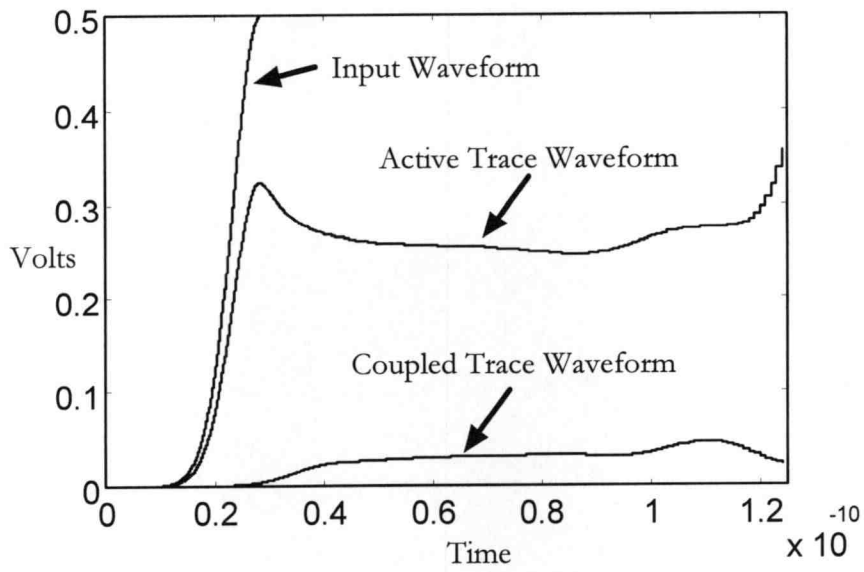

Figure 60 HSPICE Simulation Results of Full
Transmission Line Model

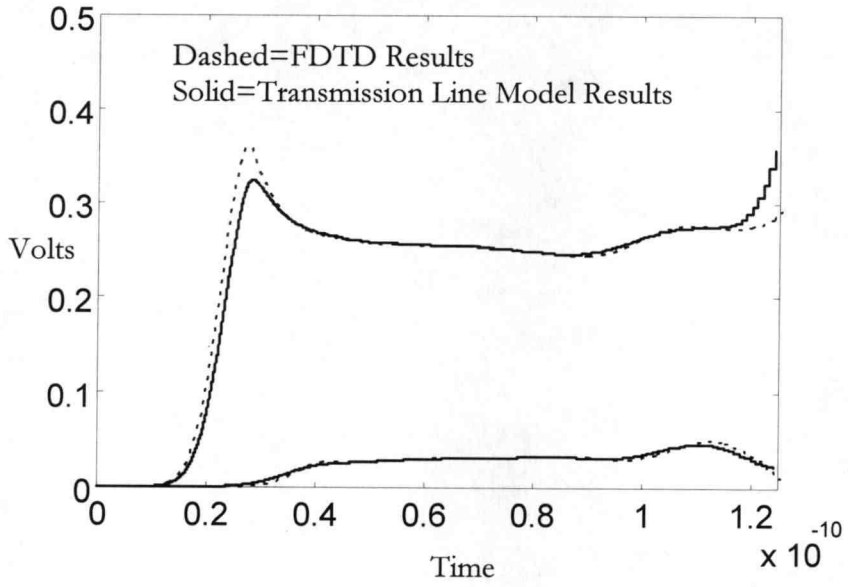

Figure 61 HSPICE Results Versus FDTD Results

The difference at the leading edge of the waveforms in Figure 61 is due to the insertion lose which is not modeled by the SPICE type transmission line circuit and the assumption that the input source was exactly 50 Ohms. Since the input source was distributed over several simulation cells, it had an effective inductance which was not captured by the two dimensional peeling algorithm. The deviation seen at the trailing edge occurs because the SPICE type model stops with an ideal open circuit, while the FDTD simulation models the effects of the nonideal open circuit inside of the IC package. In the remaining portions of the coupled transmission line sections the SPICE type circuit and the FDTD results match remarkable well for both the active line and the passive coupled line, Figure 61.

An alternative SPICE type model can be implemented using coupled inductors and capacitors as shown in Figure 62 . The lumped element type SPICE model allows a smaller circuit to be used in the simulator. The system self- and mutual- equivalent inductances and capacitances can be obtained by integrating the admittance and impedance profiles as follows[64].

$$L_{ij} = \int_{t_1}^{t_2} Z_{ij} dt \qquad i,j = 1,2 \tag{5-4}$$

$$C_{ij} = \int_{t_2}^{t_1} Y_{ij} dt \qquad i,j = 1,2 \tag{5-5}$$

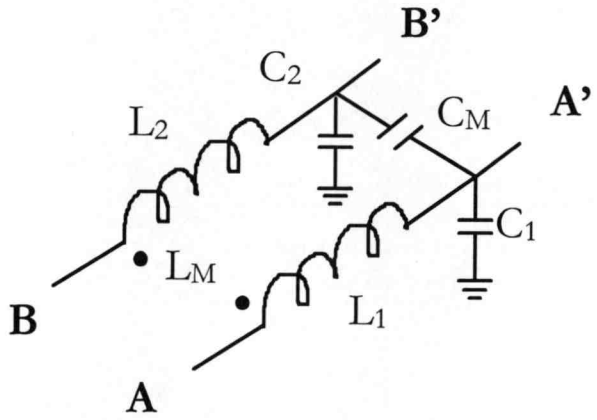

Figure 62 Lumped Element SPICE Type Circuit Model

Using the above approach several of the admittance and impedance sections can be combined to reduce the number of elements in the simulation. Figure 63 shows the simplified circuit derived for the IC package example and Figure 64 shows the comparison

between the time domain response of the reduced equivalent circuit and the original FDTD simulation voltage waveforms.

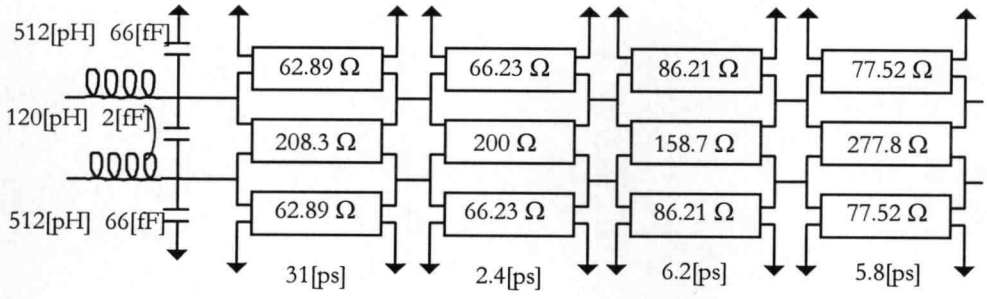

Figure 63 Simplified reduced equivalent circuit
for the coupled traces

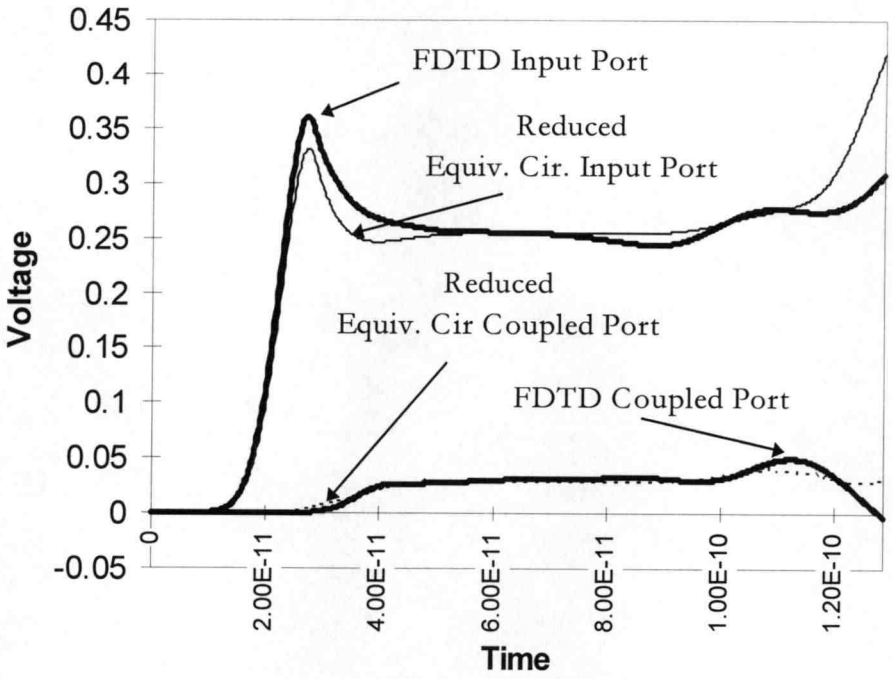

Figure 64 HSPICE simulated simplified equivalent circuit versus FDTD results

Figure 65 shows another typical example of coupled 3-D interconnects consisting of coupled striplines passing between different layers in a printed circuit board. The traces are 5[mils] wide and separated by 10[mils]. Both ends of each strip are terminated with 50 [Ω], (100[Ω] to each ground plane). The dielectric constant is 4 and the conductors are 1[mil] thick. The two dimensional peeling algorithm was applied to the V-TDR results shown in Figure 66 and simplified equivalent circuits extracted from the data are shown in Figure 67. The time domain response of the equivalent circuits is compared to the FDTD simulation results in Figure 68, to validate the accuracy of the equivalent circuit models..

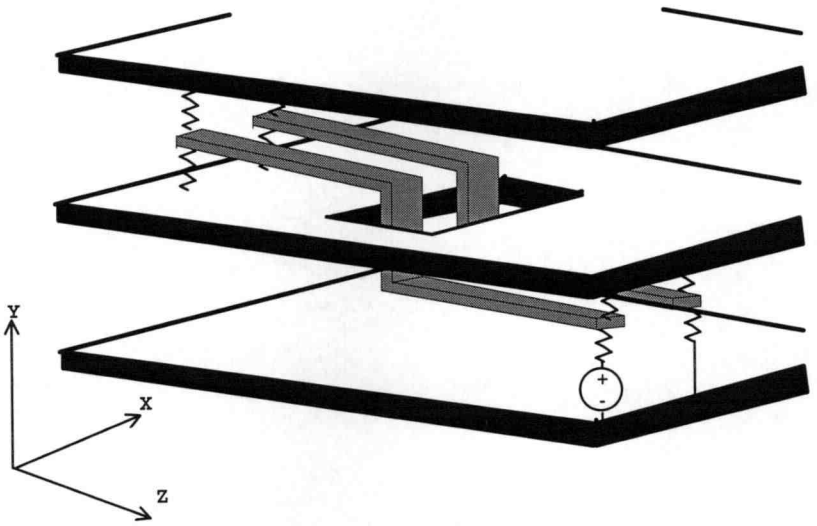

Figure 65 Coupled via structure

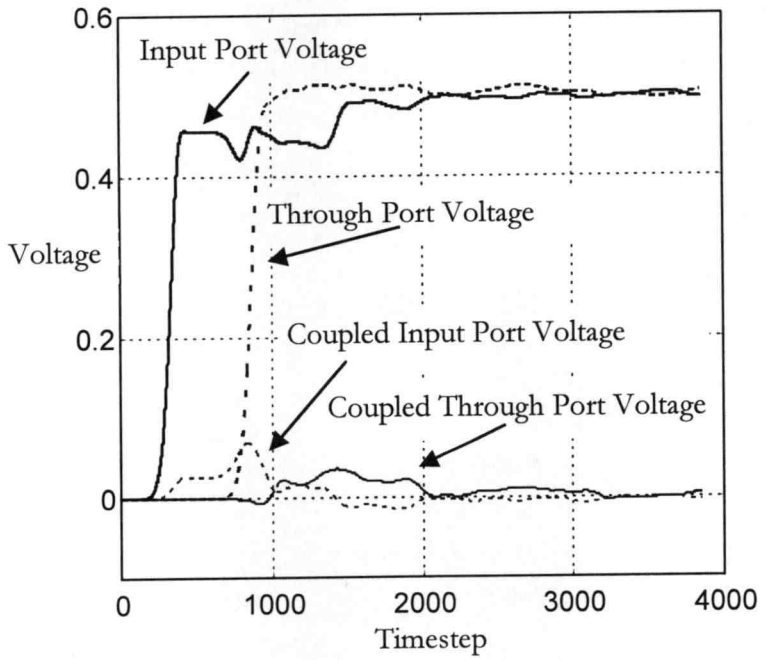

Figure 66 V-TDR voltages from FDTD simulation of coupled stripline vias

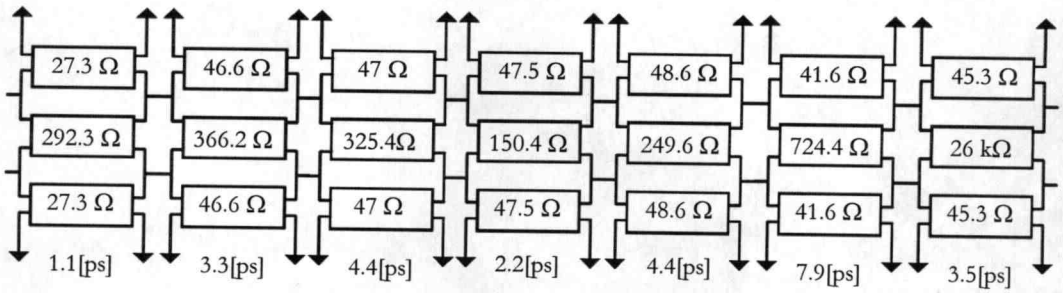

Figure 67 Extracted simplified equivalent circuit
for the coupled stripline vias

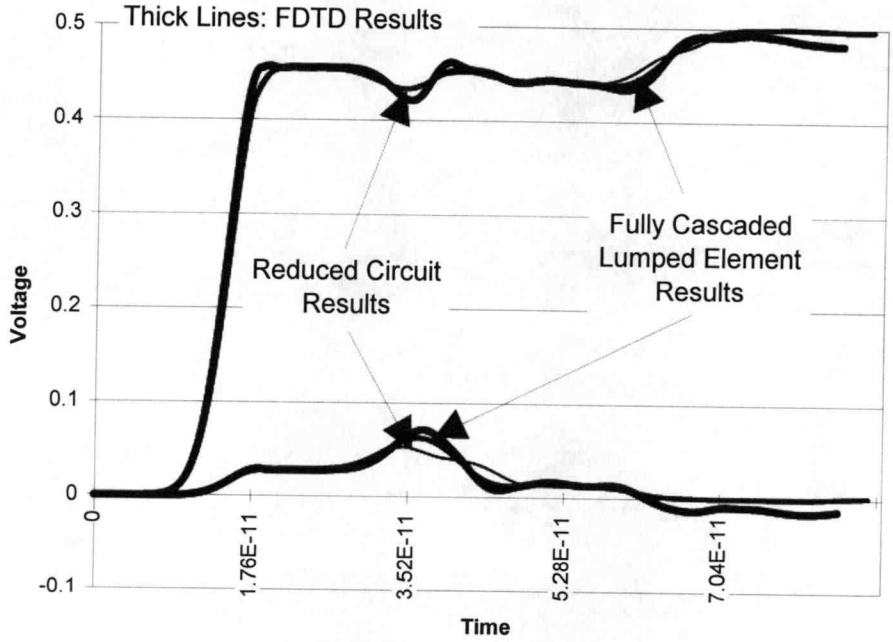

Figure 68 Simulation of extracted SPICE model
(Figure 67) and fully cascaded lumped element
model versus FDTD Results for coupled vias

The use of FDTD simulation and it's application as a V-TDR allows evaluation of package design options and other structures before prototyping. The extracted equivalent circuits can be used in board level simulations with various driver and receiver models to investigate design options and design viability. This leads to cost and time reductions in a design cycle by permitting elimination of electrically poor options before prototyping and testing. Furthermore this type of board level simulation can also be used to investigate the potential upper frequency limit and signal quality issues of a system before actual prototyping begins.

5.3. Coupled Microstrips

The FDTD technique can simulate coupled systems which are dispersive. These type of systems are more difficult to analyze using conventional techniques. As an example, Figure 69 shows a coupled microstrip structure which was simulated. A Gaussian pulse was used to excite port 1 and the voltages were monitored at each of the other ports. Each port was terminated with two 100 [Ohm] resistors, one at each edge of the conducting strips, to give a 50 [Ohm] termination. This provided good, but not ideal terminations. The structure has a dielectric constant of 4, each strip is 200 [μm] wide, separated by 180 [μm], and 100 [μm] above the ground plane. Both of the strips are 4[mm] long. Figure 70 shows the voltages at each of the ports and Figure 71 shows the absolute value of the port voltages versus frequency. The values are compensated for the frequency content of the input waveform.

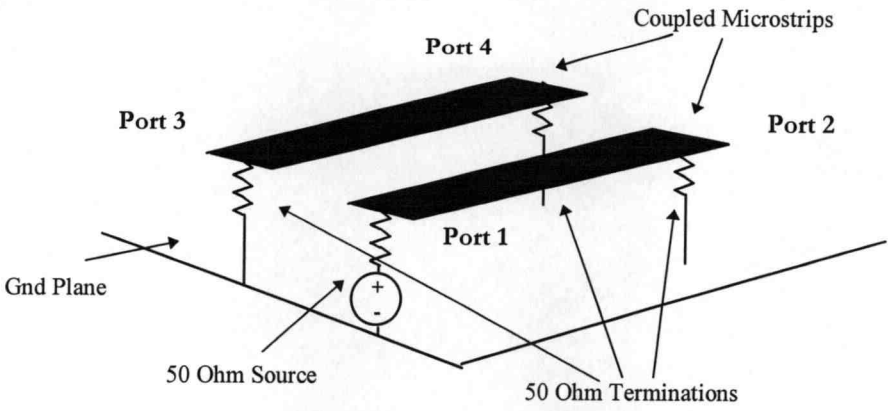

Width=200[um] Height=100[um] Dielectric=4 Δx=Δz=20[um] Δy=10[um]

Figure 69 Coupled Microstrip Structure

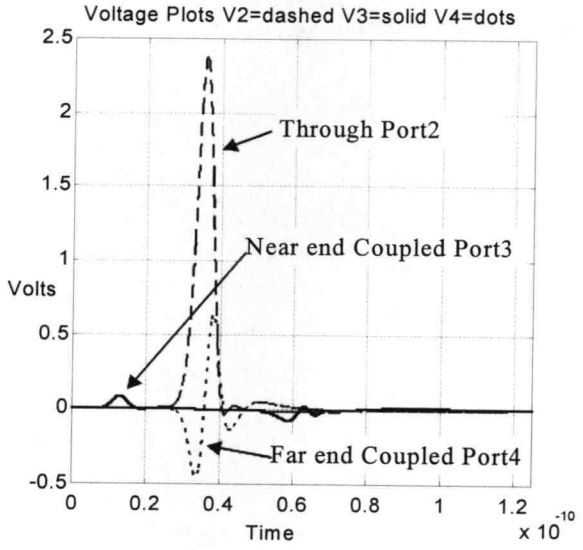

Figure 70 Coupled Microstrip Voltages

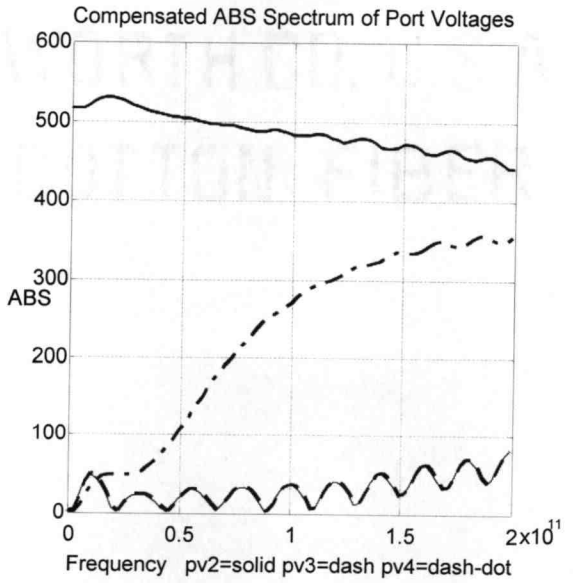

Figure 71 Port Voltages versus Frequency for Coupled Microstrips

Figure 71 shows the expected increase in coupling to port 4 as the frequency increases and the anticipated decrease in the transmitted voltage of port 2. The bumps around 150 [GHz] are believed to be from resonances due the finite width of the substrate used in the simulation.

6. Conclusions and Future Work

6.1. Conclusions

A new second order accurate technique for nonuniform FDTD electromagnetic simulation has been derived, implemented, and compared to the current first order techniques. On nonuniform grids it is seen that the new second order technique produces better results over a broader frequency range than the first order techniques.

A rigorous three dimensional stability analysis of the new second order nonuniform technique shows that the Courant stability criteria for the uniform and first order nonuniform techniques are more stringent than the stability criteria for the new second order nonuniform technique. Therefore the new second order technique does not require smaller time stepping which would increase the simulation time. Since the grid is orthogonal, the nonuniform second order technique requires virtually no additional memory and requires up to six additional multiplications and additions per nonuniform cell. The uniform cells require no additional computational power. The standard FDTD technique for lossy systems can be implemented using 36 multiplies and 24 additions per cell. The additional multiplications and additions required for the nonuniform griding are

out weighed by the computational savings provided by utilizing coarser grid spacing in regions where the simulation structure does not have fine details. There was no noticeable speed difference between the first and second order nonuniform techniques for grids with the same number of cells.

Proper treatment of the material constants, (permittivity, permeability, conductivity, and fictitious magnetic loss) in a nonuniform grid for the FDTD technique was derived and presented. This allowed the development of the general nonuniform FDTD simulator for general lossy structures which was written for this body of work.

The general nonuniform lossy FDTD simulator has been proposed and used as a V-TDR in conjunction with a two dimensional peeling algorithm to derive an equivalent circuit for 3-D coupled interconnects. Simulation results for IC ground plane current density, coupling between lines, and radiation losses were also presented. Use of FDTD simulations and it's application as a V-TDR allows evaluation of package design options and other structures before prototyping. This can lead to cost and time reductions in a package design cycle by eliminating electrically poor options before prototyping and testing.

The development of the new second order technique, it's corresponding stability criteria, and proper treatment of the material parameters in a nonuniform grid give the FDTD method much higher flexibility in modeling complex structures and helps relieve the computational and memory demands which are often the major limitations to practical implementation of the FDTD method.

There are several original or unique contributions presented in this body of work. The foremost is the development of a second order accurate technique for nonuniform grid spacings for application in the FDTD method. Derivation of the stability criteria for the nonuniform technique is another significant and original contribution performed in this work. For completion of the nonuniform technique the proper calculations and handling of the complete set of constitutive material parameters was derived. The fore mentioned contributions lead to an improved accuracy and more efficient implementation of the FDTD method for general structures.

The concept of a virtual TDR (V-TDR) is presented for the first time and used to extract the equivalent circuit from a simplified IC package. This gives designers the ability to evaluate different design options electrically before prototyping. Prototyping is an expensive and time consuming process and the concept of a V-TDR can be used to eliminate poor options thus reducing the design cycle in dollars and time.

6.2. Future Work

The same approach for generating the nonuniform space stepping can also be applied to the time stepping. Although nonuniform time stepping would increase the memory requirements, (since more past time information needs to be stored), it would allow for the FDTD method to be coupled with nonlinear simulators which rely on nonuniform time stepping. This would allow for accurate simulation of nonlinear active devices such as transistors and diodes in FDTD simulations as either single cell or multiple cell devices.

The nonuniform second order technique also works within the PML boundaries and should lead to more efficient implementations of this absorbing boundary condition. The idea is to rapidly increase the grid spacing as the PML layers get closer to the grid edge. This may work especially well since the higher frequency components will be attenuated mostly in the first couple of PML layers which will have smaller grid spacings and can support the higher frequency components. This allows for large increases in the grid spacing in the outer layers for attenuation of the lower frequency components.

It should also be possible to dynamically change the grid spacing between time steps. The new method would be able to determine the field values in the new grid based on the old grids values with an accuracy of second order. This could be used to provide finer grid spacing where high field variations are occurring during the simulation. For example a

finely gridded region could move through the simulation space tracking a propagating pulse or the simulator could increase the gridding density at locations, such as metal corners, where large field variations are occurring to insure accurate modeling. This would significantly decrease the memory demands and increase the simulation speed and accuracy. Another use would be to model objects with fine details moving through the simulation space, such as an aircraft or a super conducting body being moved by magnetic fields.

Bibliography

[1] M. Thorburn, "Analysis and Modeling of Discontinuities and Inter-Element Coupling in Microwave Integrated Circuits", Ph.D. Thesis, Oregon State University, 1991

[2] A. Hill, "Quasi-TEM and Full Wave Numerical Methods for the Characterization of Microstrip Discontinuities", Ph.D. Thesis, Oregon State University, 1990

[3] X. Zhang, "Calculations of the dispersive characteristics of microstrips by the time-domain finite difference method", IEEE Trans. MTT, vol. 36, N0. 2, pp.263-267, Feb. 1988.

[4] M. Falconer, V. Tripathi, "Time Domain Simulation of Micron and Submicron Interconnects", Proc. VLSI Multilevel Interconnections, June 1993.

[5] M. Falconer, V. Tripathi, "FDTD Simulation of Power/Ground Bounce and Crosstalk in IC Packages", Proc. Electrical Performance of Electronic Packaging, Oct. 1996, pp166-168

[6] F. Moglie, T. Rozzi, " A New Termination Condition for the Application of FDTD Techniques to Discontinuity Problems in Close Homogeneous Waveguide", IEEE Micro. Guided Wave Lett., Vol. 2, No. 12, Dec. 1992, pp.475-477

[7] C. Railton, E. Daniel, D. Paul, J. McGeehan, "Optimizing Absorbing Boundary Conditions for the Analysis of Planar Circuits Using the Finite Difference Time Domain Method", IEEE Trans on MTT, Vol. 41, No. 2, Feb. 1993, pp.290-297

[8] D. Sheen, S. Ali, "Application of the Three-Dimensional Finite-Difference Time-Domain Method to the Analysis of Planar Microstrip Circuits", IEEE Trans. MTT, Vol. 38, No. 7, July 1990, pp.849-857

[9] Z. Bi, Y. Shen, K. Wu, J. Litva, "Fast Finite-Difference Time-Domain Analysis of Resonators using Digital Filtering and Spectrum Estimation Techniques", IEEE Trans. MTT, Vol. 40, No. 8, Aug. 1992, pp.1611-1619

[10] G. Liang, Y. Liu, K. Mei, "Full-Wave Analysis of Coplanar Waveguide and Slotline Using the Time-Domain Finite-Difference Method", IEEE Trans. MTT, Vol. 37, No. 12, Dec. 1989,pp. 1949-1992

[11] M. Falconer, K. Remley, S. Goodnick, A. Weisshaar, V. Tripathi," Improved Modeling of Electromagnetic Fields Arising from the Picosecond Pulse Propagation along a Coplanar Microstrip Structure", Proc. PIERS, 1996

[12] T. Jurgens, "A Broadband Absorbing Boundary Condition for the FDTD Modeling of Circular Waveguides", IEEE MTT-S Digest, 1995, pp.35-38

[13] J. Yook, N. Dib, L. Katehi, " Characterization of High Frequency Interconnects Using Finite Difference Time Domain and Finite Elements", IEEE Trans. MTT, Vol. 42, No. 9, Sept. 1994, pp.1727-1735

[14] M. Piket-May, A. Tavlove, J. Baron, "FD-TD Modeling of Digital Signal Propagation in 3-D Circuits With Passive and Active Loads", IEEE Trans. MTT, Vol. 42, No. 8, Aug. 1994, pp. 1514-1523

[15] B. Toland, B. Houshmand, T. Itoh,"Modeling of Nonlinear Active Regions with the FDTD Method", IEEE Micro. and Guided Wave Letters, Vol. 3, No. 9, Sept 1993, pp. 333-335

[16] A. Taflove, "Computational Electrodynamics: The Finite-Difference Time-Domain Method", Artech House, Boston, pg11, 1995

[17] A. Taflove, "Computational Electrodynamics: The Finite-Difference Time-Domain Method", Artech House, Boston, pg23, 1995

[18] W. Press, "Numerical Recipes in C, The art of Scientific Computing, 2nd Edition",Cambridge University Press, New York, 1992, pp.102-104

[19] E. Yamashita, K. Atsuki, "Analysis Methods for Electromagnetic Wave Problems: The Point-Matching Method", Artech House, Boston, 1990, pp. 79-106.

[20] A. Taflove, "Computational Electrodynamics: The Finite-Difference Time-Domain Method", Artech House, Boston, pg2, 1995

[21] J. Yook, N. Dib, L. Katehi, " Characterization of High Frequency Interconnects Using Finite Difference Time Domain and Finite Elements", IEEE Trans. MTT, Vol. 42, No. 9, Sept. 1994, pp.1727-1735

[22] K. S. Yee, "Numerical solution of initial boundary value problems involving Maxwell's equations in isotropic media", IEEE Trans. Ants. Prop., vol. AP-14, pp. 302-307, May 1966.

[23] K. S. Yee, "Numerical solution of initial boundary value problems involving Maxwell's equations in isotropic media", IEEE Trans. Ants. Prop., vol. AP-14, pp. 302-307, May 1966.

[24] M. De Pourcq, "Field and power-density calculations in closed microwave systems by three-dimensional finite differences", IEEE Proceedings. Part H, Ants. Prop., vol. 132, pp.360-368, Oct. 1985.

[25] X. Zhang, "Calculations of the dispersive characteristics of microstrips by the time-domain finite difference method", IEEE Trans. MTT, vol. 36, N0. 2, pp.263-267, Feb. 1988.

[26] J. Fang, "A super-absorbing boundary algorithm for solving electromagnetic problems by the time-domain finite-difference method", Joint AP-S, URSI-B Session 27, pp. 472-474

[27] Gerrit Mur, "Absorbing Boundary Conditions for the Finite-Difference Approximation of the Time-Domain Electromagnetic-Field Equations", IEEE Trans. Electromagnetic Compatibility, vol. EMC-23, No. 4, pp.377-382, Nov. 1981.

[28] K.S. Kunz, and R.J. Luebbers, "The Finite Difference Time Domain Method for Electromagnetics", Boca Raton, Florida, CRC Press, 1993, pp. 30

[29] A. Taflove, "Computational Electrodynamics: The Finite-Difference Time-Domain Method", Artech House, Boston, pg45, 1995

[30] J.G. Maloney, G.S. Smith, "The Efficient Modeling of Thin Material Sheets in the Finite-Difference Time-Domain (FDTD Method", IEEE Trans. Ants. Prop., vol. 40, No. 3, pp 323-330, March 1992.

[31] P.A.Tirkas, K.R.Demarest, "Modeling of Thin Dielectric Structures Using the Finite-Difference Time-Domain Technique",IEEE Trans. Ants. Prop., vol. 39, No. 9, pp 1338-1344, Sept. 1991.

[32] D.S. Katz, E.T. Thiele, and A. Taflove,"Validation and Extension to Three Dimensions of the Berenger PML Absorbing Boundary Condition for FD-TD Meshes", IEEE Microwave Letters, Vol. 4, No. 8, pp.268-270, August 1994

[33] K.S. Kunz, and R.J. Luebbers, "The Finite Difference Time Domain Method for Electromagnetics", Boca Raton, Florida, CRC Press, 1993, pp. 90-91

[34] J. Veihl, R. Mittra, "An Efficient Implementation of Berenger's Perfectly matched Layer (PML) for Finite-Difference Time-Domain Mesh Truncation", IEEE Microwave and Guided Wave Letters, Vol. 6, No. 2, Feb. 1996, pp.94-96

[35] Holland, Richard, "Finite-Difference Time Domain (FDTD) Analysis of Magnetic Diffusion", IEE Trans. Electromagnetic Compatibility, Vol. 36, No. 1, Feb 1994, pg 32-39

[36] D.S. Katz, E.T.Thiele, A. Taflove, "Validation and Extension to Three Dimensions of the Berenger PML Absorbing Boundary Condition for FD-TD Meshes", IEEE Microwave and Guided Waves Letters, Vol. 4, No. 8, Aug. 1994, pp.268-270

[37] G. Mur, "Absorbing Boundary Conditions for the Finite-Difference Approximation of the Time-Domain Electromagnetic-Field Equations", IEEE Trans. Electromagnetic Compatibility, Vol. EMC-23, No. 4, Nov. 1981, pp. 377-382

[38] T.G. Moore, J.G. Blaschak, A. Taflove, G.A. Kriegsmann, "Theory and Application of Radiation Boundary Operators", IEEE Trans. on Ant. and Prop., Vol. 36, No. 12, Dec 1988, pp. 1797-1812

[39] Z. Yusheng, W. Wenbing, "The Studies of Stability of FDTD with Mur's Absorbing Boundary Condition of Second Order in 3-D Scattering Problems", IEEE Microwave and Guided Wave Let., Vol. 6, No. 3, Mar. 1996, pp. 120-122

[40] Z. Bi, K. Wu, J. Liva, "A Dispersive Boundary Condition for Microstrip Component Analysis Using The FD-TD Method", IEEE Trans. MTT, Vol. 40, No. 4, April 1992, pp. 774-777

[41] V. Betz, R. Mitra, "Comparison and Evaluation of Boundary Conditions for the Absorption of Guided Waves in an FDTD Simulation", IEEE Microwave and Guided Wave Let., Vol. 2, No. 12, Dec. 1992, pp. 499-501

[42] R.L. Higdon, "Numerical Absorbing Boundary Conditions for the Wave Equations", Mat. Comput., Vol. 49, No. 179, Jul. 1987, pp.65-91

[43] J. Fang, Electronics Packaging Forum, Binghamton, NY, IEEE Press, 1994, pp189-244

[44] K.K. Mei, J. Fang, "Superabsorption- A Method to Improve Absorbing Boundary Conditions", IEEE trans. on Ant. and Prop., Vol. 40, No. 9, Sept. 1992, pp. 1001-1010

[45] J. Pierre, "A Perfectly Matched Layer for the Absorption of Electromagnetic Waves", Journal of Computational Physics, Vol. 114, Sept, 1994, pp 185-200

[46] D.S. Katz, E.T.Thiele, A. Taflove,"Validation and Extension to Three Dimensions of the Berenger PML Absorbing Boundary Condition for FD-TD Meshes", IEEE Microwave and Guided Wave Let., Vol. 4, No. 8, Aug 1994, pp. 268-270

[47] J. P. Berenger, "A Perfectly Matched Layer For the Absorption of the Electrictromagnetic Waves." J. Comp. Pyhsics, Vol. 114, pp. 185-200, 1994

[48] Z. Wu, J. Fang, "Numerical Implementation and Performance of Perfectly Matched Layer Boundary Condition for Waveguide Structures", IEEE Trans. MTT., Vol. 43, No. 12, Dec 1995, pp. 2676-2683

[49] D. Sheen, "Numerical Modeling of Microstrip Circuits and Antennas", Ph. D. Dissertation, Massachusetts Institute of Technology, Cambridge, MA ,June 1991

[50] P. Monk, E. Suli, "A Convergence Analysis of Yee's Scheme on Nonuniform Grids", SIAM J. Numerical Analysis, Vol. 31, No. 2, pp. 393-412, April 1994

[51] P. Monk, E. Suli, "Error Estimates for Yee's Method on Nonuniform Grids", IEEE Trans. on Magnetics, Vol. 30, No. 5, pp. 3200-3203, Sept. 1994

[52] A. Taflove, "Computational Electrodynamics: The Finite-Difference Time-Domain Method", Artech House, Boston, pg345, 1995

[53] E. Navarro, N. Sangary, J. Litva, "Some Considerations on the Accuracy of the Nonuniform FDTD Method and Its Application to Waveguide Analysis When Combined with the Perfectly Matched Layer Technique", IEEE Trans. MTT, Vol. 44, No. 7, July 1996, pp. 1115-1124

[54] B. Fornberg, "Generation of Finite Difference Formulas on Arbitrarily Spaced Grids", Mathematics of Computation, Vol. 51, Num. 184, Oct. 1988, pp. 699-706

[55] E. Navarro, N. Sangary, J. Litva, "Some Considerations on the Accuracy of the Nonuniform FDTD Method and Its Application to Waveguide Analysis When Combined with the Perfectly Matched Layer Technique", IEEE Trans. MTT, Vol. 44, No. 7, July 1996, pp. 1115-1124

[56] Kirsching, Jansen, IEEE Trans. MTT Jan 1984, errata March 1985

[57] X. Zhang, J. Fang, K. Mei, "Calculations of the Dispersive Characteristics of Microstrips by the Time-Domain Finite Difference Method", IEEE MTT, Vol. 36, No. 2, Feb. 1988, pp. 263-267

[58] R. Collin, "Field Theory of Guided Waves second edition", IEEE Press, New York, NY 1991, pp. 263-268

[59] A. Taflove, "Computational Electrodynamics: The Finite-Difference Time-Domain Method", Artech House, Boston, pg433, 1995

[60] A. Taflove, "Computational Electrodynamics: The Finite-Difference Time-Domain Method", Artech House, Boston, pg45, 1995

[61] K. Kunz, R. Luebbers, "The Finite Difference Time Domain Method for Electromagnetics", CRC Press, Boca Raton, Florida, pg. 30, 1993

[62] E. Navarro, N. Sangary, J. Litva, "Some Considerations on the Accuracy of the Nonuniform FDTD Method and its Application to Waveguide Analysis When Combined with the Perfectly Matched Layer Technique", IEEE MTT, Vol. 44, No. 7, pp.1115-1124, July 1996.

[63] L. Hayden, V. Tripathi,"Characterization and Modeling of Multiline Interconnections from the Time Domain Measurements", IEEE Trans. MTT, Vol. 42, pp. 1737-1743, Sept. 1994

[64] J. Jong,B. Janko, V. Tripathi, "Time-Domain Characterization and Circuit Modeling of Multilayer Ceramic Package", IEEE Trans. Comp. Hybrids, Manufact. Tech, Part B, vol. 19, pp. 48-56, Feb. 1996